EXPLORING THE TRANSLATIONAL CLINICAL VALUE OF CEREBROVASCULAR REACTIVITY ASSESSMENTS BY DIFFUSE COREELATION SPECTROSCOPY

A Dissertation

Presented to

The Academic Faculty

by

Kyle Robert Cowdrick, MSE

In Partial Fulfillment

of the Requirements for the Degree

Doctor of Philosophy in Biomedical Engineering in the

Wallace H. Coulter Department of Biomedical Engineering

Georgia Institute of Technology and Emory University

August 2023

EXPLORING THE TRANSLATIONAL CLINICAL VALUE OF CEREBROVASCULAR REACTIVITY MEASURED BY DIFFUSE OPTICAL SPECTROSCOPY

Approved by:

Dr. Erin M Buckley PhD, Advisor
Department of Biomedical Engineering
Georgia Institute of Technology & Emory University

Dr. Susan Margulies PhD
Department of Biomedical Engineering
Georgia Institute of Technology & Emory University

Dr. Shella Keilholz PhD
Department of Biomedical Engineering
Georgia Institute of Technology & Emory University

Dr. Deqiang Qiu PhD
Department of Biomedical Engineering
Georgia Institute of Technology & Emory University

Dr. Jocelyn Grunwell, MD, PhD
Department of Pediatrics
Division of Critical Care Medicine
Emory University School of Medicine
Children's Healthcare of Atlanta

Date Approved: July 14, 2023

Draw near to God, and he will draw near to you.

James 4:8 (NAB)

This thesis is dedicated in thanksgiving to all the sources of steadfast love in my life: To Christ the King, whom out of love for the Father and for me, and through the Holy Spirit encountered me years ago and set me upon this journey of discovering that a beautiful intersection of faith and reason in service to humanity can be joyfully lived out through a professional career in biomedical engineering; to my bride Sharon, whom has revealed His love through this beautiful life we have found and built together with our children; and to my family-physical and spiritual -who have sustained me through their love, corporal and spiritual works of mercy, and steadfast prayer.

ACKNOWLEDGEMENTS

Anyone who has ever embarked upon any meaningful endeavor in life recognizes success is not achieved in a vacuum. Whatever sentiments of gratitude I impart here cannot fully express the gratitude I have toward all those who helped me along this journey to achieve such a remarkable professional milestone.

I am incredibly thankful to Erin who was the best mentor I could have possibly asked for during my doctoral journey. Erin, not only did you facilitate my professional growth as a research scientist, but also you were unmatched in your support in matters of personal life. With you and through you, I have learned to ask meaningful questions, be systematically rigorous in my approach to data science, and estimate reasonable timelines (it seems I will still be working on that indefinitely). I could go on regarding the various aspects of my training I am thankful for under your mentorship, including the opportunity to build global relationships with the incredibly talented practitioners in our field. However, perhaps one of the most important sources of gratitude I have is for your unmatched support in matters of personal life. Through your simultaneous dedication to your craft and your family, you have demonstrated that it is possible to pursue my professional aspirations without completely sacrificing the dream of building and supporting my family, a challenging endeavor when in context of do so during graduate school. I am sincerely grateful.

I thank my thesis committee for their service in supporting me toward this doctoral milestone. Your support and constructive feedback are deeply appreciated. I would like to especially thank Deqiang Qiu Ph.D. for serving on my committee at the late stage of my training as another committee member had to step out unexpectedly. Thank you, Jocelyn Grunwell, M.D., Ph.D., for your steadfast support serving on my committee despite the reality that our early pilot projects in critical care we started at the start of my training here

did not turn out as successfully as we originally expected. Thank you, Susan Margulies Ph.D., for continuing to serve on my committee regardless of your unexpected and exciting transition to lead the engineering directorate at NSF. Thank you, Shella Keilholz Ph.D. for your gracious availability to discuss conceptual matters of data analysis with Erin and I on a moment's notice.

I am thankful to all my colleagues in the Buckley Lab who made my graduate school journey a positive experience. The level of professionalism maintained in the culture of our lab team and dedication for collaborating on clinical data acquisition at all hours of the day is greatly appreciated. I thank all our clinical collaborators including our partners at Children Healthcare of Atlanta: Drs. Michael Wolf M.D., Kirshma Khemani M.D., Beatrice Gee M.D. I also thank all the research subject volunteers, CHOA patients, and their families/guardians: without your partnership and commitment to building a healthier world with more birthdays through participation in research, none of these investigations would have been possible.

While I certainly grew as a professional research scientist in the context of this academic research, undoubtedly the most impactful aspect of my professional development journey as a biomedical engineer and medtech consultant was made possible through my partnership with Georgia Tech's Biomedical Engineering Capstone Design community. I am thankful for my managers and mentors James Rains P.E. and James Stubbs Ph.D. who took a chance on me to start working with our students first as a TA and subsequently as a program manager and the New Partnerships Liaison for BME Capstone. These experiences have opened a world of opportunities for my growth as a card-carrying biomedical engineer with the capacity to turn science fiction into science fact. Through your trust in my skillsets and competencies, you allowed me to effectively "run free" in this function and shape this role into a new dynamic set of functions beyond the client-facing sales role supporting our program. Through your guidance, I have practiced, enhanced, and learned a vast array of knowledge and skills in medical device

innovation, project management, and program management. Through your mentorship, I have become wise in matters pertaining to Biodesign education and the complexities of undergraduate education in BME. I have always appreciated your honest dialogue and entrepreneurial guidance as I support our students and clients/project sponsors to bridge the gap between concepts and early-stage validation of medical technologies to address unmet clinical needs. Finally, I am grateful for the opportunity to support our organization as this opportunity has provided such necessary additional capacity to be able to financially support my family during graduate school.

Everyone who attempts to reach this doctoral training milestone needs a robust support system to make it to the finish line and often our support system takes many forms. First, I would like to express my gratitude to my (and my family's) spiritual community through the Georgia Tech Catholic Center and the Cathedral of Christ the King. The friends we have met over the years at each of these spiritual homes have been immense resources of social and spiritual support during the many trying and challenging times presented along my graduate school journey. Particularly, my wife Sharon and I are blessed and thankful for the friendship and ministry we have found in the priesthood through Father Mark White, Father Branson Hipp, and Father Joe Wagner. Father Mark, Sharon and I cannot thank you enough for the ways you blessed us during our engagement and spiritual growth at Christ the King. We will always remember the day of our engagement where you prayed for our future marriage to be a light to others while surrounded by our dear friends after Mass that beautiful day. Further, without you coming to our aid in the few weeks preceding the onset of the 2020 COVID-19 pandemic in the United States, we would not have been able to get married the night the City of Atlanta shut down on March 24th nor would we have given birth specifically to our beloved Margot. May she and our family present and future continue to pay it forward sharing the beautiful grace and love of Christ you showed us in those challenging, uncertain days. Father Branson, thank you for supporting our family through administering the sacraments and

making them so accessible, for administering Margot's Baptism, and being her favorite friend after every Mass. Father Joe, thank you for your friendship to Sharon and I and especially to Margot during family dinners. We have such a fond appreciation for the friendship that can be found through amazing ministers to souls witnessing to truth, goodness, and beauty such as yourself.

I am grateful for the unwavering support of my parents Bob and Emily Cowdrick, my first mentors in life, who have steadfastly encouraged me throughout all my educational and professional journeys. Now being a father myself, I know I can never fully comprehend all the ways you have loved me throughout my life and selflessly put my needs before your own. I am grateful you have cultivated a spirit of excellence in everything I do and because of the tremendous, yet loving value you placed on education in my life, I was motivated to pursue doctoral research at the highest level. I am grateful for the support of my sister Kara as well throughout this journey, especially through your acts of love through service to my girls and I.

I am thankful to my daughter Margot, with whom I have been extraordinarily blessed to share my dissertation journey. How unexpectedly grateful I am to have had the pleasure of watching you grow into a beautiful, intelligent, compassionate girl while rarely missing a single moment since the world transitioned to a fully remote and now hybrid work model. The best parts of my day are coming home to you and mommy after a long day at Emory or taking many breaks from our home office (i.e., also your room; thanks for lending it to me!) for hugs & snugs, reading, dance parties, and mealtimes. I love it when you want to "work together" with Dad standing next to me while at my office desk at home. Thanks for all the help you gave me "organizing" my desk (i.e., mostly taking everything out of carefully ordered locations to make my desk more entropic), making scans of all the artwork we made together, and all the ways you helped me escape the monotony of dissertation writing.

Finally, and most importantly, thank you Sharon, my love, for everything you are and all you have done to support not only me but also our supporting family throughout this journey. I could not have asked for a more supportive spouse, especially as we prepare to welcome Pascal, our new son we love so dearly already, into our lives later this year. You are as much a partner in this doctoral journey that Emory/Georgia Tech might as well give you an honorary one just for putting up with all of this! I am thankful for the love you show me as it reflects the love of our Father in heaven. No words can truly express my love and thanksgiving for you.

Ad Majorem Dei Gloriam

For the Greater Glory of God

PREFACE

Test everything; retain what is good.

1 Thessalonians 5:21 (NAB)

This thesis is intended to benefit those interested in exploring the clinical utility of bedside cerebrovascular reactivity (CVR) assessments using an emerging optical neuromonitoring technology termed diffuse correlation spectroscopy (DCS). The work herein describes exploratory evaluations of DCS-measured CVR for clinical use and serves as an initial foundation for others in the diffuse optics field to validate and continue to expand upon. Commentaries exploring the clinical value of addressing this unmet need from the perspective of bringing novel technology to market realization are provided.

TABLE OF CONTENTS

LIST OF TABLES

LIST OF FIGURES

LIST OF SYMBOLS AND ABBREVIATIONS

AA	Arachidonic Acid
ABP	Arterial Blood Pressure
ASL-MRI	Arterial Spin-labeling Magnetic Resonance Imaging
BF_i	Index of blood flow
BH	Breath-hold
BOLD-fMRI	Blood Oxygen Level-Dependent Functional MRI
CaO2	Arterial Oxygen Concentration
CBF	Cerebral Blood Flow
CBFV	Cerebral Blood Flow Velocity
CBV	Cerebral Blood Volume
CCC	Concordance Correlation Coefficient
CDE	Correlation Diffusion Equation
CO_2	Carbon Dioxide
CPP	Cerebral Perfusion Pressure
CVR	Cerebrovascular Reactivity
CVAR	Cerebrovascular Autoregulation
D_b	Effective Brownian Diffusion Coefficient
DPF	Differential Path (Length) Factor
$EtCO_2$	End-tidal Carbon Dioxide
ε	Error (i.e., fit residual)
FDA	Food and Drug Administration
fdNIRS	Frequency-Domain Near-Infrared Spectroscopy
fMRI	Functional Magnetic Resonance Imaging

G_1	Unnormalized Temporal Electric Field Autocorrelation Function
g_1	Normalized Temporal Intensity Autocorrelation Function
g_2	Normalized Temporal Electric Field Autocorrelation Function
Hb	Hemoglobin
HbF	Fetal Hemoglobin
HbO	Oxygenated Hemoglobin
HbR	Deoxygenated Hemoglobin
HbS	Sickle hemoglobin
ICP	Intracranial Pressure
ICU	Intensive Care Unit
MAP	Mean Arterial Blood Pressure
MBLL	Modified Beer-Lambert Law
MCA	Middle Cerebral Artery
MRI	Magnetic Resonance Imaging
NIRS	Near-Infrared Spectroscopy
NMDA	N-Methyl D-Aspartate (neuronal receptors)
nNOS	Neuronal Nitric Oxide Synthase
NO	Nitric Oxide
PaO_2	Partial Pressure of Oxygen in Arterial Blood
$PaCO_2$	Partial Pressure of Carbon Dioxide in Arterial Blood
PET	Positron Emission Tomography
ρ	Source-Detector Separation
RBCs	Red Blood Cells
rSO2	Regional (Tissue) Oxygen Saturation
RS	Resting State

SCD	Sickle Cell Disease
SCI	Silent Cerebral Infarct(s)
SPECT	Single-Photon Emission Computed Tomography
TBI	Traumatic Brain Injury
TCD	Transcranial Doppler (Ultrasound)
trNIRS	Time-Resolved Near-Infrared Spectroscopy
μ_a	Optical Absorption Coefficient
μ_s'	Optical Reduced Scattering Coefficient
VoC	Voice of the Customer

SUMMARY

Cerebrovascular reactivity (CVR), i.e., the ability of cerebral vasculature to dilate or constrict in response to vasoactive stimuli, is a biomarker of vascular health. The available literature suggests CVR quantification may benefit clinical care and consequently, CVR quantification is considered an unmet clinical need. However, the value of addressing this unmet need is not clear. Acknowledging limited investigations exploring the clinical value proposition of bedside CVR assessments, there is a clear gap in existing research seeking to validate new medical technologies that can feasibly quantify CVR in a bedside clinical setting, to identify an underserved patient population that would benefit from such assessments, and to demonstrate that new solutions are able to detect clinically meaningful differences in CVR. This thesis focuses on enhancing the clinical value proposition of CVR assessments by exploring novel experimental approaches to quantify CVR and investigating CVR assessments in a previously unexplored pediatric patient population using an emerging optical neuromonitoring technology termed Diffuse Correlation Spectroscopy (DCS).

DCS is an emerging low-cost, noninvasive, and portable optical tool that utilizes near-infrared light to assess cerebral hemodynamics (i.e., cerebral blood flow, cerebrovascular reactivity) at the microvascular length scale. Numerous investigations have explored the potential of DCS as a clinical tool to monitor hemodynamic function in response to disease states or interventions that may adversely disrupt hemodynamic function. To successfully achieve translation of this promising neuromonitoring capability from research concept to routine clinical reality, a convincing value proposition must be established demonstrating the ability of DCS neuromonitoring to detect signs of cerebrovascular dysfunction and provide compelling data showing if on-demand CVR was available to physicians, actionable, timely, and appropriate therapeutic interventions could occur to reverse a CVR abnormality that is itself a determinant of clinical outcome.

The overall goal of this work is to explore and enhance the clinical value proposition DCS-mediated CVR assessments in pediatric patients. This work has two primary aims. In Aim #1, I hypothesize that CVR assessed with DCS using more tolerable experimental protocols will agree well with the gold standard hypercapnia challenge. In Aim #2, I hypothesize that children with SCD experience markedly reduced CVR when compared to healthy children in response to a breath-hold challenge. The ultimate outcome of this work lends support to the clinical value of DCS-measured CVR assessed in a routine outpatient clinical workflow for a pediatric population with sickle cell disease.

CHAPTER 1. Cerebrovascular Reactivity as an Unmet Clinical Need and Biomarker of Disease

1.1 Introduction/Motivation

1.1.1 Defining Cerebrovascular Reactivity (CVR)

Cerebrovascular health is related to the ability of the cerebrovascular system to balance supply of cerebral blood flow (CBF), oxygen, nutrients, and waste elimination with metabolic demand.[1] While comprising ~2% body mass, the brain's energy demand accounts for ~20% of a resting adult's total body metabolism and in young children, can be as high as 50% by 5 years of age.[2] Highly coordinated, tightly regulated physiological mechanisms – namely, cerebral autoregulation and neurovascular coupling— have evolved to meet the unique metabolic needs of the brain. Cerebral autoregulation refers to the hemodynamic process of regulating CBF in response to reductions in cerebral perfusion pressure over a timescale of minutes to hours.[3] Neurovascular coupling refers to the ability of cerebral vasculature to provide an acute (~seconds) surge in supply at the microvascular/neurovascular unit length scale.[4] These two regulatory mechanisms are highly interconnected and involve multifactorial control inputs including chemical and neurogenic factors. However, when a disease state is presented (e.g., cerebrovascular disease), these mechanisms can be compromised in a multitude of ways (e.g., vascular stenosis) that either reduce or reroute CBF. Sufficient perfusion can only be restored if either CBF can bypass the occlusion via an alternative route (i.e., the collateral blood supply), or in response to medical intervention (e.g., balloon angioplasty with stent placement; a common interventional cardiology procedure). If reductions in perfusion are detected and not restored in a timely manner, neural tissue may suffer temporary impairment or irreversible damage (**Figure 1**).

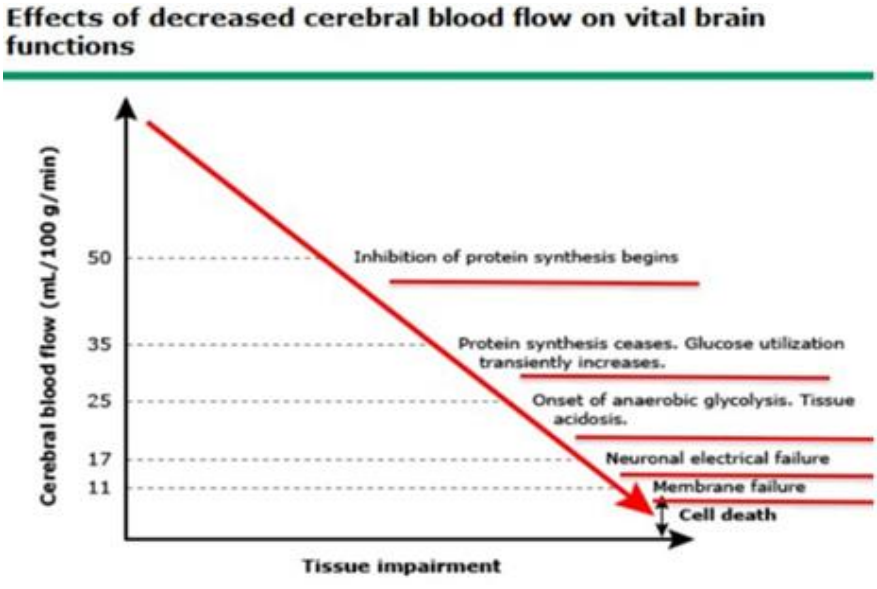

Figure 1. Effect of CBF on neuronal function during ischemia.
The degree of impaired neuronal function is a function of decreasing CBF, where an irreversible threshold is reached at sufficiently low flow (<11mL/(100g tissue *min). Figure adapted from Markus et al 2004.[5]

The status of cerebrovascular health regardless of the presence of neurological symptoms is of notable importance to physicians. Assessments of cerebrovascular reactivity (CVR) may provide a quantitative measure of the neurovascular unit's ability to respond to acute changes in metabolic need.[1] CVR, broadly defined as the ability of cerebral vasculature to dilate or constrict in response to vasoactive stimuli, is an integral regulatory mechanism in brain hemodynamic homeostasis. Indeed, this cerebrovascular biomarker is thought to be an important indicator of the brain's vascular health.[6] In recent years, interest in CVR as a prognostic biomarker of disease has accelerated (2008: N=27 PubMed publications published in that year; 2021: N=171; search terms: "cerebrovascular reactivity") with potential clinical applications in a multiplicity of disease states and physiological phenomenon including but not limited to: cerebrovascular disease[7–13],

stroke[14,15,15–19], cardiac arrest[20], traumatic brain injury[21–27] (including mild-TBI[28,29]), and cognition[30–41]. For example, in patients with carotid artery stenosis, measurements of impaired CVR are suggested to be more robust predictors of poor neurologic outcome compared to standard static neuroimaging based scoring systems.[17] CVR quantification is thought to have the potential to reduce morbidity and mortality in critically ill, brain-injured patients.[17,42] If providers had the ability to provide accurate, on-demand assessments at the bedside, interventions aimed to restore abnormal CVR may reduce neuronal injury resulting from vascular dysregulation. The growth of the available literature suggests CVR quantification may benefit clinical care, but a critical question remains: how does one take the many insights gathered from this growing field of research and translate them into the development of a medical device that can realistically benefit patient care? To address this question, it is instructive to first explore how a viable solution to an unmet clinical need is translated from concept to reality in the medical device industry.

1.1.2 How is an unmet clinical need translated into a viable solution in the medical device industry?

A fundamental mission of academic research centers on the impact research and discovery can bring to broader society, yet desired societal benefits cannot be realized without the successful transfer new technologies from the academic enterprise to a commercial reality. As is often the case in emerging technical fields, the path from basic science discovery or technology advancement to commercialization can be a confoundingly unclear journey among academic practitioners fraught with professional risk. There are undoubtedly many reasons for this and a thorough root cause analysis is beyond the scope of this dissertation. However, I affirm and others assert[43] the principal root cause is the processes, models, and economic incentives that work well when

supporting university-based basic and translational research programs are fundamentally different than those that facilitate new medical device creation.

Historically, academic research has contributed to medical technology innovation through the discovery and advancement of basic science used to develop fundamentally new technologies that form the basis for medical devices. The economic model of scientific research thrives on using new discoveries and technology development to generate publications in peer-reviewed academic journals offering proof-of-concept perspectives or initial technology or clinical validations which are then leveraged to solicit grant funding to sustain research programs and facilitate new discoveries. Most research proposals necessarily describe a vision of "impact to society" centering on the question "where can my new technology be applied"? However, sustaining this research economy is fundamentally different than the effort involved in the design, development, and sustainment of a new medical device. Consequently, this question may be prone to bias[43,44] and restructuring it to focus first on validating the value of an unmet clinical need can yield a more goal-directed, de-risked pathway to successfully achieving the impact to society researchers strive to attain through their scientific work.

One must not look too far to realize that well-validated processes and models exist to guide medical device innovation and academic research programs can leverage these best practices to focus future research effort in support of bringing new technologies to a point where patients may truly benefit from during routine care. Some of these models will be familiar to most academic scientists, most notably the technology-push "bench to bedside" or clinician-driven "beside to bench" models.[44] These traditional approaches have limitations and biases that substantially increase the risk of successful technology transfer as discussed extensively elsewhere.[44] However, one model for medical technology innovation – the spiral innovation model – can provide an excellent conceptual

roadmap for guiding academic research. This model for medtech innovation, championed by leadership at the Center for Bioengineering Innovation and Design at the Johns Hopkins University Department of Biomedical Engineering, is a derivative of the Stanford Biodesign process well-known among practitioners in the medical device entrepreneurial community.

The spiral innovation model proposes that any successful healthcare innovation must address various needs and constraints across diverse stakeholders according to four broad categories and activities: 1) defining and validating an unmet clinical need; 2) assessing market need/commercialization potential; 3) technology development, design, and validating its viability for clinical use; 4) organizational and strategic alignment (**Figure 2**).[44] The first theme centers on "voice of the customer (VoC) activities" in which the perspectives, clinical evidence, and operating environment of health care works, patients and their families, and the healthcare facility are systematically identified. Often these insights are gathered through informational interviewing among relevant stakeholders, clinical observations performed using ethnographic research techniques, and an extensive review of the available clinical literature. Then, these insights are aggregated and analyzed to properly define an unmet clinical need and validate the extent to which that unmet clinical need is valuable to as many stakeholders as possible. The second "market-oriented" theme focuses on assessing reimbursement potential and payor needs, assessing whether the competitive landscape of existing solutions allows a "whitespace" for innovation, and assessing legal constraints to define a regulatory strategy. The third "technical" theme follows the FDA "design controls" framework, where inputs from the first two themes are used to define need specifications (i.e. converting stakeholder/user insights into actionable design specifications), generate solution concepts, create technical prototypes, and verify/validate their technical performance.[45] Finally, the "organizational" theme seeks to implement best practices in management, small business

finance, fundraising, team formation, and strategic consulting to discern a viable pathway to market. This innovation model is highly iterative by nature, where innovators must frequently attend to forming and testing critical hypotheses in each thematic area with the ultimate goal of de-risking future efforts. The area under the curve represents the cumulative investment in time and financial resources required to advance the project to the next stage of development. Finally, after a full iteration among these four themes are completed, the project necessarily reaches a series of reviews cumulating in decisions to either proceed with further development, pivot the project (e.g. change a technical feature, focus on a new clinical need or patient population), or kill the project in favor of higher-priority areas of interest.

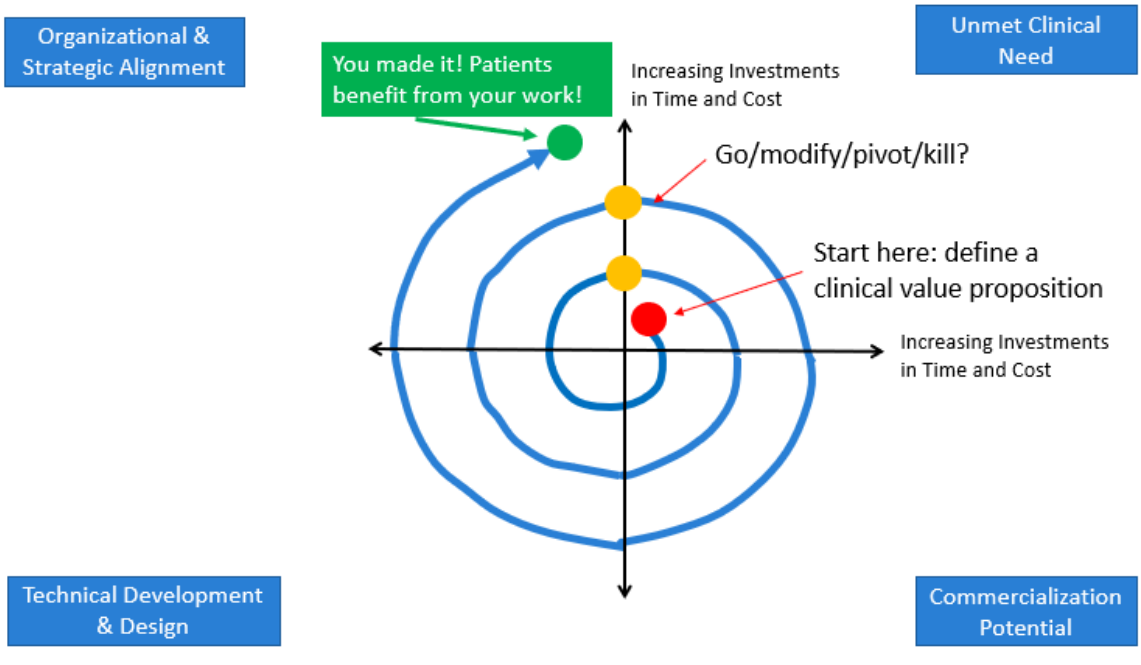

Figure 2. Spiral product development model for medical technology innovation
Spiral innovation model depicting high-level categories (blue boxes) that must be continuously addressed to take a medical device from idea to clinical reality. The X and Y axis represent time and cost and the spiral pathway, extending outward, represents increasing relative investments in time and cost. Periodically (yellow dots), a team arrives at a stage-gate in which the team evaluates progress among all four categories to determine whether future investments should continue, the commercialization approach should be modified, the innovation project should pivot entirely to a new approach, or simply kill the project if it is no longer promising. Adapted from Yazdi, Y. & Acharya et al., Annals of BME 2013.

Academic research programs are historically most adept at supporting activities in the third technical-focused theme, where in a “bench to bedside” innovation model, an academic community or faculty member develops a fundamentally new technology and later seeks to identify clinical problems that might be solved using the new platform. However, there are considerable challenges with this approach which can increase the risk for successfully translating new technology to clinical use.[44] First, exclusive effort on technology development requires substantial up-front time and financial investment yet if not properly guided by “voice of the customer” insights from key stakeholders early in the process, runs the risk of developing a solution that is not ultimately useful for the end user (see the recent case of Israeli startup Ornim Medical for a representative example[46] related to the field of optical neuromonitoring). Second, “technology looking for a problem to solve” can bias the researcher toward defining a specific clinical need that fits well with the existing technology previously developed. This approach introduces unnecessary bias and risk by potentially compelling a researcher to pursue a given clinical problem that might not result in the highest value, highest impact problem that physicians and patients need solved. Aspects of the clinical need that are well-aligned for one’s existing solution are emphasized, and other aspects that do not fit with the existing solution but may be important to clinical stakeholders are deemphasized.[44]

While each of these product development themes are revisited frequently and are all important, the spiral innovation model asserts that the best-spent effort to de-risk early technology transfer from academic research is on the initial theme in this stage-gated product development framework. In other words, the first and most critical step of bringing a medtech innovation from concept to clinical reality is to define an unmet clinical need and then demonstrate it has a unique clinical value proposition worthy of further investments in time and resources. Academic research that is carried out through this

philosophical lens exhibits a higher likelihood of both identifying an unmet need worth solving and successfully translating a new technology into clinical application.

1.1.3 CVR assessment as an unmet clinical need

CVR quantification as an unmet clinical need is discussed elsewhere in the available literature for a wide range of disease states as briefly referenced in Section 1.1.1. To specifically highlight the unmet need for CVR quantification and how these assessments may be clinically useful, two pediatric use cases are provided. The first describes an application in the inpatient critical care setting, which is exemplary of a high risk to patient, high cost to payors environment that would greatly benefit from innovations designed to reduce risk, increase patient outcome, and reduce costs to the healthcare system. The second describes an outpatient environment in hematology, in which routine CVR assessment may provide enhanced means to guide therapeutic management.

1.1.3.1 Inpatient critical care use case

Pediatric cardiac arrest is a devastating event associated with high morbidity and mortality affecting >16,000 children/year in the United States.[47] The majority of pediatric patients experience arrest at <1 year old, and survival to discharge approximates to ~13%.[47] While clinical guidelines inform management after successful resuscitation[48,49], evidence-based, patient-specific neuroprotective interventions are lacking owing to a limited ability to longitudinally monitor an individual patient's perfusion and neurovascular function status post-arrest.[50] During post-resuscitation, it is imperative that a patient

receives proper cerebral perfusion to meet metabolic needs after a global-ischemic insult to prevent secondary injury (i.e., Post-cardiac arrest syndrome). Post–cardiac arrest syndrome is a unique and complex combination of pathophysiological processes which include brain injury, myocardial dysfunction, and a systemic ischemia/reperfusion response. The clinical presentation (i.e., "signs") of this syndrome includes impaired cerebrovascular dysfunction, cerebral edema, and post-ischemic neurodegeneration, usually in a progressive order.[51,52] Observational studies strongly indicate post-arrest patients experience abnormal "cerebral vital signs" including CBF[53–59] and cerebrovascular autoregulation (CVAR). CVAR refers to the homeostatic mechanism that minimizes longitudinal deviations (e.g. deficits) in CBF due to changes in cerebral perfusion pressure (CPP, defined as the difference between mean arterial blood pressure (MAP) and intracranial pressure (ICP); i.e. CPP=MAP-ICP) through regulation of CVR.[60] Note that the terms "cerebrovascular reactivity" and "cerebrovascular autoregulation" are often used interchangeably in the literature but in this dissertation, CVAR refers to the specific aspect of CVR that is characterized by the MAP-CBF relationship.

CVR/CVAR quantification is an unmet clinical need as evidenced by recent studies which suggest impaired cerebral autoregulation is associated with neurocognitive deficits[61] and mortality[58]. For example, in a secondary analysis of a March 2016-2017 clinical trial, CVAR assessed in an adult cohort of comatose, mechanically ventilated survivors if cardiac arrest was impaired in patients with a poor 6-month clinical outcome[62] assessed by the Pittsburgh Cerebral Performance Categories.[63,64] Further, patients with a narrower MAP range for maintaining CVAR was associated with poor outcome highlighting the inherent variability in patient-specific cerebrovascular function. Unfortunately, current bedside technologies do not give physicians quantitative, on-demand, direct measures of CVAR. Rather, it is often inferred through indirect assessment of MAP. As a result, patient-specific therapeutic management of cerebrovascular function post-cardiac arrest

effectively is practically not possible. Physicians instead are forced to provide less accurate, care using population-based thresholds from large cohorts which are not necessarily applicable for each individual patient.[50,65] If physicians had the means of performing on demand CVAR assessment, a patient's individual autoregulatory limits can be quantified to then direct fluid status and vasopressor support in a manner that is tailored to maintain the CPP of a specific individual, thereby mitigating risk of secondary neurological injury post-cardiac arrest.

1.1.3.2 Outpatient hematology use case

CVR quantification may benefit pediatric clinical populations vulnerable to ischemic brain injury such as in patients with sickle cell disease (SCD). Children with SCD, an autosomal recessive inherited hemoglobinopathy caused by a single-gene DNA base-pair alteration that produces hemoglobin in the characteristic sickle shape (HbS), face an urgent unmet need for solutions that mitigate lifetime risk to ischemic injury. Affecting millions of children globally, individuals with SCD experience an average life expectancy 20 years lower than the general population in developed nations. In developing sub-Saharan African nations, this disparity in healthcare is exacerbated given between 50-95% of children with the HbSS genotype die by 5 years of age depending on the study referenced.[66] All individuals face a life-long high risk of neurocognitive comorbidities most commonly including stroke, silent cerebral infarction, and reduced executive function.[67] Brain injury in SCD is understood as a chronic mismatch in brain oxygen supply and demand where this homeostatic balance is affected by multiple hematologic factors including but not limited to hemoglobin concentration, arterial oxygen saturation, oxygen delivery to the brain (e.g., CBF), and oxygen saturation fraction.[67,68] White matter tissue in the watershed areas or "border zones" between cerebral arterial territories are particularly

vulnerable to ischemic injury as these microenvironments are prone to low cerebral blood flow and receive flow last with respect to other brain regions.[67,69] Sickled red blood cells differ from normal red blood cells in that they are prone to vaso-occlusion and hemolyze rapidly, leading to an array of local microenvironmental and system-wide physiological compensatory mechanisms aimed to maintain adequate oxygen supply to the brain. For example, the brain's cerebral vasculature will dilate to increase cerebral blood flow to maintain sufficient oxygen metabolism in the presence of a global reduction in hemoglobin concentration and oxygen saturation (**Figure 3**). Prior work over the past three decades demonstrates that each of the aforementioned hematological factors are abnormal in SCD and may serve as biomarkers used to identify and medically mitigate a patient's lifetime risk to accumulated brain injury.

Silent cerebral infarcts (SCI) are the most common ischemic injury in SCD affecting ~40% of patients by age 15[70]. Although SCI often accumulate undetected, they can be seen on brain imaging scans and are associated with poor school performance, lower IQ, and impaired executive skills, as well as with increased risk for progressive silent infarcts and overt stroke[70–72]. The etiology of SCI is due to many physiological factors including hyperemic vascular instability due to chronic anemia, impaired cerebral autoregulatory mechanisms[73] and limited vascular reserve (i.e. impaired CVR) [74–80] which increases oxygen extraction to critical levels.[81–85] (**Figure 3**). These phenomena position the brain in a vulnerable state where it must constantly, sufficiently respond to global and local increases in metabolic demand. Brain tissue is notoriously susceptible to infarction when blood flow is insufficient to maintain adequate oxygen metabolism.[81,86–88]

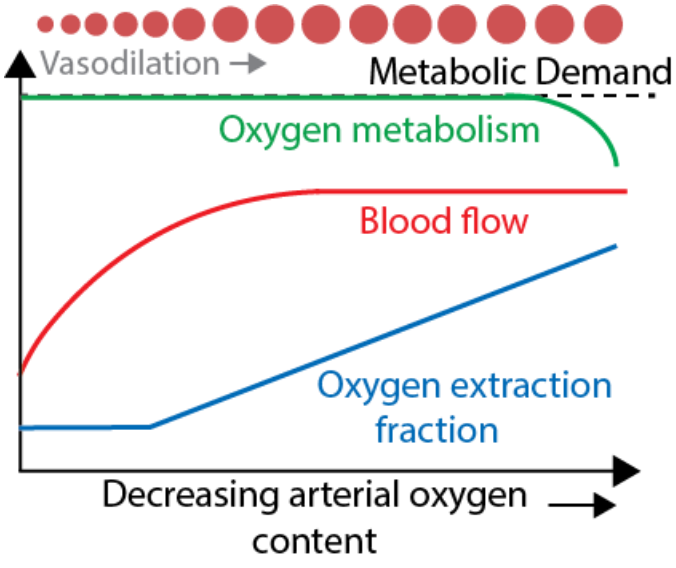

Figure 3. Hypothesized mechanism of ischemic injury in pediatric sickle cell disease
As anemia worsens, arterial oxygen content is reduced. To compensate for this reduction, the cerebrovasculature dilates to increase cerebral blood flow (CBF, red). As vascular reserve is exhausted and CBF plateaus, oxygen extraction fraction (blue) increases to preserve oxygen metabolism (green). Eventually there is a mismatch between tissue metabolic demand (dotted black) and oxygen metabolism, and infarction ensues. *Adapted from Juttukonda et al., JMRI 2019*.[68]

The current standard of care for SCI screening in SCD children entails at minimum a 1-time screening by magnetic resonance imaging (MRI) to detect SCI in early-school-age children when MRI can commonly be performed without sedation.[89] While MRI neuroimaging without sedation is effective at detecting SCIs before neurological manifestations present as overt symptoms (e.g. cognitive impairment, poor school performance), this screening approach is not a particularly patient-friendly solution. The modality is prohibitively expensive for patients in addition to payors. MRI can induce anxiety and adverse claustrophobic reactions, especially in young children.[90,91] Most importantly, the biological mechanism of ischemic injury (**Figure 3**) suggests that CVR quantification may provide an early warning of cerebral hemodynamic stress before overt symptoms clinically present. As CBF plateaus and oxygen extraction fraction increases to maintain metabolic demand, CVR would necessarily be impaired given the patient has a decreased cerebrovascular reserve due to chronic vasodilation. If clinicians could assess

cerebrovascular status on a regular basis, such as at the bedside during a routine outpatient hematology exam occurring at minimum once a year but often more frequently, then any indication of impaired CVR may prompt a change in medical management (e.g., adjusting hydroxyurea dosing) to rectify the dysfunction before permanent brain damage through SCI occurs. Very few studies[74–80] have directly investigated the relationship of CVR in the presence of SCI in SCD populations,. Therefore, there is an unmet clinical need to first explore the ability of neuromonitoring modalities to feasibly quantify microvascular CVR in children with SCD before further investigating the role of CVR in children at risk for SCI.

Using these two use cases as representative clinical vignettes, we have established that assessment of CVR is considered an unmet clinical need and innovation is needed to provide solutions that adequately address this need. Given there are plenty of unmet needs in the healthcare environment, there are plenty of problems to be solved and prioritization can be challenging with limited societal resources. If CVR quantification is an unmet clinical need, this claim necessarily begs the question “Is it a valuable” one?

1.1.4 Translational Clinical Value of Addressing Unmet Needs in CVR Needs Further Enhancement

When a clinical need is identified, it is essential that the value proposition of solving that unmet need is properly assessed to de-risk further investments of time and resources when translating a new medical technology to clinical reality. This begs the question: “how is the *value proposition* of a novel medical device innovation defined?”.

Defining a value proposition is a multifaceted, complex activity for the value of an innovation is evaluated across the four domains as depicted by the spiral innovation

model: e.g., the clinical value proposition, the business value proposition, the technical value proposition, and the organization value proposition. Furthermore, assessing the value of addressing a particular unmet need or a proposed solution may yield diverging results depending on the unique needs and constraints of the stakeholder group in question. A physician might define the value of a CVR assessment on a qualitatively relative scale with respect to other clinical needs he or she encounters in daily practice. For example, while a physician may find CVR quantification useful in the outpatient hematology clinic setting for assessing ischemic risk in SCD children, it might take a lesser priority than addressing the clinical need of remote patient monitoring for hydroxyurea medication adherence. Payors, whether they are patients or insurance entities, would certainly be interested in reducing costs to the individual and the broader healthcare system. CVR assessments using lower cost neuromonitoring modalities (see **Section 1.3**) such as transcranial doppler (TCD) ultrasound or near infrared spectroscopy (NIRS)-based approaches are advantageous to healthcare facilities given the modalities require less capital investment to procure and maintain that traditional neuroimaging modalities such as MRI. However, innovators must consider through economic analysis how adding an additional diagnostic procedure into the existing established care pathway may positively or negatively impact the patient, the hospital, and insurance providers.

Recall that the spiral innovation model involves assessment and alignment of as many stakeholder needs and incentives as possible, typically identified using informational interviewing and ethnographic VoC research. Defining the value proposition for a new medical technology innovation necessarily includes development of a robust business case and go to market strategy. Across the CVR literature, no such ethnographic or health economics research exists to date (discussed in **Chapter 4.2.2**), suggesting a whitespace opportunity for further investigation in this field. While it is at least equally – and it can be

argued to be more— important to identify and focus research on the right problem guided by market research as it is to advance the science and technology used to address unmet clinical needs, this kind of market analysis is beyond the scope of this dissertation.

Acknowledging the lack of systematic research investigating the clinical value proposition of CVR assessment, there is a clear gap in existing research that seeks to validate new medical technologies that can feasibly quantify CVR in a clinical setting, to identify an underserved patient population that would benefit from such assessments, and to demonstrate that new solutions are able to detect clinically meaningful differences in CVR. This thesis focuses on exploring and enhancing the clinical value proposition of CVR assessments through validating novel experimental approaches to quantify CVR and investigating CVR assessments in previously unexplored patient populations using emerging an optical neuromonitoring technology termed Diffuse Correlation Spectroscopy (DCS). In the proceeding subchapters, the specific aims of this work are presented (**Chapter 1.2**), followed by the underlying background supporting these aims. This background includes the biological mechanisms of CVR (**Chapter 1.3**), existing CVR quantifying modalities (**Chapter 1.4**), and a discussion regarding the potential for optical neuromonitoring by DCS to provide CVR assessments (**Chapter 1.5**).

1.2 Hypotheses and Specific Aims

On-demand, bedside assessments of CVR may help guide clinical management of patients at risk for ischemic injury, such as in pediatric patients with sickle cell disease. There is an unmet clinical need for neuromonitoring tools that can assess microvascular CVR and provide physicians with actionable information that may be used to guide individualized treatment plans. The overall goal of this work is to explore and enhance

clinical value proposition of DCS for assessing CVR in pediatric patients. This work has two primary aims:

Specific Aim #1: Develop methods to noninvasively assess cerebrovascular reactivity (CVR) using DCS.

Rationale: CVR, defined as the ability of cerebral vasculature to respond to vasoactive stimuli, is an important indicator of the brain's vascular health. Impairment of CVR assessed with MRI or Transcranial Doppler Ultrasound (TCD) using a hypercapnia challenge has been shown to predict poor neurologic outcomes in various disease states. However, CVR cannot be feasibly quantified longitudinally using existing perfusion neuroimaging modalities and measuring CVR using existing experimental protocols presents burdensome implementation challenges. DCS provides an attractive alternative as a CBF monitoring tool to assess CVR in the microvasculature. Further, DCS combined with more tolerable experimental protocols such as breath-holding or resting state intermittent breath modulation may enable routine monitoring in children.

Hypothesis: I hypothesize that CVR assessed using more tolerable experimental protocols will agree well with the gold standard hypercapnia challenge.

Approach: I will continuously measure cerebral blood flow, end-tidal CO_2, and blood pressure in healthy adults during 3 experimental methods: 1) resting state observations followed by 2) a breath-hold challenge and 3) a hypercapnic challenge. CVR will be quantified using multiple analytical methods. I will compare CVR from methods 2-3 to the "gold standard" hypercapnic challenge to determine agreement. The results of this work are presented in **Chapter 2**.

Specific Aim #2: Demonstrate clinical utility of novel CVR methods in children with sickle cell disease (SCD).

Rationale: CVR is thought to be impaired in pediatric SCD due to chronic anemia causing vascular instability. Routine quantification may help provide a biomarker of silent infarction and/or overt stroke risk.

Hypothesis: I hypothesize that children with SCD experience markedly reduced CVR when compared to healthy children in response to a breath-hold challenge.

Approach: SCD children and healthy pediatric controls will be subjected to the resting state and breath-hold paradigms developed in Aim #1. The results of this work are presented in **Chapter 3**.

1.3 Biological mechanisms regulating CVR

1.3.1 Cerebrovascular resistance: the physiological basis for CVR

The brain has evolved many unique anatomical characteristics and physiological mechanisms to protect the neuronal microenvironment against a loss of CBF supply. CBF is distributed through an increasingly complex network of macrovascular and microvascular structures beginning with bilateral internal carotid arteries and vertebral arteries.[4] These feeding arteries provide approximately 70% and 30% of total supply respectively into the Circle of Willis, a central anastomosis within the brain which serves to redistribute CBF entering the brain upon failure of a proximal supplying artery. Three bilateral sets intracerebral arteries branch off from the Circle of Willis to supply vascular territories - the anterior cerebral arteries, middle cerebral arteries (MCA), and the posterior cerebral arteries. These arteries bifurcate extensively across the brain surface forming highly redundant networks of arterioles within the pia mater (i.e., pial arterioles) before penetrating deep into the cerebral cortex (i.e., penetrating arterioles) to form capillary networks. All arteries proximal to capillary networks share smooth muscle cells that line the endothelial walls and range from multiple thick layers within the cerebral arteries to a single cell layer in the penetrating arterioles.

Changes in cerebrovascular resistance form the physiological basis for CVR. Three major mechanisms control vascular smooth muscle cells through manipulating vascular resistance to adjust vascular tone (i.e., diameter) and consequently regulate localized blood flow.[92] First, cerebrovascular autoregulation regulates vasodilation across long timescales (i.e., minutes to hours) to maintain relatively consistent CBF regardless of variations in CPP. A thorough presentation of CVAR is not provided in this thesis but is

reviewed sufficiently elsewhere.[93–97] Second, cerebrovascular resistance responds to dynamic changes in arterial CO_2, in which global increases in CO_2 result decrease resistance causing a progressive increase in blood flow in most regions of the brain.[4,98–100] This increase is typically characterized by a sigmoidal function in instances where MAP remains constant. Third, neurovascular coupling—the link between neural activity and CBF— drives increases in local CBF in response to increases in metabolic demand.[92,101]

There are differing perspectives concerning the importance of the macrovascular system in CBF regulation through the CVR response. A commonly historical perspective posits that large cerebral arteries and veins are dedicated to blood distribution and storage of blood volume and effectively act exclusively as a non-vasoactive conduit for the pulsatile arterial flow from the aorta to the brain.[100] It is more commonly understood today that cerebral arteries and pial arterioles are vasoactive, characterized by layers of smooth muscle that are consequently responsive to changes in blood gasses (e.g. the partial pressure of oxygen/carbon dioxide in arterial blood; PaO_2, $PaCO_2$), oxygen concentration (CaO_2), and arterial pH (e.g. H+ concentration; [H+]).[98] This phenomenon, particularly the response to chances in $PaCO_2$, enables assessment of CVR through use of TCD (described in **Section 1.3.2**). However, recent compelling evidence suggests that microvascular capillary networks, specifically the precapillary sphincter residing at the transition between penetrating arterioles and first order capillaries, are of prime importance as they generate the largest changes in cerebrovascular flow resistance among all brain vessel segments.[102] Given the importance of microvascular CBF regulation, brief biological contexts concerning the influence of arterial CO_2, the role of cellular constituents facilitating neurovascular coupling, and the role of precapillary sphincters on CVR in the microvasculature are provided.

1.3.2 Microvascular regulation of CVR through changes in arterial CO_2

The influence of $PaCO_2$ on localized CBF control mediated through the CVR response is well established.[100] The strong relationship between $PaCO_2$ and CBF exists as a homeostatic function tightly linked to respiratory chemoreceptor function and is evolved to finely regulate pH in the local neuronal microenvironment. Changes in $PaCO_2$ induce vasodilation and contraction predominantly at the microvascular length scale, exerting its effect through penetrating arterioles and precapillary sphincters.[103–105] For example, it has been shown that increases in CO_2 relaxes the smooth muscle of all cerebral vessels yet the most responsive were arterioles with smaller diameters than pial arteries.[106] The exact biochemical mechanisms and cellular signaling pathways involved in the $PaCO_2$-CBF relationship have been the subject of extensive research over the past two decades[4,98] and are discussed extensively elsewhere.[4,98,107] At a high level, it is generally understood that changes in cerebrovascular resistance due to CO_2 occur when dissolved CO_2 in the bloodstream traverses the blood-brain barrier (BBB) to induce changes in extracellular pH. In response, changes in cerebrovascular resistance occur quickly (i.e., 5-10 seconds) as smooth muscle relaxes to vasodilate, facilitating an increase in CBF which restores chemical equilibrium through enhanced oxygen delivery. While the CVR response due to CO_2 is relatively fast, it is suggested that the brain may take up to 2 minutes to achieve a new steady state CBF when breathing a fixed concentration of ~5% CO_2.[100] This physiological mechanism is the underlying principle that enables assessment of CVR through the hypercapnia (HC) challenge, a commonly used experimental paradigm often considered the “gold-standard” approach for CVR quantification.

1.3.3 Microvascular regulation of CVR through neurovascular coupling

Neurovascular coupling refers to the dynamic, interconnected relationship between neural microenvironmental cells and localized changes in CBF. When considering the cellular constituents that comprise the blood brain barrier, CBF is primarily regulated by neurons and astrocytes. The role of both cells in CBF regulation through CVR are briefly summarized.

When neurons in proximity to an arteriole are activated, the release of neurotransmitter glutamate from a proximal synapse acts on distal neuronal N-methyl D-aspartate (NMDA) receptors responsible for facilitating calcium ion entry into the neuronal cell bodies.[107] This influx in electric potential results in a downstream signaling effect by increasing the enzymatic activity of neuronal nitric oxide synthase (nNOS) resulting in the release of extracellular nitric oxide (NO) into the microenvironment. When NO diffuses into the arteriole smooth muscle, it facilitates additional signaling pathways culminating in the generation of the secondary messenger cyclic guanosine monophosphate and resulting in a decrease in cerebrovascular resistance and blood vessel dilation. NO signaling, while required for stimulating an increase in CBF through neurovascular coupling, is thought to be a modulatory influence in vessel dilation that works in tandem with and modulating the effect of astrocyte signaling to blood vessels.[108]

Astrocytes are a class of glial cells[109] that are highly interconnected with neuronal signaling, neural metabolism, and intercellular signaling between neurons and smooth muscle cells lining penetrating arterioles in the brain.[107] Astrocytes have spiny projections with end feet that fully encapsulate blood vessels to form the blood-brain barrier. When stimulated by localized neuronal activity, astrocytes facilitate cellular signaling to arteriole smooth muscle through multiple pathways that either dilate or constrict vessels according to need. One theory suggests that astrocytes respond to neurotransmitter signaling by releasing potassium ions [K+] at their end feet effecting a change in the electrical gradient

between astrocytes and smooth muscle.[107] This gradient reduces the influx of calcium ion [Ca^{2+}] in smooth muscle resulting in decreased vascular resistance, increased relaxation, increased dilation, and increased CBF. While there remains a lack of evidence-based consensus on this mechanism's importance in CBF regulation, there is strong evidence to support the role of metabolites of arachidonic acid (AA) in CBF regulation.[107] Release of glutamate activates glutamate receptors on an astrocyte, resulting in an increase of [Ca^{2+}] causing downstream production of AA formed from the astrocyte's phospholipid membrane. The corresponding increase in intracellular AA stimulates the production of metabolites which include prostaglandins and epoxyeicosatrieonic acids which traverse intracellular space to nearby smooth muscle to then dilate arterioles. Interestingly, AA is also known to constrict vessels when it enters smooth muscle and is enzymatically converted to 20-hydroxy-eicosatetraenoic acid.[107] The relative importance of neuronal and astrocytic signaling mechanisms in vasodilation continues to be debated, but the existing evidence asserts that these two cellular constituents are highly interconnected and involved in microvascular CBF regulation.

1.3.4 Microvascular regulation of CVR through flow regulation by precapillary sphincters

Recent works have demonstrated compelling evidence describing the fundamental role the precapillary sphincter exerts on localized CBF regulation. Historically prior to 2010, neurovascular coupling was thought to primarily occur through the mechanistic regulation of smooth muscle tone at the arteriole level.[107] However, the discovery of pericytes introduced a paradigm shift in our understanding of microvascular CBF regulation. Pericytes are cells present at ~50μM intervals along the walls of capillaries and post-capillary venules, are involved in the creation of the BBB, and regulate immune cell transport across the BBB.[110] Most relevant to CVR, pericytes are involved in the regulation

of capillary CBF as they form precapillary sphincters. Pericytes comprise contractile proteins that are demonstrated to constrict or dilate in response to neurotransmitters (e.g. glutamate).[107] Observations of pericyte contraction were demonstrated in response to ischemia (i.e. a lack of blood flow to the brain) in which pericytes were responsible for impaired capillary reperfusion after a temporary cessation of CBF (e.g., in the case of a cardiac arrest).[111] Furthermore, pericyte death induced by chronic periods of localized ischemia has been shown to irreversibly constrict capillaries indicating pericytes are vitally important regulators of CBF in pathological conditions.[112] Interestingly, other works[113,114] have confirmed prior theories[107] that cellular signals can migrate across pericytes occurring through gap junctions either between pericytes themselves or between endothelial cells. Thus, it is understood that pericytes are responsible for mediating upstream signaling from capillary units to higher order branches in the penetrating arteriole network. Today, it has been experimentally demonstrated using microscopic imaging in animal models that precapillary sphincter pericytes generate the most significant changes in cerebrovascular resistance and flow compared to other larger brain vessels and are the principal chokepoint for the brain's microenvironmental cerebral blood flow.[102] Taken together, these insights represent a paradigm shift in our understanding of the role of capillary CBF regulation and underscore the importance of microvascular cerebrovascular function in clinical medicine. Improving microcirculation after an acute ischemic event is now considered a primary goal of post-ischemic clinical care.[111]

In summary, the existing body of biological evidence supports the important role the microvasculature system has on neurovascular regulation of CBF. Whether it is regulation through arterial blood gases like CO_2 or neurovascular coupling, the penetrating arterioles play an essential role in finely controlling cerebrovascular resistance to mediate changes in CBF. Further, recent investigations challenge the historical dogma that neurovascular coupling is regulated exclusively by changes in smooth muscle tone around

arterioles, especially those on the surface of the cortical brain. Discovering the presence of precapillary sphincters and quantifying the relationship between CBF and sphincter dilation, microvascular control of CVR to regulate CBF is arguably of critical importance. These biological realities emphasize the unmet clinical need for developing new neuromonitoring solutions that can effectively and feasibly quantify CVR through observations of microvascular-level cerebrovascular function.

1.4 Existing CVR-quantifying neuroimaging modalities

CVR assessment necessitates a neuroimaging modality that can measure changes in CBF and a vasoactive stimulus paradigm. Discussed at length in **Section 3.1**, the latter includes infusion of acetazolamide, the "gold-standard" hypercapnia challenge, the bread-hold challenge, and resting state observations. Regarding the former, CBF changes can be quantified using a diverse array of neuromonitoring techniques, many of which are ubiquitous in a clinical research environment. Presented in order of most feasibly integrated into routine clinical workflows, existing modalities used clinically to monitor CBF changes include: positron emission tomography (PET), single-photon emission computed tomography (SPECT), arterial spin-labeling magnetic resonance imaging (ASL-MRI), blood oxygen level dependent functional MRI (BOLD-fMRI), transcranial Doppler ultrasound (TCD), and near-infrared spectroscopy-based regional cerebral oximetry monitors ("commercial NIRS"). Each modality naturally has its inherent strengths and limitations and are presented in terms of modalities that measure macrovascular CBF (**Section 1.4.1**) and microvascular CBF (**Section 1.4.2**).

1.4.1 Macrovascular CVR-quantifying modalities

Nuclear medicine modalities that directly measure CBF are neuroimaging procedures used in clinical practice but are rarely used for CVR assessment outside of clinical research studies. PET is based on the assumption that areas of high radioactive tracer uptake are associated with brain activity and CBF to different parts of the brain is correlated with brain activity.[115] Although PET has the unique ability to monitor specific metabolic tracers (oxygen utilization and glucose metabolism) that are indirect signs of CBF, SPECT is widely available and relatively simple making it more clinically practical. SPECT detection hardware is different than PET, yet the principle of operation is similar: injection of a radioactive tracer is rapidly taken up by the brain within ~60s reflecting the CBF at the time of the injection. These nuclear neuroimaging modalities can provide absolute quantification of CBF in units of X mL CBF / 100 g tissue yet are limited in their use of ionizing radiation in CBF assessments and capacity for longitudinal monitoring of brain-injured patients. Thus, while these nuclear imaging modalities have been historically used for CBF assessment including the validating CBF measurements from newer techniques[116], they have not been widely applied to CVR quantification.

Perfusion weighted ASL-MRI imaging utilizes the signal change from water endogenous to arterial blood as it flows from the neck to the brain, also providing a direct assessment of CBF in units of X mL CBF / 100 g tissue.[115] ASL-MRI can be used for measuring CBF in macrovascular (e.g. internal carotid arteries, vertebral arteries) and to some extent the cortical microvasculature. ASL-MRI imaging of the microvasculature requires long averaging times on order of 3-5 minutes to represent a single snapshot in time given the signal tends to be temporally and spatially noisy. A comparatively limited set of literature has utilized ASL-MRI for direct quantification of CVR[117] yet BOLD-fMRI is generally the most preferred neuroimaging technique. However, CVR studies that use BOLD-fMRI as the CBF quantifying technique occasionally use ASL-MRI in tandem to

provide baseline assessments of CBF before the CVR vasoactive stimulus to assess associations between the these[75,118] and other variables (e.g. age[119,120]). Most clinical MRI scanners are not as fast as a CT-based technique (i.e., SPECT) and image quality is easily compromised by motion, thus limiting its routine use in pediatrics by requiring sedation in most infants and younger children. All MRI neuroimaging systems require substantial capital investment to procure and maintain. Most healthcare entities cannot provide on-demand or high-temporal resolution neuromonitoring intraoperatively or at the bedside.

TCD provides the most direct and clinically feasible bedside CBF quantification in macrovasculature. TCD uses a low-frequency ultrasound transducer placed on the scalp to insonate the main cerebral arteries (most commonly, the MCA) and measures the cerebral blood flow velocity (CBFV).[121] CBFV is determined by measuring the frequency change (i.e. Doppler shift) in the ultrasound beam which is directly proportional to red blood cell velocity. TCD signal traverses relatively thin bone windows, which are not present in 10-20% of patients[121] and are especially limited in Black and Asian patients or elderly individuals.[122] Physical limitations of the Doppler effect in addition to locations of accessible bone windows make TCD an exclusively macrovascular CBF imaging technique. As a result, while TCD is ubiquitous in the clinic[3,123,124], it cannot capture dynamics of cerebral perfusion in microvasculature which is especially important for evaluating brain-injured patients whom often have impaired neurovascular coupling[125] and microvascular occlusions[51]. TCD transducers can be fixed to the scalp with a headband to enable continuous high temporal resolution CBFV recording during a given examination (typically lasting only a few minutes in total). Interestingly, the use of TCD to quantify CVAR and ICP has been explored and are potentially useful diagnostic biomarkers of cerebrovascular disease and brain injury respectively.[126]

The clinical adoption of continuous TCD monitoring to assess cerebral perfusion long-term is practically negligible at present even though long-term (>1hr) monitoring of CBFV is technically achievable as demonstrated from recent technology developments[127,128] leading to a 2013[129] and 2018[130] FDA clearance. This is possibly attributed to the bulky hardware required for a TCD headset, though within the past ~3 years two Phase I clinical trials have initiated (SONAS[131], NeuralBot[132]) to explore the viability of techniques that use more ergonomic designs. Regardless of progress, none of these continuous TCD devices are designed for pediatric applications and it is further unlikely existing devices could be feasibly adapted in select populations (e.g., younger children in ICUs with smaller head circumferences). TCD is not typically utilized as a longitudinal monitor in routine clinical practice owing to the requirement for a skilled operator (e.g., physicians, radiology technician) to monitor any TCD procedure. The calculation of CBFV requires a precise angle of insonation with respect to CBF, a notable and nontrivial limitation of the technique.[122] The most accurate measure of CBF necessitates an angle of zero (i.e. parallel) with to the direction of blood flow. The larger the angle, the greater degree of error is introduced in the CBFV measure and thus, sonographers must limit the angle to <30º and keep the error below 15%. Another notable limitation of TCD especially relevant for CVR quantification is that accurate CBFV calculation assumes that the diameter of the insonated blood vessel is constant, which has been shown to respond to changes in blood pressure or a vasoactive stimulus[122].

1.4.2 Microvascular CVR-quantifying modalities

BOLD fMRI detects changes in the blood oxygen level dependent (BOLD) MRI signal that results when a change in brain state induces changes in neuronal activity and is considered an indirect measure of microvascular CBF.[133] This technique exploits the link between neural activity in the brain and coupled regulation of local microvascular

blood flow, in which neural activation increases the delivery of glucose and oxygen in concert with electrical activity.[134,135] When the brain responds to a given stimulus, increases in cortical neural activity induces an increases in localized CBF in order to match supply with increased metabolic demand. The change in CBF usually overshoots the minimum increase in oxygen and nutrients required to respond to a stimulus, resulting in an oversupply of oxygenated blood in the microenvironment and a decrease in the relative concentration of deoxyhemoglobin.[133] This phenomenon directly affects the BOLD signal used to produce MRI images owing to the observation that deoxygenated hemoglobin is considerably paramagnetic. Decreases in deoxyhemoglobin generate contrast in MRI by effectively resulting in a small (on the order of ~1%) increase signal strength and this increase is the BOLD signal measured in fMRI. Unfortunately, a critical limitation of the BOLD signal is that it is inherently a composite signal comprising the effects of multiple hemodynamic parameters. The exact magnitude of the signal change is dependent not only on changes in CBF, but also changes in cerebral blood volume (CBV) and oxygen tension (i.e., PaO_2). Thus, the BOLD signal does not represent an absolute quantification of CBF unlike nuclear imaging modalities (e.g., SPECT). Further complicating analysis of CBF by BOLD-fMRI is the "hemodynamic response" phenomenon in which there is a delay between an increase in neural activity and vasodilation to increase flow and a subsequent wash-out phase in which the proportion of deoxyhemoglobin slowly returns to baseline.[135] Quantification of the BOLD-signal usually entails accounting for this phenomenon through numerical techniques that use a "hemodynamic response function" (HRF) in tandem with general linear models (GLM).[136,137] The HRF represents the dynamics of the BOLD signal and the use of GLMs enables accounting of noisy/nuisance signals ultimately allowing for subsequent individual and group-level statistical analysis.[138]

Among the CVR literature, BOLD fMRI is the most extensively utilized CVR quantifying modality across a wide range of experimental paradigms and appears to be

the preferred modality for CVR research (**Table 1**). BOLD fMRI hosts numerous advantages compared to other neuroimaging modalities for microvascular perfusion monitoring including the ability to assess CVR in white matter and deep brain regions, capacity for whole brain as well as regional CVR assessments, and repeatability.[139,140] Unfortunately, with respect to CVR quantification as a clinical need in intensive care or outpatient clinic environments, BOLD fMRI exhibits significant barriers for translating this clinical research-focused neuroimaging modality to routine clinical care. The principal technical limitation is the BOLD signal itself, which is inherently an indirect and confounded measure of CBF. From a human factors engineering perspective, BOLD-fMRI is increasingly challenging to enact in younger pediatric populations (e.g., <6 years old) requiring sedation and in critically ill individuals where any transportation outside of the intensive care environment is not without risk. MRI-based techniques can induce anxiety and adverse claustrophobic reactions, especially in young children.[90,91] Furthermore, MRI is expensive given its high initial capital investment costs and ongoing maintenance costs which largely limit its availability to patients and clinical providers at large academic medical centers.

Table 1. High-level CVR literature review by modality
PubMed literature search highlighting the various CVR-quantifying modalities mentioned in the existing literature. Retrieved 3/22/23.

Search Query	Results (N references)
"cerebrovascular reactivity"	1,708
"cerebrovascular reactivity" AND ("BOLD" OR "BOLD MRI" OR "BOLD fMRI")	246
"cerebrovascular reactivity" AND ("TCD" OR "Transcranial Doppler ultrasound")	190
"cerebrovascular reactivity" AND ("PET" or "positron emission")	86
"cerebrovascular reactivity" AND ("SPECT")	78
"cerebrovascular reactivity" AND ("NIRS" or "near-infrared spectroscopy")	60

Given the importance of the microvasculature to regulate CBF through the CVR response and the limitations of existing neuromonitoring modalities for CVR assessments, there is a fundamental need for tools that allow feasible quantification of microvascular cerebral perfusion status at the bedside. Optical neuromonitoring modalities, otherwise known as diffuse optical spectroscopies, may be more realistic medical technologies to address this unmet need. The following sections will first provide a summary of the existing state of the art regarding commercially available NIRS regional oximeters (i.e., continuous wave near infrared spectroscopy) and their potential for facilitating CVR assessment (**Section 1.4.1**). Then, the promise of diffuse correlation spectroscopy (DCS) for routine microvascular CVR assessments is presented (**Section 1.4.2**).

1.5 Diffuse Optical Spectroscopies are potential CVR-quantifying modalities

1.5.1 Near Infrared Spectroscopy (NIRS)

1.5.1.1 Principles of Operation

Continuous wave near infrared spectroscopy (cwNIRS) is a real-time noninvasive optical monitoring method that uses NIR spectrum photons (700-1300nm) to calculate regional cerebral tissue oxygenation (rSO2) in the microvasculature which participates in oxygen exchange with the local tissue microenvironment. cwNIRS is often referred to as "commercial NIRS" as the underlying scientific principles of operation in cwNIRS comprise the majority of commercial NIRS devices for clinical use.[141] cwNIRS utilizes the modified Beer-Lambert Law (MBLL), which states that the concentration of a substance can be measured based on the degree of wavelength-dependent light absorption in tissue.[142] A full mathematical treatment of cwNIRS is discussed extensively elsewhere in the literature.[143,144] cwNIRS sensors are placed on the forehead and emit near-infrared light into the which penetrates into the scalp, skull, dura, and brain tissue (**Figure 4**). Photons are optically absorbed at multiple wavelengths by tissue chromophores (primarily oxy- and deoxy-hemoglobin; hereafter, HbO and HbR) whereas the remaining light is collected by detectors spaced a specific distance away from the light source (i.e., a source-detector separation; ρ), counted, and applied to algorithms to calculate the change in ratio of HbO/HbR, thus providing a value for the relative change of oxygen saturation in tissues.

The measured rSO2 represents a venous-weighted measurement of blood oxygen saturation under the assumption that 70-80% of cerebral blood volume exists in the

venous compartment of cerebral tissue.[145] rSO2 describes the cerebral venous oxygen reserve capacity following tissue oxygen extraction.[146,147] In other words, rSO2 represents the oxygen not used by oxidative metabolism in the brain tissue, hence why it is considered a regional measure of the tissue oxygen saturation available to the brain for additional metabolic activity. Various assumptions are made in the calculation algorithm of cerebral oxygen saturation with NIRS, which may not always be valid.[148,149] For example, the MBLL assumes that the absorption of tissue changes homogeneously with a change in brain state.[143] However, it is well understood that absorption changes are inhomogeneous across the tissue volume interrogated by a NIRS sensor. This can result in the MBLL underestimating changes in concentrations of HbO and HbR. While cwNIRS is advantageous for its noninvasive assessment of the microvasculature and ability to enable long-term (~hours) observations of local cerebral hemodynamics, it is limited by signal contamination inherent to extracerebral tissues and the ambient environment, and enables only monitoring relative trends in rSO2 against a given baseline which is demonstrated to be prone to misinterpretation[150] instead of measuring absolute hemoglobin concentrations. Perhaps the greatest technical limitation of cwNIRS is the nature of the measured signal: just as the BOLD fMRI signal is not a direct measure of cerebral perfusion status, rSO2 is similarly limited given it measures oxygenation as a proxy to CBF.

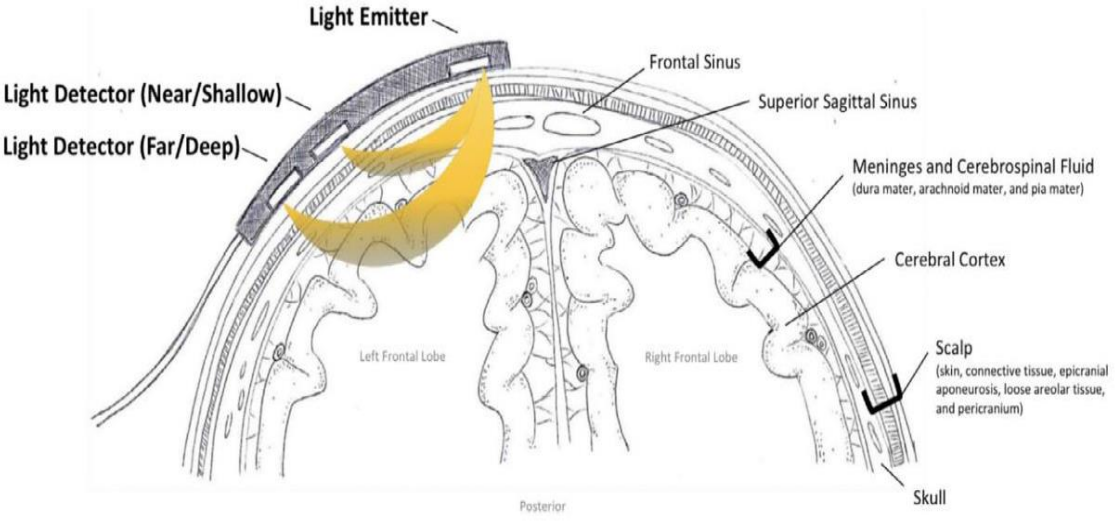

Figure 4. Neuromonitoring with Diffuse Optical Spectroscopies.
Schematic demonstrating mode of operation for cwNIRS with respect to optical light paths traversing through differencing volumes of cerebral anatomy for each source-detector separation. Figure adapted from Finucane et al 2020.[147]

1.5.1.2 Clinical adoption of cwNIRS validates market need for optical neuromonitoring systems.

Both progress in instrumentation and quick adoption of diffuse optics by researchers in several fields have accelerated the translation of diffuse optical spectroscopy techniques to commercially available systems.[141] Numerous commercial NIRS products are available for clinical use and are rigorously compared in the literature.[151–155] Broadly summarizing, commercially available NIRS systems are categorized as either bedside-portable or wearable/wireless systems. Bedside-portable devices represent the earliest entrants to commercial translation, with widespread market adoption demonstrated as early as 1991 (*e.g.*, INVOS 3100c, Covidien (Now Medtronic), USA). Wearable/wireless systems reflect the recent paradigm shift in the commercial market responding to consumer preferences for digital health technologies that are ergonomic, highly portable, and lend data-driven insights into consumer lifestyle (*e.g.*, Apple Watch, various Masimo product lines). Leading clinical, bedside-portable cwNIRS devices include

Medtronic's INVOS 5100c/7100c product line[156], Masimo's Root with O3 Regional Oximetry device[157], Edwards Life Sciences' ForeSight device[158], and Nonin Medical Corporation's SenSmart X-100[159]. Clinically approved cwNIRS oximeters primarily operate in intensive care unit (ICU) environments and surgical environments where neuroprotection through preventing ischemic events is highly valued from both a clinical and economic perspective. This is due to the reality that there is no consistent reimbursement[160] from public or private insurance providers for the use of cwNIRS for cerebral oximetry monitoring. As a result, to justify the cost of capital investment for hospitals to utilize cwNIRS, these modalities are primarily used in clinical settings with high rates of reimbursement that result in a single lump sum payment to hospitals for a primary diagnostic ICD-10 and DRG reimbursement code. This payment structure incentivizes hospitals and providers to manage a patient's care economically as possible. Any additional *preventable* neurologic injury that may result from a specific diagnosis that admits a patient to the ICU or a specific surgical procedure must be managed at cost to the healthcare provider. Therefore, the value in cerebral oximetry to hospitals is primarily to manage and reduce patient risk of preventable ischemic events. Outside of these clinical environments, cwNIRS is not well adopted for routine clinical care because sufficient clinical value to enhancing patient outcomes has not been sufficiently demonstrated to warrant the investment by providers necessary to operate commercial NIRS devices.

1.5.1.3 Ongoing debate on the clinical utility of cwNIRS

Notably, despite its commercial adoption since the 1991 launch of Covidien's INVOS product platform, the inherent analytical assumptions and technical limitations of cwNIRS systems have incited strong debate[146,148–150,161–164] regarding the ability of these devices to provide targeted therapy to reduce incidence of adverse neurologic outcomes.

For example, some monitors susceptible to ambient light interference display normal rSO2 values when sensors are unattached and completely exposed to ambient light.[150] Other studies have demonstrated quantification of rSO2 typically characteristic of healthy adult subjects in dead subjects pre/post autopsy[161] (>60% rSO2), during intraoperative cardiac arrest[150] (rSO2 initially at 60% increasing to 75% by time of death), and in an assortment of common vegetables[149] when compared to a control group of cardiothoracic surgeons (rSO2 71% in controls, ~75% in yellow squashes, 63% in butternut squash). These cases when taken together strongly support the argument that rSO2 measured by commercial cwNIRS systems cannot be used as an accurate measure for absolute rSO2 but rather is most useful as a relative trends monitor for assessing cerebral oximetry status changes with respect to a baseline which necessarily changes with each new application of a sensor to the patient's forehead.[165] rSO2 monitoring is an imperfect substitute[162] for quantifying CBF and neural metabolism despite its commercialization and modest clinical adoption.[166–168]

Clinical validation of cwNIRS systems lacks robust outcomes-based research and there remains ongoing debate whether a cerebral perfusion monitor that only measures one hemodynamic biomarker is sufficient to improve clinical outcome. The utility of NIRS-based neuromonitoring in pediatrics are broadly explored in anesthesia[147,169], cardiac surgery[170], and neurocritical care[171–174]. Consensus among these specialties suggests that these modalities are improving our understanding of cerebral perfusion in disease states yet it generally remains to be shown these cwNIRS modalities substantially improve short-term morbidity and mortality.[169] There is a dearth of validation studies correlating measured hemodynamic vital signs such as rSO2 with onset or ongoing neurologic outcome.[173] There are many clinical researchers who have evaluated cwNIRS and do not recommend it for routine clinical use in part due to a scarcity of well-validated definitions for ischemic thresholds in adults and children.[162,163,175,176] As one author suggests, despite

significant investigation regarding the usefulness of cwNIRS, “these modalities remain an unfulfilled promise of a reliable and clinically useful [cerebral perfusion] monitor”.[162] In summary, there is a clinical need for developing affordable hemodynamic neuromonitoring solutions that enable high-fidelity, direct quantification of cerebral perfusion – and by extension CVR – and are readily integrated in clinical workflow at the point-of-care clinical care. Most importantly, there is a need for developing robust studies that show measured hemodynamic vital signs are correlative—and hopefully predictive—of an adverse neurologic outcome.

1.5.2 Diffuse Correlation Spectroscopy (DCS)

1.5.2.1 Principles of operation

Compared to cwNIRS, DCS is a relatively new optical neuromonitoring technology that when applied to the cerebral neuromonitoring, measures an index of cerebral blood flow (CBF_i) which reflects the average flow of red blood cells within the interrogated tissue volume[144,177–179]. Although the units of CBF_i (cm^2/s) do not match the volumetric units of blood flow measured from traditional neuroimaging techniques (X mL/min/100g tissue), numerous validations studies against these “gold-standard” perfusion modalities (i.e. ASL-MRI, SPECT/CT) in adults, children, and animals demonstrate that CBF_i correlates with cerebral blood flow in young children, and relative changes in this CBF_i agree well with relative changes in CBF (summarized in detail by Durduran *et al.*[180]) measured in adults and children. Fundamentally, DCS quantifies the temporal fluctuation of light intensity generated from the propagation of coherent NIR light multiply scattered through tissue. This detected intensity fluctuation indirectly represents the fluctuation of electric fields at a single point (i.e., a detector) on a tissue surface. Mathematical theory ultimately relates temporal fluctuations in electric fields to light scattered from moving particles (i.e., red

blood cells, RBCs, as the dominant source of moving particles in tissue) in a highly scattering medium.[144,181,182] (**Figure 5**)

Mathematically, the unnormalized temporal electric field autocorrelation function $G_1(\rho, \tau)$ (Eq. 1) should obey a correlation transfer equation based on modifications to the governing radiation transport equation described extensively elsewhere[182,183], and after various assumptions[144,177,178] can be presented as a steady-state mathematical equation describing the transport of electric field temporal autocorrelation through tissue termed the correlation diffusion equation (CDE) (Eq. 2):

$$G_1(\rho, \tau) = \langle E(\rho, \tau)\, E^*(\rho, t + \tau) \rangle \qquad \text{(Eq. 1)}$$

$$\nabla \cdot \left(D(\rho)\nabla G_1(\rho,\tau)\right) - v\left(\mu_a(\rho) + \frac{\alpha}{3}\mu'_s\, k_0^2\, \langle \Delta r^2(\tau) \rangle\right) G_1(\rho,\tau) = vS(\rho,\tau) \quad \text{(Eq. 2)}$$

***E*(ρ , *t*)** refers to the electric field at any given at position **r** (i.e., SDS) and time **t**

$\boldsymbol{\tau}$ is the autocorrelation function time delay.

<> brackets denote the ensemble average (approximated by a time average)

D ≅ 1/(3μ'$_s$(λ, ρ)) is the light diffusion coefficient in tissue

$\boldsymbol{v}$ is the speed of light in tissue.

S(ρ , t) represents the isotropic light source.

$\boldsymbol{k_0 = 2\pi n/\lambda}$ is the wavenumber of light diffusing through tissue where *n* is the index of refraction of tissue

⟨Δr^2(τ)⟩ is the mean-square particle displacement in time τ

(i.e., in tissue, characterizing the motion of RBCs in the microvasculature)

α is the fraction of light-scattering events (i.e., from moving RBCs)

μ_s' is the wavelength-dependent reduced scatting coefficient assessed by fdNIRS or trNIRS

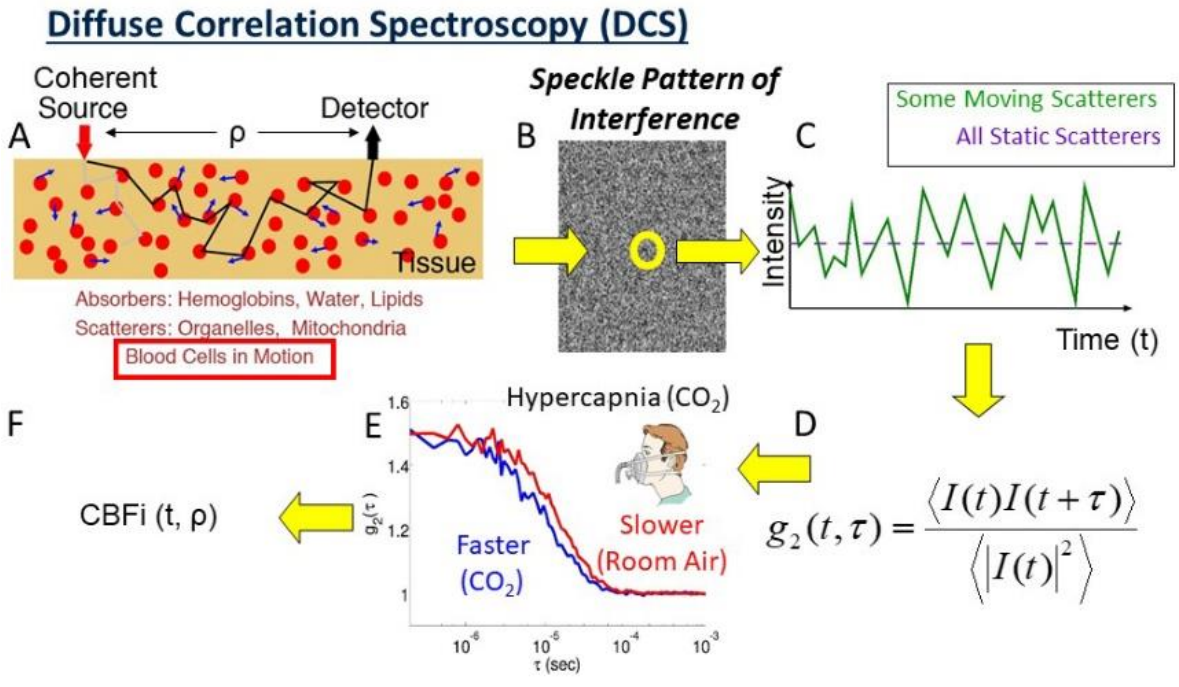

Figure 5. DCS principle of operation
(A) Coherent light is scattered through tissue and is detected at distance ρ **(B)** Speckle pattern generated from the constructive and destructive interference due to moving scatters (i.e., RBCs) results in **(C)** a measured temporal intensity fluctuation. **(D)** I(t) is transformed into the normalized temporal intensity autocorrelation function $g_2(\rho, \tau)$ **(E)** $g_2(\rho, \tau)$ reflects the diffusive-like motion of RBCs in the tissue; the speed of $g_2(\rho, \tau)$ decay represents the change in motion due to a perturbation **(F)** Using Eq. 1-10, an index of cerebral blood flow (CBFi) is determined for each source-detector separation ρ.

While it may be initially intuitive to assume the motion of RBCs moving through arterioles and capillaries to be a convective nature similar to the way that fluid moves through a pipe, prior studies[181] have confirmed that motion of RBCs can be best modeled using a Brownian or diffusive-like motion when measured by DCS (Eq. 3):

$$\alpha \langle \Delta r^2(\tau) \rangle = \alpha D_b = CBF_i \qquad \text{(Eq. 3)}$$

D_b is an "*effective* Brownian diffusion coefficient" of cells in blood within the studied tissue and represents an index of blood flow that describes the shear-induced diffusion of

RBCs at the microvascular/tissue microenvironment length scale.[184] This coefficient is orders of magnitude higher than the Brownian diffusion coefficient for an RBC. Numerically solving the CDE for this mean-square particle displacement $\langle \Delta r^2(\tau) \rangle$ displacement enables the calculation of CBF_i.

To solve for CBF_i in practice, one must relate the measured intensity to the electric field and solve the CDE for a given geometry. While the detail surrounding this derivation is explained extensively elsewhere[181,182], the Siegert relation (Eq. 4) bridges the normalized intensity g_2 and electric field g_1 autocorrelation functions and the CDE can be solved for a tissue modeled as a semi-infinite homogenous medium (Eq. 5) where various constituent variables are related to the geometry of the medium (Eq. 6-10):

$$g_2 = 1 + \beta |g_1(\tau)|^2 \qquad \text{(Eq. 4)}$$

$$g_1(\rho, \tau) = \frac{\left[\frac{e^{K(\tau)\rho_1}}{\rho_1} - \frac{e^{K(\tau)\rho_2}}{\rho_2}\right]}{\left[\frac{e^{K(0)\rho_1}}{\rho_1} - \frac{e^{K(0)\rho_2}}{\rho_2}\right]} \qquad \text{(Eq. 5)}$$

$$K(\tau)^2 = 3\mu_a(\lambda)\mu'_s(\lambda) + (\mu'_s(\lambda)^2 k_0^2 \alpha \langle \Delta r^2(\tau) \rangle) \qquad \text{(Eq. 6)}$$

$$\rho_1 = \sqrt{\rho_2 + z_0^2} \qquad \text{(Eq. 7)}$$

$$\rho_2 = \sqrt{\rho_2 + (z_0 + 2z_b)^2} \qquad \text{(Eq. 8)}$$

$$z_0 = 1/(\mu'_s) \qquad \text{(Eq. 9)}$$

$$z_b = \left(\frac{2}{3\,\mu'_s}\right)\left(\frac{1+R_{eff}}{1-R_{eff}}\right) \qquad \text{(Eq. 10)}$$

$\mathbf{z_o}$ and $\mathbf{z_b}$ are geometric constants described by the method of images[182]

$\boldsymbol{R_{eff}}$ = 0.493 is the effective reflection coefficient.[185]

Using the expressions in Equations 1-10, we have the ability able to solve for Eq. 3 by fitting the measured normalized intensity autocorrelation function $g_2(\rho, \tau)$ with Eq. 4-5 and determine CBF_i.

The accuracy of continuous CBF_i changes can be enhanced by incorporating both baseline optical properties and the continuous change in μ_a throughout each exam using the MBLL. These optical properties are quantified not by a cwNIRS platform by more modern frequency-domain NIRS (fdNIRS) or time-resolved NIRS (trNIRS) platforms reviewed elsewhere.[141] The MBLL (Eq. 11)[182,186] accounts for changes in the concentration of chromophores within a highly scattering medium by measuring the change wavelength-dependent signal intensity relative to baseline while also accounting for the distribution of light path lengths for a given SDS (e.g. differential path length factor, DPF, Eq. 12)[186]:

$$ln\left(\frac{I_{DC}(\rho,\lambda,t)}{I_{DC}(\rho,\lambda,0)}\right) \equiv \Delta OD(\rho,\lambda,t) \cong -\Delta\mu_a(\lambda,t)L_{eff}(\lambda) = -\Delta\mu_a(\lambda,t)\, DPF(\lambda)\, \rho \quad (\text{Eq. } 11)$$

$$DPF(\lambda) = \frac{1}{2}\left(\frac{\mu'_s(\lambda)}{\mu_a(\lambda)}\right)^{\frac{1}{2}}\left[1 - \frac{1}{1+\rho(3\mu_a(\lambda)\mu'_s(\lambda))^{1/2}}\right] \approx \frac{1}{2}\left(\frac{\mu'_s(\lambda)}{\mu_a(\lambda)}\right)^{\frac{1}{2}} \quad (Eq. 12)$$

$L_{eff}(\lambda)$ is the mean optical path length a photon travels from the source to detector and is affected by the SDS, medium geometry, and wavelength.

$L_{eff}(\lambda)$ can be approximated by calculating the DPF for each wavelength and SDS used in continuous NIRS monitoring.[182] The MBLL can be used to determine $\Delta\mu_a$ when specific assumptions are met: changes in scattering are negligible, absorption changes are global, the tissue examined is homogeneous, and the absorption changes are small relatively to their baseline values (<100%).

A typical setup comprises a multi-modal instrumentation with a means of measuring optical properties (e.g. fdNIRS) and a DCS system.[187] The DCS component consists of a 852nm long-coherence laser, two four-channel single photon counting modules, and a software correlator[188] using a dedicated 8 channel PCIe/PXIe6612 counter/timer data acquisition board allowing fast data acquisition at ~20-50Hz. (**Figure 6**). Auxiliary recordings of arterial blood pressure allow users to also calculate MAP using the raw arterial blood pressure (ABP) captured by a data acquisition board (National Instruments). All acquisition hardware is controlled by a custom software program (LabVIEW) running on a dedicated desktop computer.

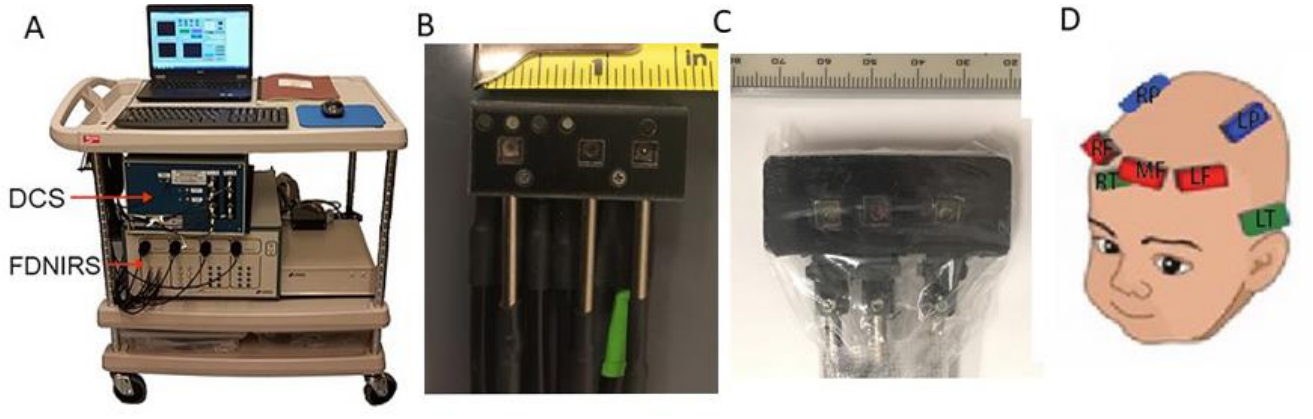

Figure 6. Optical instrumentation and measurement approach.
(A) DOS mobile instrumentation (B) Handheld rigid "absolute sensor" for baseline measurements (C) Flexible "continuous sensor" for continuous observations as required for CVR assessments in Aim 2. (D) Example measurement locations on patient's head. Red = frontal, blue = parietal, green = temporal

A typical patient interface consists of a rigid fdNIRS/DCS sensor constructed for baseline quantification of optical properties, hemoglobin concentration, and CBF_i (i.e., "absolute sensor", **Figure 6B**) and a flexible sensor (**Figure 6C**) for continuous

assessment of CBF_i and changes in μ_a. Two DCS detectors comprised of single-mode fibers are positioned at two SDS (ρ_{short} = 1cm, ρ_{long} = 2.5cm), respectively chosen to measure superficial scalp blood flow and to balance signal-to-noise with depth penetration. Collectively, the specifications of this and subsequent sensors are designed to meet the relevant ANSI standards for maximum permissible exposure according to FDA guidance.[189–191]

1.5.2.2 Strategic advantages of DCS for clinical neuromonitoring

DCS offers several advantages over other neuromonitoring modalities. DCS measures of CBF have demonstrated strong agreement with cwNIRS[176,192] rSO2 and MRI-measured[193,194] CBF respectively in prior clinical validation studies. Unlike MRI or CT, DCS systems are relatively low-cost (~$50K USD), involve no ionizing radiation exposure, are portable, enable long-term (>1hr) continuous and high temporal (>20Hz) monitoring at the bedside, and are easily integrated in a provider's clinical workflow. Although DCS is limited by spatial resolution and extracerebral signal contamination similarly to cwNIRS, this is less of a concern in younger pediatric populations. In summary, the strategic advantages of DCS provide a unique opportunity to enable longitudinal evaluation of cerebral perfusion and related biomarkers and has potential to alter clinical management of patients at risk of experiencing cerebrovascular dysfunction.

1.5.2.3 CVR quantification opportunity for DCS

CVR assessments necessitate accurate, moderately high (~1Hz) temporal quantification of CBF and the strategic advantages of DCS compared to existing modalities make it a potentially valuable CVR quantifying platform. As discussed

extensively in **Section 1.4**, traditional methods for quantifying CBF in the human brain (SPECT[13] and Xenon-CT inhalation[19]) require expensive instrumentation, injectable contrast agents, and/or ionizing radiation. Today, CVR is most commonly quantified by functional (fMRI) and perfusion MRI (i.e. ASL-MRI).[6,25,195–197] MRI techniques have shown promise as a safe, non-invasive method for global and local measures of CVR. However, there are prohibitive limitations for routine practice beyond clinical research studies. MRI techniques are prohibitively expensive for serial measurements and routine monitoring, it requires patient transport to the scanner, which is challenging in critically ill patients, and it requires sedation in children under 6, thereby especially limiting its applicability in pediatrics. Alternatively, TCD is also commonly used to assess CVR as it avoids the limitations of MRI and allows for bedside assessment of CVR in the macrovasculature. While useful, TCD assessments of CVR are typically limited to a single vessel and should be interpreted with caution in brain injured cohorts wherein mismatch between macrovascular and microvascular perfusion is commonly observed (i.e., macrovascular reactivity may be intact while microvascular reactivity is significantly impaired.[187,198] Finally, cwNIRS is also often employed to assess CVR; however, given the poor association between NIRS-measured oxygenation and cerebral blood flow, the utility of these assessments is highly suspect.[198]

Compared to these existing modalities, the innovative use of DCS to quantify CVR directly is relatively new and consequently, remains unproven and unexplored. To date, only a handful (N=9)*[1] small cohort pilot studies[144,193,199–205] have utilized DCS to quantify the CBF response with respect to a vasoactive stimulus in comparison to the extensive

*[1] PUBMED search performed on 2/25/21 using the following search criteria: "Cerebrovascular reactivity" AND ("Diffuse Correlation Spectroscopy"). Some studies included in this basic search may inadvertently include reviews vs. exclusively observational/prospective human subject studies.

studies performed to assess CVR by TCD (N=455)*[2] or MRI (N=451)*[3]. Two of these DCS studies utilize intravenous infusion of ACZ[204,205] to induce vasodilation and the remaining seven utilize an HC challenge in healthy adults[144,202], in children with congenital heart disease[193,199–201,203,206] , and in children with sleep apnea[200]. Notably, most of these studies were designed to validate DCS measures of blood flow against other gold standard perfusion modalities and not to explicitly quantify CVR in absolute terms (%/mmHg).

Using DCS to monitor changes in CBF and consequently, quantify CVR has many advantages. First, DCS has the advantage of being exquisitely sensitive to microvascular CBF changes thereby being the first available neuromonitoring modality to feasibly enable bedside microvascular assessments of CVR. Second, like cwNIRS, DCS is well tolerated in all patient cohorts as it only requires a minimally obtrusive sensor attached to a patient's scalp. DCS is certainly not without limitations including sensitivity to superficial cortical perfusion[203] (~1-2cm average optical depth penetration) and the signal contamination[203,207–209] owing to extracerebral perfusion which confounds the cortical CBF assessments. However, these limitations can be acceptable in certain clinical scenarios. For example, these technical concerns while currenting being addressed with novel technology development[141] are largely reduced in pediatric subjects. Additionally, CVR impairment is a global phenomenon in patients with sickle cell disease[210], suggesting this neuromonitoring technique should be capable of assessing microvascular optical CVR occurring anywhere in the superficial cortex.

1.5.2.4 Need for research targeted toward enhancing the clinical value proposition of DCS

*[2] PUBMED search performed on 2/25/21 using the following search criteria: "Cerebrovascular reactivity" AND ("TCD" OR "Ultrasound" OR "Doppler"). Some studies included in this basic search may inadvertently include reviews vs. exclusively observational/prospective human subject studies.
*[3] PUBMED search performed on 2/25/21 using the following search criteria: "Cerebrovascular reactivity" AND ("MRI" OR "Magnetic" OR "BOLD"). Some studies included in this basic search may inadvertently include reviews vs. exclusively observational/prospective human subject studies.

For successful translation of next generation optical neuromonitoring tools to facilitate the routine adoption of CVR assessments in clinical practice, a number of broad criteria must be met in which the clinical/scientific, commercial, technical, and strategic value propositions align to produce a compelling data-backed argument which would confidently support commercialization efforts (recall **Figure 2**).[44] Given the technical development of DCS is well established and the existence of predicate optical neuromonitoring devices such as cwNIRS validate the market need for cerebral hemodynamic monitoring, the utmost area of need for further CVR research with DCS relates to enhancing the clinical/scientific value proposition. Further work is needed to 1) identify a promising clinical indication, ideally one previously unexplored in the DCS literature, 2) demonstrate the ability of DCS neuromonitoring to detect signs of cerebral hemodynamic dysfunction and 3) provide compelling data showing if measured hemodynamic vital signs were available in real time, actionable, timely, and appropriate therapeutic interventions could occur to reverse a CVR abnormality that is itself a determinant of outcome.[175] *If these criteria are not met, DCS will continue to encounter significant barriers to successful translation to the marketplace and ultimately, CVR assessments may never be adopted in routine clinical care.*

Chapter 2. Verification of CVR Assessments Using Diffuse Optical Spectroscopies in Healthy Adults

Results detailed in this chapter have been published in Neurophotonics[211]

Abstract

Significance: Cerebrovascular reactivity (CVR), i.e., the ability of cerebral vasculature to dilate or constrict in response to vasoactive stimuli, is a biomarker of vascular health. Exogenous administration of inhaled carbon dioxide, i.e., hypercapnia, remains the "gold-standard" intervention to assess CVR. More tolerable paradigms have been proposed that enable CVR quantification when hypercapnia is difficult/contraindicated. However, because these paradigms feature mechanistic differences in action, assessment of agreement of these more tolerable paradigms to hypercapnia is needed.

Aim: To determine the agreement of CVR assessed during hypercapnia, breath-hold, and resting state.

Approach: Healthy adults were subject to hypercapnia, breath-hold, and resting state paradigms. End tidal carbon dioxide (E_tCO_2) and cerebral blood flow (CBF, assessed with Diffuse Correlation Spectroscopy) were monitored continuously. CVR (%/mmHg) was quantified via linear regression of CBF vs E_tCO_2 or via a general linear model that was used to minimize the influence of systemic and extracerebral signal contributions.

Results: Strong agreement (CCC≥0.69; R≥0.76) among CVR paradigms was demonstrated when utilizing a general linear model to regress out systemic/extracerebral signal contributions. Linear regression alone showed poor agreement across paradigms (CCC≤0.35; R≤0.45).

Conclusions: More tolerable experimental paradigms coupled with regression of systemic/extracerebral signal contributions may offer a viable alternative to hypercapnia for assessing CVR.

2.1 Introduction

2.1.1 CVR Quantification Among Experimental Paradigms

Cerebrovascular reactivity (CVR), defined as the ability of cerebral vasculature to dilate or constrict in response to a vasoactive stimulus, is an integral mechanism in brain homeostasis. Interest in CVR as a diagnostic and prognostic biomarker has accelerated in recent years because impaired CVR has been observed in numerous disease states, including cerebrovascular disease[7–13], stroke[14–19], cardiac arrest[20], and traumatic brain injury.[21–29] Quantification of CVR coupled with interventions aimed at restoring abnormal CVR has the potential to reduce morbidity and mortality.

Several well-established experimental paradigms exist to study CVR non-invasively in humans. These methods typically involve quantification of the cerebral blood flow (CBF) response to changes in arterial carbon dioxide content via acetazolamide infusion, inhalation of carbon dioxide (CO_2), or breath-holding. Intravenous acetazolamide administration has historically served as the preferred method to quantify CVR in clinical settings.[212] While the single dose injection is relatively simple, differences in pharmacokinetic/dynamic profiles among subjects lead to poor repeatability, and it is associated with a high incidence of side effects that preclude its modern use in many patient cohorts (e.g., children).[12,13,16,19,212,213] In research settings, the most common method to quantify CVR is inhalation of CO_2 to induce hypercapnia (HC), which is considered by many to be the “gold standard” experimental paradigm. A standard HC challenge involves a limited duration inhalation of medical-grade CO_2 (e.g., 5% CO_2, 21%

oxygen, balance nitrogen) coupled with monitoring of CBF and end tidal CO_2 (E_tCO_2). This approach is increasingly used due to the potency of CO_2 as a vasodilator, rapid onset and cessation of the CBF response, and repeatability.[6,212,214–222] However, hypercapnia requires complex gas delivery equipment, time and expertise to perform the procedure, and it can induce anxiety in some subjects. Moreover, hypercapnia may be clinically contraindicated in patients with acute illness and/or compromised hemodynamics for whom the benefits of CVR assessment do not outweigh the risks of rapid or prolonged hyperemia (e.g., sickle cell disease).[223] A breath-hold (BH) challenge, wherein a subject briefly holds their breath, offers a simpler alternative to manipulate arterial CO_2. This approach offers many advantages over CO_2 inhalation, including a lack of complex gas delivery equipment and improved patient tolerability given the self-directed nature of the breath-hold.[42,197,224,225] However, the BH approach requires an individual's cooperation, which limits applicability in children < ~6y and in patients with severe conditions, and entirely excludes its use in other cohorts (e.g., patients on a mechanical ventilator).

To bypass the limitations of existing experimental paradigms, recent investigations have explored the potential for measuring CVR using the intrinsic vasoactive stimulus of natural arterial CO_2 fluctuations that occur when a subject is freely breathing.[34,216,225–228] This resting state (RS) approach is attractive because it does not require patient compliance or intentional manipulation of arterial CO_2. Thus, it has potential in those who have lost consciousness or who are sedated. However, the approach is thought to be susceptible to poor signal-to-noise due to the relatively small fluctuations in E_tCO_2 that occur during spontaneous breathing. Thus CVR estimations at rest may be unreliable.[229]

2.1.2 Need for Validation Among Experimental Paradigms

While the use of more tolerable experimental paradigms to assess CVR is clinically appealing, there has been limited investigation into the agreement of CVR measured by these approaches. Liu *et al.* recently demonstrated poor agreement of hypercapnia vs breath-hold and of hypercapnia vs resting state.[229] The other handful of studies that have compared CVR across hypercapnia/breath-hold/resting state paradigms are limited in interpretation. These studies either compare relative changes in blood flow without accounting for differences in elicited E_tCO_2 response[222,229,230], which can vary appreciably across subjects and/or paradigms, or they focus on the spatial correlation of cohort-averaged, qualitative, regional CVR maps attained from two experimental paradigms.[36,225,231] Given that these paradigms act on the vasculature in different ways and that each has relative merit in terms of robustness of response and ease of implementation, a systematic and rigorous comparison of CVR across paradigms is warranted.

2.1.3 Objectives and Hypothesis

Herein we quantify agreement of CVR across hypercapnia, breath-hold, and resting state paradigms in healthy adults. To quantify cerebral blood flow, we employ a non-invasive optical technique known as diffuse correlation spectroscopy (DCS). Diffuse correlation spectroscopy (DCS) offers many strategic advantages over more traditional modalities used to assess CBF (e.g., computed tomography, perfusion magnetic resonance imaging, transcranial Doppler ultrasound) including portability, low cost, high temporal resolution, direct measure of microvascular blood flow, and ease of use in both adults and children in a wide array of clinical indications and environments. Indeed, several studies[144,193,199–205,232] have explored the use of DCS to quantify the CBF response to a vasoactive stimulus (ACZ, hypercapnia), although the majority of these investigations

were designed to demonstrate the sensitivity of DCS measured blood flow changes after proposing advances in the underlying platform technology (whether hardware, software, or numerical), not to explicitly quantify CVR. Thus, in this study, we use DCS to quantify CVR, and we hypothesize that CVR measured during hypercapnia will agree strongly with CVR assessed with more tolerable and more practical breath-hold and resting state paradigms.

2.2 Methods

Healthy adult subjects without prior history of cardiovascular, neurological, respiratory, or hematological disorders were recruited at Emory University. Exclusion criteria further included history of major head injury within the past 2 years or history of significant acute illness within one month of the study. Subjects were instructed to abstain from stimulants (e.g., caffeine) or depressants (e.g., alcohol) for at least 12h prior to the study. Written informed consent was obtained for all participants. All protocols were approved by the Emory University Institutional Review Board.

Twenty-seven healthy adults (13 male) ranging in age from 22-37 years were enrolled in this study. A subset of 4 subjects was measured on multiple occasions yielding thirty-four total measurement sessions. Of these sessions, one dataset was discarded due to substantial drift in optical signal attributed to poor sensor contact, and two datasets were discarded due to an improper execution of the hypercapnia exam, yielding a total of 31 available datasets.

2.2.1 Experimental Protocol

Cerebrovascular reactivity (CVR) was quantified via three consecutive experimental paradigms: resting state (RS), breath-hold (BH), and hypercapnia (HC) (**Figure 7**). First, for resting state, the subject was directed to breath naturally (i.e.,

unpaced) for 10 minutes while minimizing bodily movements. Next, for breath-hold, the subject was asked to complete 5 breath-hold challenges, each of which consisted of 40-60s paced breathing followed by a 20-30s end-inspiration breath-hold. Paced breathing at the subject's natural respiration rate (determined during resting state) was facilitated by a custom graphical user interface written in MATLAB (MathWorks Inc., Natick, MA). End-inspiration breath-holds, which have been demonstrated to yield similar CVR magnitudes when compared to end-expiration breath-holds[197], were selected to facilitate subject comfort during the exam. Subjects were instructed to breathe in approximately half capacity before initiation of the breath-hold and to exhale entirely at the conclusion of the breath-hold. Finally, for hypercapnia, the subject was instructed to breathe naturally for 3 minutes, followed by 6 minutes of 5% CO_2/balance room air inhalation (Nexair, Memphis, TN), and 6 minutes of room air inhalation recovery. Unpaced breathing was used throughout the HC challenge.

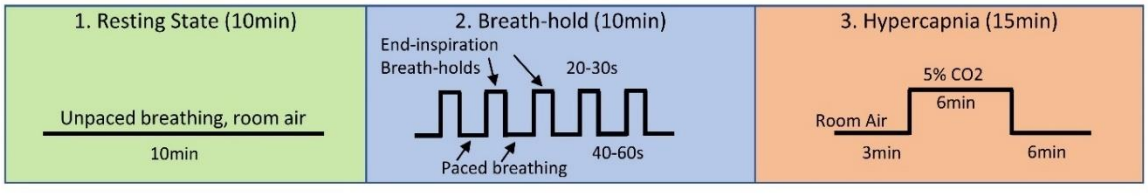

Figure 7 Experimental protocol.
CVR was quantified using 3 consecutive experimental paradigms: (1) Resting state wherein the subject breathed naturally for 10 minutes, (2) Breath-hold, wherein the subject completed 5 end-inspiration breath-holds, and (3) Hypercapnia, wherein the subject inhaled 5% CO_2 for 6 minutes. Cerebral blood flow, end tidal carbon dioxide, peripheral oxygen saturation, and arterial blood pressure were continuously monitored throughout the duration of the protocol.

Subjects sat upright for the duration of the study protocol. Continuous (20Hz) DCS measurements of cerebral blood flow were made by securing an optical sensor over the

right or left forehead. Given that CVR is a global phenomenon[233] , laterality of the sensor placement was determined based on the hemisphere that yielded the highest detected light intensities to maximize DCS signal-to-noise ratio. Trends in peripheral oxygen saturation (SpO2, LifeSense II, Nonin Medical, Inc.) and arterial blood pressure (CNAP Monitor 500, NIPD1000D-1, Biopac Systems) were also continuously monitored (1Hz for SpO2 and 125 Hz for ABP, **Figure 8A**). In post-processing, beat-to-beat mean arterial blood pressure (MAP) was determined from the ABP waveform using *BP_annotate*[234] in MATLAB. Further, a gas mask was placed over the mouth and nose to facilitate continuous monitoring of expelled CO_2 (4Hz, LifeSense II, Nonin Medical Inc., Plymouth, MN) as well as to enable delivery of carbon dioxide during hypercapnia. For resting state and breath-hold paradigms, the mask was configured such that the subject breathed room air. For the hypercapnia challenge, the mask was attached to a reservoir of 5% CO_2. One-way, non-rebreathing valves were used to maintain a constant inhaled CO_2 concentration (**Figure 8B, Table 2**). In post-processing, a peak detection algorithm in MATLAB (*findpeaks*) was used to estimate end tidal CO_2 (E_tCO_2) from the expelled CO_2 waveform. The E_tCO_2 time series was then visually inspected to remove obvious outliers attributed to irregular breathing or incomplete exhalation.

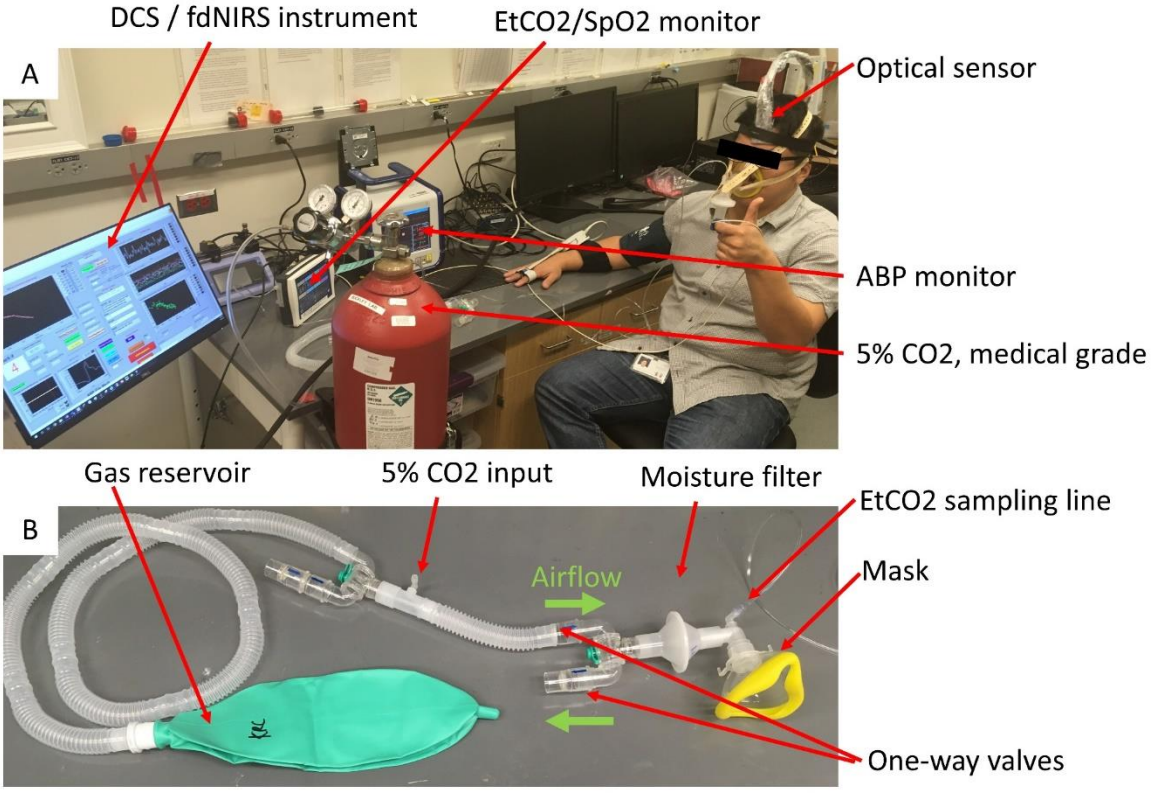

Figure 8. Experimental setup and respiratory equipment.
(A) Depiction of experimental setup with all monitoring instrumentation displayed. The respiratory mask is configured for the resting state and breath-hold paradigms. (B) Respiratory circuit configuration with relevant components annotated configured for hypercapnic gas inhalation.

Table 2. Respiratory circuit components.
Component, manufacturer, and part numbers are displayed for all pieces of the respiratory circuit.

Component	Manufacturer (Distributor)	Distributor Part Number
5% medical grade CO_2 (Balance N_2/O_2)	NexAir	SGV BG NICDOXC9-K
Standard anesthesia circuit tubing including: Moisture Filter E_tCO_2 sampling line Gas reservoir T-Splitter	McKesson Medical Surgical	1016896
5% CO_2 input Pressure Line Adaptor	Teleflex Medical (Medline)	HUD1642
One-way valves		HUD1665 HUD1664
Elbow adaptor with CO_2 sampling line		HUD1624
Standard Tubing Adaptors		HUD 1640
Masks	McKesson Medical Surgical	854706 854707 854708
Mask harnesses	Teleflex Medical (McKesson Medical Surgical)	336156 248120

2.2.2 Diffuse Optical Instrumentation

DCS measures of blood flow were acquired using a custom-built device consisting of a 852 nm long-coherence near-infrared laser (iBeam Smart, TOPTICA Photonics, Farmington, New York), two four-channel single photon counting modules (SPCM AQ4C-IO, Perkin-Elmer, Quebec, Canada), and an 8 channel counter/timer data acquisition board (PCIe6612, National Instruments, Austin, TX) that allowed for fast (20Hz) quantification of the intensity autocorrection function, $g_2(t,\tau)$, at time, t, and delay time, τ.[188]

Frequency-domain near-infrared spectroscopy (fdNIRS) was also employed to assess baseline tissue optical properties (namely, the wavelength-dependent absorption and scattering coefficients, $\mu_a(\lambda)$ and $\mu_s'(\lambda)$) as well as changes in $\mu_a(\lambda)$ over time.[235] The fdNIRS system is a customized, commercially-available device with 8 rapidly (20Hz) multiplexed sources (690, 730, 750, 775, 785, 800, 825, 830nm) that are modulated at 110 MHz and four photomultiplier tube (PMT) detectors with gain modulation of 110 MHz + 5 kHz for heterodyne detection at 5 kHz (Imagent, ISS, Urbana Champaign, IL). To assess baseline optical properties, measurements were made over the right and left frontal hemispheres with a rigid fdNIRS sensor containing one source and 4 detectors spaced 2.0, 2.5, 3.0, and 3.5 cm[235]. Resulting values were averaged to yield a global estimate of $\mu_a(\lambda)$ and $\mu_s'(\lambda)$.

Continuous DCS + fdNIRS data were acquired with a flexible sensor containing one source fiber bundle and two detector bundles spaced 1.0 and 2.5 cm from the source (ρ_{short} and ρ_{long}, respectively). The source bundle contained a 1000 μm multimode fiber for DCS (FT1000EMT, Thorlabs, Newton, NJ) and three 400 μm multimode fibers for fdNIRS acquisition at 690, 800, and 830 nm (FT400EMT, Thorlabs). The ρ_{short} detector bundle contained one single mode fiber for DCS (780HP, Thorlabs) and one multimode fiber for fdNIRS (FT600EMT, Thorlabs). The ρ_{long} detector bundle contained seven single mode fibers for DCS (780HP, Thorlabs) and three multimode fibers for fdNIRS (FT600EMT, Thorlabs). Each source and detection fiber bundle was mechanically coupled to a 5 mm right-angle prism mirror (MRA05-E03, Thorlabs) using a custom 3D printed prism/fiber holder. Prism/fiber holders were cast within a polyurethane mold (Vytaflex30, Smooth-On Inc., Macungie, PA colored black with PearlEx Carbon Black #640, Jacquard, Healdsburg, CA). The sensor was designed to be compliant with ANSI maximum permissible exposure standards of skin to laser radiation of < 4 mW/mm^2 at 852 nm.

2.2.3 DCS Data Analysis

Measured $g_2(\rho_{long},t,\tau)$ were first averaged across all 7 detectors. Next, $g_2(t,\tau)$ at ρ_{short} and the averaged $g_2(t,\tau)$ at ρ_{long} were down sampled from 20Hz to 1Hz to enhance the signal-to-noise ratio. These averaged and down sampled $g_2(t,\tau)$ curves were then fit for an index of blood flow using two separate models. First, $g_2(t,\tau)$ curves were fit to the semi-infinite homogenous solution to the correlation diffusion equation to extract an index of blood flow ($BF_i(t)$, cm^2/s) at each source detector separation. For ρ_{long}, fits were restricted to g_2 >1.2 to enhance sensitivity to cortical blood flow.[203] For all g_2 fits, we assumed a fixed index of refraction of 1.4, and we incorporated fdNIRS-estimated, subject-specific $\mu_a(852nm)$, $\mu_s'(852nm)$, and $\Delta\mu_a(852nm,t)$, as described elsewhere[235], to avoid the confounding influence of optical properties on BF_i estimation[236]. When resting state fdNIRS measurements were not available (N=3), group averaged optical properties were used. For each source detector separation, data were fit simultaneously for the coherence factor (β) and BF_i. Next, to minimize extracerebral signal contributions, we also fit data from ρ_{long} and ρ_{short} simultaneously to a three-layer model[237] (assuming scalp, skull, brain) for scalp and brain blood flow (SBF_i and CBF_i, respectively) using a single cost function.[238]

$$\chi^2 = \sum_{j=1}^{N_r}\sum_{k=1}^{N_\tau}\left[g_2\left(r_f,\tau_k,CBFi_{true},SBFi_{true}\right) - g_2\left(r_f,\tau_k,CBFi_{estimated},SBFi_{estimated}\right)\right]^2 \quad \text{(Eq. 13)}$$

Here, N_r is the number of detectors, N_τ is the number of τ delay times. The cost function minimizes χ^2 using *fminsearchbnd* in MATLAB with bounds for both CBF_i and SBF_i defined as [$1x10^{-11}$, $1*10^{-6}$] cm^2/s. For these fits, we assumed negligible (0) flow in the skull and fixed values for layer optical properties and thicknesses according to literature (**Table**

3).[239] To improve the stability of fits, β for each separation were estimated by averaging the first five points of the autocorrelation curves.

Table 3. Assumed layer optical properties.
Assumed optical properties for absorption and scattering coefficients ($\boldsymbol{\mu_a}$ **and** $\boldsymbol{\mu_s'}$) at 852nm, as well as layer thicknesses (L) for scalp, skull and brain.

Layer	μ_a (cm^{-1})	μ_s' (cm^{-1})	L (cm)
Scalp	0.10	15	0.4
Skull	0.10	9	0.8
Brain	0.16	3.0	Inf

For each experimental paradigm, relative change in blood flow as a function of time ($rCBF(t)$) was calculated as $(BFi(\rho_{\mathrm{long}}, t) - BFi_0(\rho_{long}))/BFi_0(\rho_{long}) \times 100\%$ for the semi-infinite model and as $(CBFi_{3-layer}(t) - CBFi_{3-layer,0})/CBFi_{3-layer,0} \times 100\%$ for the 3-layer model. Here the subscript 0 denotes the mean flow index during the baseline of the given paradigm. For resting state, baseline was chosen as the 2 minutes at the start of the resting state period. For breath-hold, baseline was chosen as the 30 seconds prior to the first breath-hold epoch. For hypercapnia, baseline was chosen as the 3 minute period of room air inhalation immediately prior to CO_2 initiation. Change in E_tCO_2 as a function of time was estimated as $\Delta EtCO2(t) = EtCO2(t) - EtCO2_0$ using the same baseline periods as rCBF. To account for the gas transit time from the mask to the capnogram and the physiological delay between alveolar diffusion of CO_2 in the lungs and arterial CO_2 reaching the cerebrovasculature, we time-aligned $rCBF(t)$ and $\Delta EtCO2(t)$ via cross correlation. For this analysis, the E_tCO_2 timeseries was incrementally shifted at 0.01s intervals up to 10s. For each shift, $\Delta EtCO2(t)$ was interpolated to the $rCBF(t)$ time

axis, and Pearson's correlation coefficient between $rCBF(t)$ and $\Delta EtCO2(t)$ was estimated. Finally, $\Delta EtCO2(t)$ was shifted by the time lag that yielded the highest correlation coefficient between $rCBF(t)$ and $\Delta EtCO2(t)$.

2.2.4 Estimation of CVR

We employed 2 numerical methods to estimate CVR (%/mmHg) for each experimental paradigm: 1) linear regression, and 2) a general linear model that regresses out systemic contributions to the DCS measured blood flow. The latter approach was included to minimize the known confounding extracerebral contributions to the DCS signal[232,240] as well as the influence of heart rate and blood pressure variability.

2.2.4.1 Linear Regression

Linear regression is commonly used to assess CVR by modeling a simple linear relationship between $rCBF(t)$ and $\Delta EtCO2(t)$:

$$rCBF(t) = \beta_0 + \beta_1 * \Delta EtCO2\,(t) + \mathcal{E}\,(Eq.14)$$

Here β_1 reflects CVR (%/mmHg), β_0 is the intercept, and $\mathcal{E}$ is the fit residual. For each experimental paradigm, linear regression (*regress*, MATLAB) was applied between the cross-correlated, time-aligned $rCBF(t)$ and $\Delta EtCO2(t)$ signals to obtain an estimate of CVR. To ensure that the model explains a significant amount of variability in the data, we discarded CVR estimates for which the model p-value for β_1 was > 0.05. We further discarded any CVR value <0.1.

2.2.4.2 General Linear Model

By the nature of the DCS measurement, detected light carries information about both cerebral and extracerebral (i.e., scalp and skull) hemodynamics. To minimize extracerebral contributions, we took a cue from best practices in functional near-infrared spectroscopy.[241,242,243] We employed a general linear model (GLM) to regress out the relative changes in BF_i at ρ_{short} (assumed to reflect scalp hemodynamics) from the relative changes in BF_i at ρ_{long} (assumed to be sensitive to both superficial and brain layers):

$$rBFi(\rho_{long}, t) = \beta_0 + \beta_1 * \Delta EtCO2\,(t) + \beta_2 * rBFi(\rho_{short}, t) + \mathcal{E}\,(Eq.15)$$

Here β_1 reflects CVR (which we call $CVR_{GLM\text{-}SS}$, %/mmHg) and β_2 represents the relative influence that the rBF_i at ρ_{short} has on rBF_i measured at ρ_{long}.

We also explored the use of a GLM to regress out systemic contributions to the $CBF_{i,3\text{-}layer}$ signal that are reflected in $SBF_{i,3\text{-}layer}$. Here the GLM took the form of:

$$rCBFi\ \ (t) = \beta_0 + \beta_1 * \Delta EtCO2\,(t) + \beta_2 * rSBFi\ \ (t) + \mathcal{E}\,(Eq.16)$$

Here β_1 reflects CVR (which we call $CVR_{GLM,\ 3\text{-}layer}$), and β_2 represents the relative influence that the scalp perfusion ($rSBF_i$) has on measured cerebral blood flow index ($rCBF_i$).

CVR estimated for each experimental paradigm using the cross-correlated, time-aligned signals by solving the system of linear equations utilizing the Moore-Penrose pseudoinverse (*pinv* MATLAB function). To ensure that the model explains a significant

amount of variability in the data, we discarded CVR estimates when the model p-value for β_1 was > 0.05. We further discarded any CVR value <0.1.

2.2.5 Statistical Analysis

Data are reported as median (interquartile range) unless stated otherwise. Paired Wilcoxon sign-rank tests were used to assess whether MAP, HR, and E_tCO_2 were statistically different from baseline for breath-hold and hypercapnia paradigms. Wilcoxon rank-sum tests were used to assess differences in the change of these systemic parameters between hypercapnia and breath-hold paradigms. To compare CVR across experimental paradigms, we performed Wilcoxon rank-sum tests between all combinations of paradigms for a given numerical method (e.g., linear-regression CVR compared between HC and BH), between all combinations of numerical methods for a given paradigm (e.g., HC CVR compared between linear regression and GLM methods), and between DCS analytical models for a given paradigm (e.g., linear regression HC CVR compared between semi-infinite and 3-layer models). To quantify agreement of CVR across experimental paradigms, we calculate Pearson's correlation coefficient (R) as well as Lin's Concordance Correlation Coefficient (CCC), which is a measure of how well a set of bivariate data compares to a "gold standard" measurement (hypercapnia CVR, in our case).[244] We define the following agreement thresholds for CCC: poor (0-0.5), moderate (0.5-0.7), strong (0.7-0.9), excellent (>0.9) agreements. We further visualized agreement through a Bland-Altman plots, and we quantify the mean bias (95% confidence interval).[245] All statistical analyses were performed in MATLAB. Statistical significance was assessed at the 0.05 confidence level.

2.3 Results

2.3.1 Systemic changes Across Experimental Paradigms

As expected, E_tCO_2 significantly increased during both breath-hold and hypercapnia paradigms (both $p<0.05$, **Table 4**). E_tCO_2 changes were more pronounced during hypercapnia (13.0 vs. 7.5 mmHg in HC vs. BH; $p<0.001$). During the resting state paradigm, E_tCO_2 varied appreciably, with a median range (i.e., max – min over the 10 min period) of 6.5 mmHg. MAP significantly increased by 8.0 (5.6, 11.6) mmHg during breath-hold and 4.9 (1.9, 10.3) mmHg during hypercapnia (both $p<0.001$) (**Table 4**). Heart rate significantly increased by 11.5 (9.1, 19.2) bpm during breath-hold ($p<0.001$); no changes were observed during hypercapnia.

Table 4. Systemic changes during each CVR paradigm.
Median (interquartile range) change in end-tidal carbon dioxide (E_tCO_2), mean arterial blood pressure (MAP) and heart rate (HR) for each experimental paradigm. For hypercapnia, this change reflects the steady state change from room-air inhalation, for breath-hold, this change reflects the peak increase during breath-hold. For resting state, the median (IQRs) of the range (max – min over the 10 min period) is reported. $^{+}$ denotes significant difference from baseline ($p<0.05$); * denotes significant difference between hypercapnia and breath-hold ($p<0.05$).

	E_tCO_2 (mmHg)	**MAP (mmHg)**	**HR (Beats/minute)**
	Delta from baseline		
Hypercapnia	13.0 (7.80, 19.0)$^{+}$*	4.9 (1.9, 10.3)$^{+}$	2.1 (-3.1, 4.7) *
Breath-hold	7.5 (5.9, 9.2)$^{+}$	8.0 (5.6, 11.6)$^{+}$	11.5 (9.1, 19.2)$^{+}$
	Range: Median (IQR)		
Resting State	6.5 (5.3, 8.8)	1.9 (1.4, 2.3)	3.3 (2.9, 5.3)

2.3.2 CVR Across Experimental Paradigms

Of the 31 available datasets, a subset of CVR estimates for each experimental paradigm was discarded due to a failure to meet quality control criteria. The exact number of datasets included for each paradigm are included in **Table 5** along with median (IQR) CVR for each experimental paradigm and numerical method. CVR was statistically indistinguishable when compared across experimental paradigms for a given numerical method (e.g., linear regression) or for a given DCS analytical model (e.g., semi-infinite, **Table 5, Figure 9**). Within a given paradigm, the use of the 3-layer model increased CVR compared to the semi-infinite model. Further, the use of a general linear model with short separation regression depressed the median CVR and constrained the range compared to the linear regression approach.

Table 5. CVR across experimental paradigms.
CVR (%/mmHg) for hypercapnia, breath-hold, and resting state experimental paradigms estimated with linear regression and general linear models using the semi-infinite and 3-layer models for DCS analysis. Data are reported as median (IQR), N datasets (out of 31) that passed quality control metrics. *denotes significant difference between semi-infinite and 3-layer for a given CVR paradigm and numerical method ($p<0.05$). $^{+}$denotes significant difference between linear regression and the general linear model estimate of CVR for a given experimental paradigm ($p<0.05$).

	Linear Regression		**General Linear Model**	
	Semi-Infinite	**3-layer**	**Semi-Infinite**	**3-layer**
Hypercapnia	1.95 (0.92, 3.38)$^{+}$, 29	3.14 (1.48, 5.11), 24	1.30 (0.49, 2.06)$^{+}$, 26	3.27 (1.55, 5.48)*, 21
Breath-hold	2.15 (1.24, 5.68)$^{+}$, 28	4.86 (2.70, 8.34)*, 21	1.17 (0.73, 2.48)$^{+}$, 19	2.73 (1.87, 5.03)*, 20
Resting State	1.89 (1.36, 2.44), 20	3.51 (2.37, 4.33)*, 18	1.67 (0.98, 2.02), 18	3.33 (1.95, 4.40)*, 19

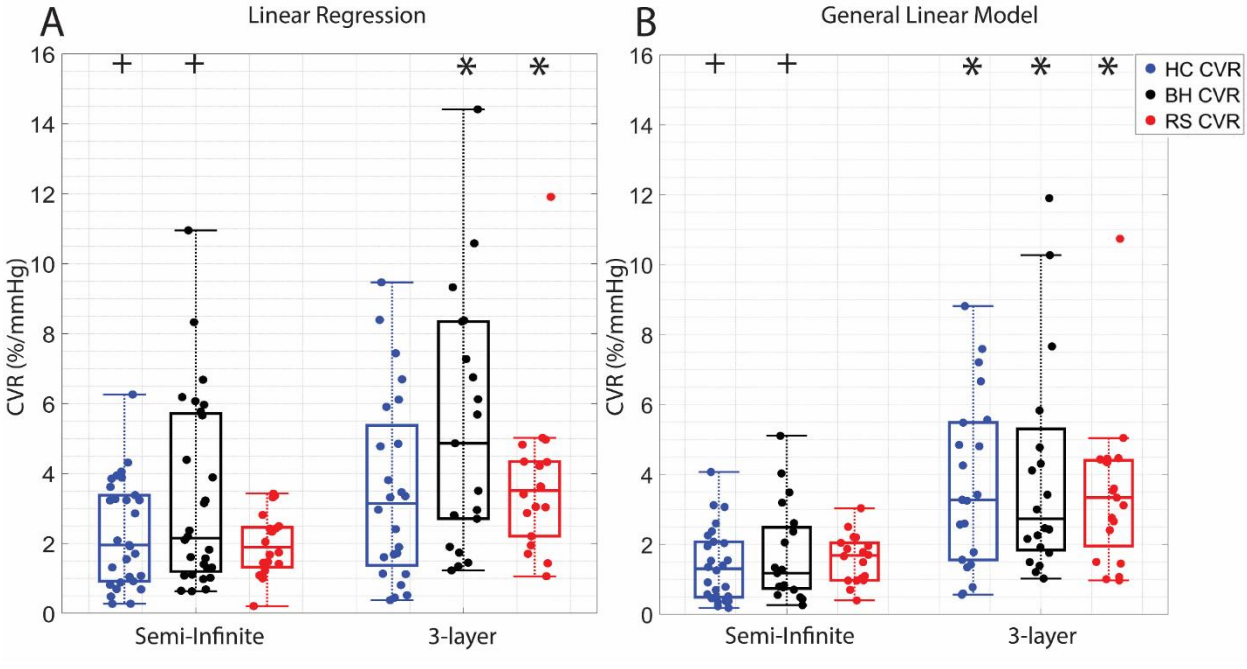

Figure 9. CVR across experimental paradigms.
Boxplots of CVR (%/mmHg) estimated with (A) linear regression and (B) a general linear model using both semi-infinite and 3-layer DCS analytical models during hypercapnia (HC, blue), breath-hold (BH, black), and resting state (red) experimental paradigms. For each boxplot, the central line denotes the median, and the bottom and top edges of the box indicate the 25th and 75th percentiles, respectively. The whiskers extend to the most extreme data points not considered outliers. Individual data are also included. *denotes significant difference between semi-infinite and 3-layer for a given CVR paradigm and numerical method ($p<0.05$). $^{+}$ denotes significant difference between linear regression and the general linear model estimate of CVR for a given experimental paradigm ($p<0.05$).

2.3.3 Agreement Between Hypercapnia and Breath-hold

The relationship between CVR during hypercapnia versus breath-hold is shown in **Figure 10** and summarized in **Table 6**. When using linear regression to estimate CVR, the correlation between HC and BH was only statistically significant for the 3-layer model ($R = 0.58$, $p<0.01$, **Figure 10C**); however, agreement was poor (CCC = 0.45). No association between HC and BH was observed with linear regression for the semi-infinite model (**Figure 10A**). The strength of the HC vs. BH CVR relationship greatly improved when using a GLM-SS to estimate CVR (**Figure 10 E,G**). Strong correlation and

agreement were observed using the GLM on the semi-infinite data (R = 0.80, CCC = 0.75, **Figure 10E**), where the mean bias from the line of equivalence of -0.12 %/mmHg was not significant (**Figure 10F**). Further, modest correlation and moderate agreement were observed using the GLM on 3-layer data with scalp flow regression (R = 0.69, CCC = 0.52, **Figure 10G**), with a non-significant mean bias of +0.76 %/mmHg (**Figure 10H**).

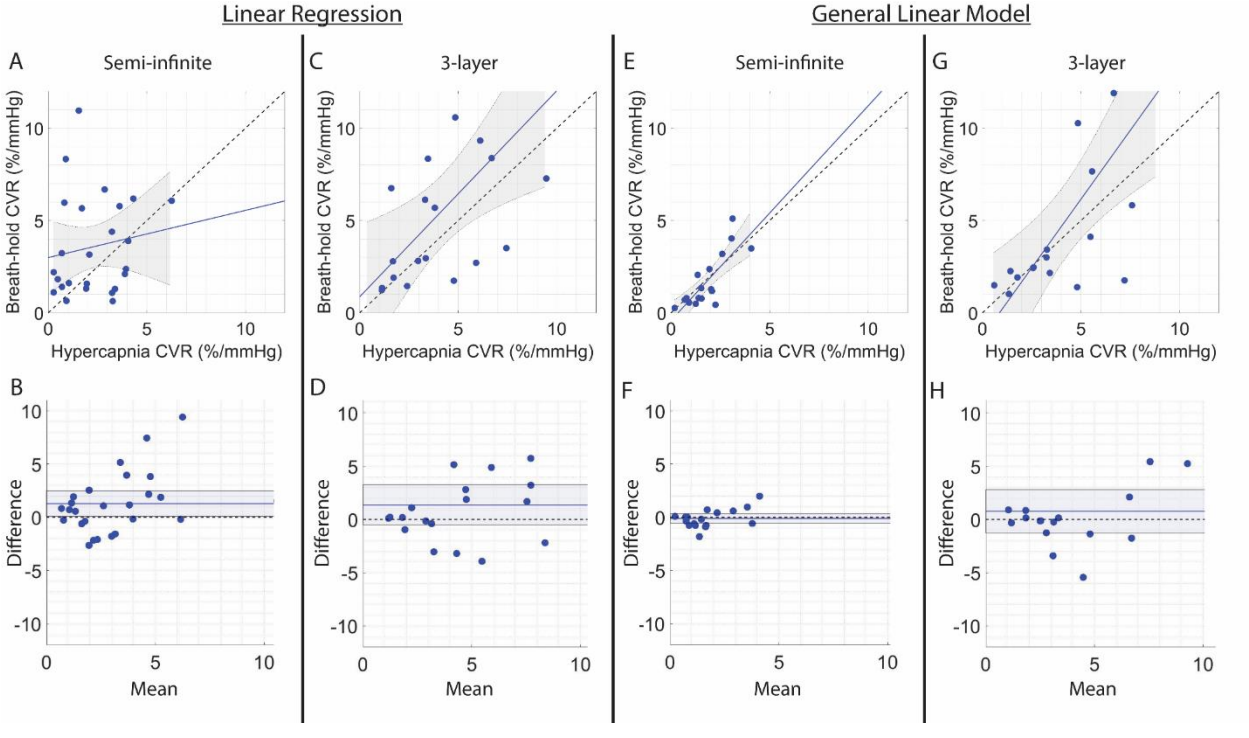

Figure 10. Relationship between hypercapnia and breath-hold CVR.
Relationship between CVR estimated during hypercapnia vs. breath-hold (top row) and corresponding Bland-Altman plots of the difference versus mean CVR (bottom row) estimated with linear regression (left columns) and general linear models (right columns) using the semi-infinite or 3-layer model for DCS analysis. In the top row, the dotted line represents the line of unity, while the solid line represents the best linear fit and 95% confidence interval (grey shaded). In the bottom row, the mean bias (solid line) and its 95% confidence interval (shaded region) are compared to the line of equality (dotted black line).

Table 6. Relationship between hypercapnia and breath-hold.
Relationship between CVR estimated during hypercapnia versus breath-hold using each numerical method and DCS analytical model corresponding to Figure 3. N denotes the number of datasets that met quality inclusion criteria for both hypercapnia and breath-hold, R denotes Pearson's correlation coefficient and its corresponding p-value (p), CCC denotes Lin's concordance correlation coefficient with 95% confidence intervals, and Mean Bias (95% confidence interval).

	Hypercapnia vs. Breath-hold			
	Linear Regression		General Linear Model	
	Semi-Infinite	3-layer	Semi-Infinite	3-layer
N	25	18	17	16
R	0.15	0.58	0.80	0.69
p-value	0.48	0.0087	0.00011	0.0021
CCC	0.11 (-0.19, 0.39)	0.45 (0.14, 0.68)	0.75 (0.49, 0.88)	0.52 (0.24, 0.72)
Mean Bias	1.28 (0.08, 2.49)	1.36 (-0.53, 3.25)	-0.12 (-0.57, 0.33)	0.76 (-1.28, 2.80)

2.3.4 Agreement Between Hypercapnia and Resting State

We next compared CVR agreement between hypercapnia and resting state paradigms (**Figure 11,**

Table 7). When using linear regression to estimate CVR, the correlation between HC and RS was statistically significant, but the agreement was poor for the semi-infinite model (R = 0.45, p=0.045, CCC = 0.35, **Figure 11A**); no association between RS and HC was observed for the 3-layer model (**Figure 11C**). In a similar manner to the HC vs. BH comparison, the strength of the HC vs. RS CVR relationship greatly improved when using a GLM to estimate CVR (**Figure 11E,G**). Strong, statistically significant correlation and borderline strong agreement were observed using the GLM with short separation regression on the semi-infinite data (R = 0.76, p<0.001, CCC = 0.69, **Figure 11E**) with a non-significant mean bias of -0.12 %/mmHg (**Figure 11F**). Significant correlation and moderate agreement were observed using the GLM on 3-layer data with scalp signal regression (R = 0.65, CCC = 0.55, **Figure 11G**), with a non-significant mean bias of -0.68 %/mmHg (**Figure 11H**).

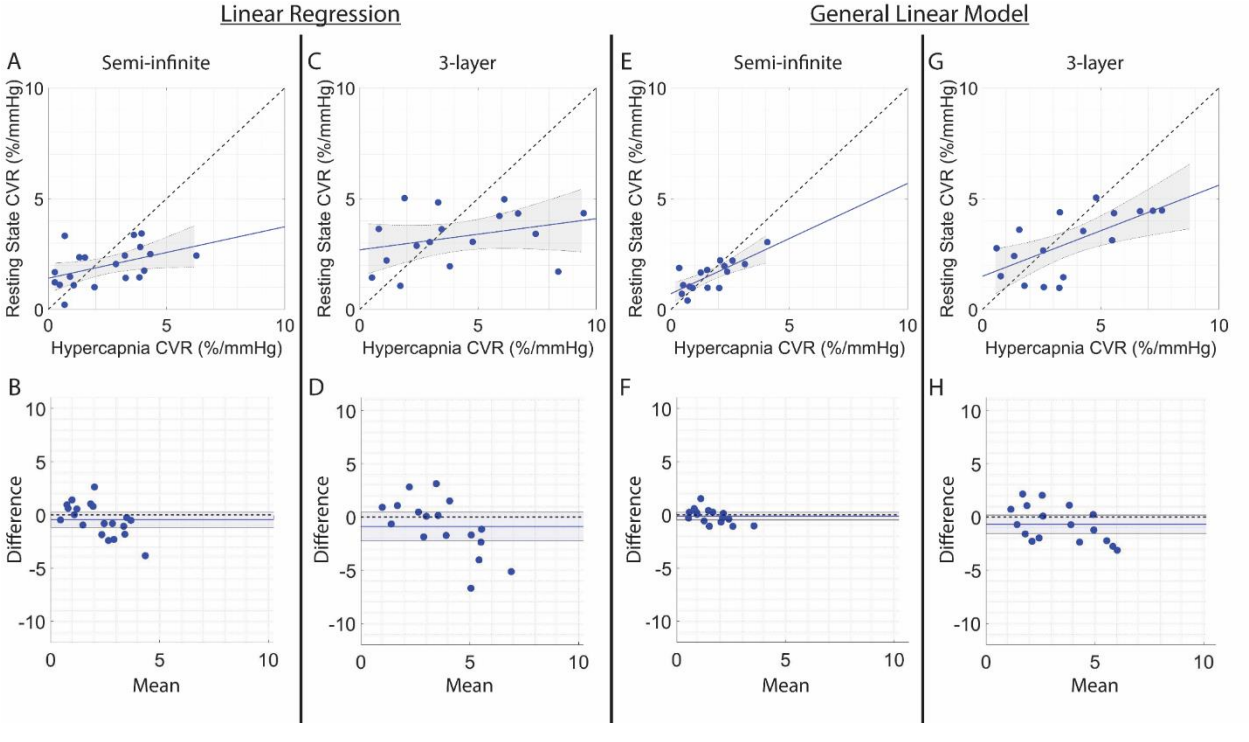

Figure 11. Relationship between hypercapnia and resting state.

Relationship between CVR estimated during hypercapnia vs. resting state (top row) and corresponding Bland-Altman plots of the difference versus mean CVR (bottom) estimated with linear regression (left columns) and general linear models (right columns) using the semi-infinite or 3-layer models for DCS analysis. In the top row, the dotted line represents the line of unity, while the solid line represents the best linear fit and 95% confidence interval (grey shaded). In the bottom row, the mean bias (solid line) and its 95% confidence interval (shaded region) are compared to the line of equality (dotted black line).

Table 7 Relationship between hypercapnia and resting state.
Relationship between CVR estimated during hypercapnia versus resting state using each numerical method and DCS analytical model corresponding to Figure 4. N denotes the number of datasets that met quality inclusion criteria, R denotes Pearson's correlation coefficient and its corresponding p-value (p), CCC denotes Lin's concordance correlation coefficient with 95% confidence intervals, and Mean Bias (95% confidence interval).

	Hypercapnia vs. Resting State			
	Linear Regression		General Linear Model	
	Semi-Infinite	3-layer	Semi-Infinite	3-layer
N	20	17	16	17
R	0.45	0.31	0.76	0.65
p-value	0.045	0.23	0.00058	0.0048
CCC	0.35 (0.02, 0.61)	0.21 (-0.13, 0.51)	0.69 (0.40, 0.86)	0.55 (0.20, 0.77)
Mean Bias	-0.46 (-1.17, 0.26)	-0.89 (-2.26, 0.47)	-0.12 (-0.50, 0.25)	-0.68 (-1.55, 0.19)

2.4 Discussion

2.4.1 CVR Measured by DCS Demonstrates Strong Agreement Among More Tolerable Paradigms When Employing Short-Separation Regression With A General Linear Model

Herein we used DCS to quantify the agreement between CVR measured during hypercapnia compared to more tolerable and more practical breath-hold and resting state paradigms. Although these experimental paradigms are often used interchangeably in the literature as vehicles to assess CVR, we found surprisingly poor agreement between CVR assessed with each of these paradigms when using a simple linear regression to estimate CVR. This poor agreement was observed when using both the semi-infinite and 3-layer models for DCS blood flow estimation. However, by employing a general linear model to

regress out extracerebral contributions, we found strong agreement between the "gold-standard" hypercapnia challenge and both breath-hold and resting state. This result suggests that the more CVR tolerable paradigms may serve as a substantially equivalent substitution for the hypercapnia challenge, thereby enabling bedside assessment of microvascular CVR with DCS in patient cohorts for whom hypercapnia is contraindicated or not feasible.

The use of a general linear model with short separation regression (GLM-SS) is designed to remove extracerebral and systemic contributions to the long separation blood flow signal and, by extension, to enhance sensitivity to changes in brain-layer blood flow caused by dissolved CO_2 in the bloodstream. While commonly employed by the functional near-infrared spectroscopy community to improve detection of evoked brain activity[241,243,246], this approach is novel in the assessment of CVR with DCS. Furthermore, this approach offers a unique advantage over other CVR-quantifying modalities such as TCD that lack easy access to information regarding systemic changes without the use of supplemental monitoring of arterial blood pressure, heart rate, etc. Functional MRI commonly employs a global signal regression to account for systemic influences, among other contributors[247]; however, when applied to the assessment of CVR, this approach yields only qualitative estimates that complicate inter-subject comparisons and is non-ideal for use in breath-hold or hypercapnia.[248] By employing short separation regression with DCS, we regress out extracerebral and systemic contributions to the signal in a manner that is comparatively more feasible to fMRI but provides quantitative assessment of CVR across a wider range of experimental paradigms.

2.4.2 Need for Further Validation in DCS-Derived CVR

While we have demonstrated strong agreement among experimental paradigms using the GLM-SS approach, more work is needed to validate that CVR estimated with this approach reflects the true CVR. For reference, literature commonly reports hypercapnic CVR in healthy adults ~4-8 %/mmHg.[222,233,202] Our median (range) of 1.3 (0.5-4%/mmHg) is comparatively lower, possibly because the systemic influences that we regress out are known to be caused by factors that change cerebral blood flow in tandem with the effects of dissolved CO_2 (e.g., blood pressure, cardiac output). Alternatively, the blunted values may be due to the choice of source detector separations, which may regress out too much of the desired brain-layer BF_i signal due to a lack of optimal short separation or which may not have sufficient brain sensitivity due to the 2.5 cm long separation. Finally, the blunted values could reflect that our assessments were made while the subjects were seated. Many literature reports, particularly with MRI, are performed while supine, and a supine posture is a known factor that increases the magnitude of CVR.[249] Regardless, validation studies against other modalities (e.g., MRI) and clinical studies demonstrating the ability to detect abnormalities in CVR with this approach are warranted.

2.4.3. Current Technical Limitations in DCS Brain Sensitivity May Limit Adoption in a Clinical Environment

While the strong agreement between hypercapnia and breath-hold/resting state with the GLM-SS approach is promising, we note the overall rejection rate is high (23, 28, and 42 % for hypercapnia, breath-hold, and resting state, respectively). We explored several explanations for this high rejection rate. For a subset of subjects (N=13/31), we observed that baseline BF_i (ρ_{short})>BF_i (ρ_{long}), which may suggest a lack of brain sensitivity. For the resting state paradigm, BF_i (ρ_{long})/BF_i (ρ_{short}) was significantly lower in rejected vs. passing datasets (0.81 vs. 1.40; $p<0.01$); however, this trend was not

observed for hypercapnia or breath-hold paradigms. Further, in a subset of 6 subjects, we briefly applied pressure to the sensor to reduce scalp flow. Although the sample size was small, we observed that the relative change in BF_i at ρ_{long} compared to ρ_{short} during this pressure manipulation was higher but not significantly different in rejected data (2/6) across all paradigms (e.g., for resting state, 0.88 vs. 0.67). Taken together, these observations may suggest that the high rejection rate may be partially due to either regressing out too much brain signal with the 1cm separation or not enough brain sensitivity with the 2.5cm separation. Literature suggests the latter is more likely, as limited brain sensitivity is a well-known challenge in DCS measurements. Multiple ongoing, long-term efforts aim to address this brain sensitivity limitation[141] including novel hardware developments (e.g., time-domain[250,251], and interferometric DCS[252,253], along with moving to the second optical window[254]) and improved analytical approaches.[232,237,255] As a mitigating near-term strategy, computational simulations are warranted to optimize source-detector separations, akin to what has been done with functional NIRS.[241,256] For the resting state paradigm, another explanation we investigated for the high rejection rate was that the natural fluctuations in E_tCO_2 observed during unpaced breathing (typically a difference 1-3 mmHg on a breath-by-breath basis) may be too small to elicit reliable fluctuations in CBF, as has been previously suggested.[6,225,229] However, median resting state E_tCO_2 IQRs and beat-to-beat E_tCO_2 changes between accepted and rejected data were not statistically different ($p>0.1$), contradicting this previously offered explanation. Future work should be directed to better understand the factors that contribute to this high rejection rate to increase clinical viability of the CVR assessment with the GLM-SS approach.

Quantifying CVR with DCS is a particularly attractive opportunity for technology transfer as a diagnostic medical device for use in clinical settings given the unique economic, ergonomic, and clinical workflow integration benefits conferred by this optical neuromonitoring modality. Notable advantages include microvascular sensitivity in

contrast to TCD, bedside portability in contrast to MRI, and ease of use in all patient cohorts in contrast to both TCD and MRI. Indeed, given these positive attributes, several studies[144,193,199–205,232] have utilized DCS to quantify the CBF response to a vasoactive stimulus (e.g., ACZ, hypercapnia). Nevertheless, despite the advantages of DCS as a CVR-quantifying platform, drawbacks remain. The penetration depth of DCS is limited to the superficial cortex and the spatial sensitivity is poor unlike MRI, and as previously discussed, the measurement can be significantly confounded by the influence of extracerebral layers (i.e., skull, scalp, cerebrospinal fluid). With regards to the latter limitation, we explored both the GLM-SS and the use of the 3-layer model. With the 3-layer model, we found that the magnitude of CVR significantly increased for most experimental paradigms and numerical approaches compared to the semi-infinite model, suggesting the model did increase brain sensitivity. However, agreement amongst experimental paradigms was strongest with the semi-infinite model using the GLM-SS. The weaker agreement with the 3-layer model could be due to the sensitivity of this model to errors in the model's assumed input parameters. For example, it has been shown to be sensitive to errors in both skull and scalp thickness, such that an underestimation of scalp thickness by ~20% could induce ~15% errors in the estimation of rCBF.[238] To minimize these sources of error, future studies could benefit from concurrent anatomical scans (e.g., MRI or CT) to assess layer thickness and/or from the implementation of a realistic, multi-layered Monte Carlo-based fitting process coupled with a pressure modulation paradigm to optimize model parameters.[232]

2.4.4 Limitations and Future Directions

This study is not without limitations. First, the order of the experimental paradigms was not randomized by subject. While we have no indication that order should influence agreement, the best practice to avoid unintended systematic error in experimental design

would have been to randomize the order. Second, our estimation of CVR assumes a linear relationship between blood flow and end tidal CO_2. This first-order approximation may break down outside the autoregulatory range of E_tCO_2 (~35-45 mmHg), wherein the relationship between macrovascular blood flow velocity and E_tCO_2 has been shown to be logistic.[257,258] Future work could benefit from quantifying the hemodynamic response function to step changes in E_tCO_2 to better account for possible non-linearity between CBF and E_tCO_2.[202,224,246,256,259] Third, we did not rigorously control for environmental stimuli. While the exact influence of the environment on our estimations of CVR is not well-delineated, there is evidence to suggest that environmental stimuli can influence the brain's response to changes in end tidal CO_2. For example, Peng et al. showed that the time delay between the gray matter BOLD signal change and E_tCO_2 is larger with eyes-open vs. eyes-closed states.[260] The effect of environmental influences should be the subject of rigorous further investigation. Finally, there are numerous assumptions/approximations made when fitting for BF_i with the semi-infinite model and CBF_i with the 3-layer model. For example, with the semi-infinite model, we incorporate FDNIRS-estimated optical properties into the fitting procedure, which are predicated on several assumptions, e.g., μ_s' does not change with time.[193] For the 3-layer model, we assumed that optical properties do not change with time and we also used a fixed, literature defined scalp and skull thicknesses for all subjects. While the magnitude of the errors induced by each of these approximations in isolation may be small, the cumulative effect could be significant. Future work that targets this issue by minimizing the number of assumptions needed would be merited.

2.5 Conclusions

This work provides the first systematic comparison of CVR across experimental paradigms using diffuse correlation spectroscopy. We demonstrate that using a general

linear model to regress out extracerebral and systemic contributions to the DCS-measured blood flow yields strong agreement between the gold-standard hypercapnia and the more tolerable and feasible paradigms of breath-hold and resting state. These findings suggest breath-hold and resting state paradigms may offer feasible experimental alternatives to hypercapnia for practical clinical evaluation of CVR with DCS.

Chapter 3: Impaired cerebrovascular reactivity in pediatric sickle cell disease using diffuse correlation spectroscopy

Results detailed in this chapter are in preparation for submission to Biomedical Optics Express

Abstract.

Cerebrovascular reactivity (CVR), defined as the ability of cerebral vasculature to dilate in response to a vasodilatory stimulus, is an integral mechanism in brain homeostasis that is thought to be impaired in sickle cell disease (SCD). This study used diffuse correlation spectroscopy and a simple breath-hold stimulus to quantify CVR non-invasively in a cohort of 12 children with SCD and 15 controls. Median [interquartile range] CVR was significantly decreased in SCD compared to controls (2.03 [1.31, 2.44] versus 3.49 [3.00, 4.11] %/mmHg, p=0.028). These results suggest DCS may provide a feasible means to routinely monitor CVR impairments in pediatric SCD.

3.1 Introduction

Children with sickle cell disease (SCD) face an increased, life-long risk of neurocognitive comorbidities that are exacerbated by cerebrovascular dysfunction, including stroke and silent cerebral infarction.[67] Cerebrovascular reactivity (CVR), defined as the ability of cerebral vasculature to dilate in response to a vasodilatory stimulus, is an integral mechanism in brain homeostasis. It is thought that CVR is impaired in SCD due to both endothelial dysfunction and persistent vasodilation caused by chronic anemia.[68] Indeed, a handful of publications have demonstrated impairments in both the magnitude and response time of CVR in children [198,261–263] and adults [264–266] with SCD compared to healthy controls. These impairments are observed globally[262,265,267,268], and the extent of CVR impairment has been shown to be correlated with the degree of amenia.[210,264] Quantification of CVR coupled with medical interventions aimed at restoring abnormal CVR has potential to reduce morbidity and mortality in patients with SCD.

Routine assessment of CVR in the clinical environment requires tolerable vasodilatory stimulus paradigms that can detect deficits in CVR as well as bedside tools capable of quantifying the dynamic cerebral blood flow (CBF) response to the stimulus. Several well-established experimental paradigms exist to study CVR non-invasively.[6,269] The majority of work to date has quantified the CBF response to changes in arterial carbon dioxide content via acetazolamide infusion or inhalation of carbon dioxide (CO2), neither of which are feasible solutions for routine CVR assessment in a clinical environment, particularly in children.[6] More tolerable experimental paradigms, such as a breath-hold challenge [6,15] or natural arterial CO2 fluctuations that occur at rest when freely breathing[269], are largely unexplored in SCD. CBF can be quantified using several neuroimaging techniques, e.g., magnetic resonance imaging (MRI), transcranial Doppler ultrasound (TCD). However, most of these modalities are limited to the research setting

and are not feasible for routine CVR assessment in patient care environments due to cost, availability, etc.

Diffuse correlation spectroscopy (DCS) is a non-invasive optical technique to assess CBF that offers many strategic advantages over more traditional perfusion modalities, including portability, low cost, high temporal resolution, direct measure of cortical-level microvascular blood flow, and ease of use in both adults and children in a wide array of clinical indications and environments.[201,226,235,270] In this pilot feasibility study, we use DCS to quantify CVR in a cohort of children with SCD along with a population of healthy pediatric controls. We make these assessments both at rest and during a breath-hold challenge. We hypothesize that CVR is reduced in SCD children compared to controls. Further, we hypothesize that CVR obtained during breath-hold agrees with CVR obtained at rest. Finally, we explore whether CVR is associated with age, sex, and hematological biomarkers of anemia.

3.2 Methods

3.2.1 Participants

Children ages 6-18 years (inclusive) with and without sickle cell disease were recruited at Emory University and Children's Healthcare of Atlanta as part of a prospective, cross-sectional pilot study. All protocols were approved by the Emory University Institutional Review Board. Written informed consent was obtained from all parental guardians and written (11-17 y) or verbal assent (6-10 y) was acquired from each child. For the SCD group, all participants had a diagnosis of sickle cell anemia (SS or $S\beta_0$ genotypes), as confirmed by electrophoresis. Exclusion criteria included history of prior curative therapy (e.g., bone marrow transplant), hypertension, prior overt stroke, transient ischemic attack, vasculopathy, Moyamoya disease, major head injury, or neurological

indications not related to SCD (e.g., seizure disorder). Temporary exclusion criteria included recent hospitalization or acute vaso-occlusive crisis within the past 2 weeks or blood transfusion within the past 2 months. For the control group, participants were eligible if they did not have sickle cell disease (any genotype), as reported by family. Exclusion criteria included prior history of anemia-related disorders, cardiovascular disease (e.g., hypertension), chronic respiratory dysfunction (e.g., cystic fibrosis), seizure disorders, cerebrovascular disease, stroke, transient ischemic attack, or renal disease.

3.2.2 Experimental Protocol

All participants were instructed to abstain from stimulants (e.g., caffeine, Adderall) for at least 12 hours prior to study participation. Cerebrovascular reactivity was quantified via two consecutive experimental paradigms: resting state and breath-hold. For resting-state, the participant was directed to breathe naturally, i.e., unpaced, for 10 minutes. For breath-hold, the participant completed 5 end-inspiration breath-hold challenges facilitated by a custom graphical user interface (MATLAB, Mathworks Inc., Natick, MA; **Appendix 2, Figure 19-20**). Each challenge consisted of 60 seconds (s) paced breathing tuned to the participant's native resting respiration rate followed by a 20-30s end-inspiration breath-hold. A training session was performed prior to the start of the protocol to familiarize participant with the user interface and the breath-hold exercise. This practice was also used to tailor the breath-hold duration to the individual's comfort (typically 20-30s) and to promote compliance with the exercise. Participants sat upright for the duration of the study protocol.

Continuous (20 Hz) DCS measurements of cerebral blood flow were made by securing an optical sensor on the forehead over the hemisphere that yielded the highest

detected light intensities to maximize signal-to-noise ratio. A mask or nasal cannula was placed over the mouth and/or nose to facilitate continuous monitoring of expelled CO_2 (4Hz, LifeSense II, Nonin Medical Inc., Plymouth, MN). In post-processing, a peak detection algorithm in MATLAB (*findpeaks*) was used to estimate end tidal CO2 (EtCO2) from the expelled CO2 waveform. The EtCO2 time series was visually inspected to remove obvious outliers attributed to irregular breathing or incomplete exhalation. Peripheral oxygen saturation (SpO2, LifeSense II, Nonin Medical, Inc.) and arterial blood pressure (ABP, CNAP Monitor 500, NIPD1000D-1, Biopac Systems) were also continuously monitored at 1 and 125 Hz, respectively. For the SCD group, a small venous blood sample was acquired within 1 month of CVR assessment (typically on the same day), either as part of routine clinical care or for research. Hemoglobin (Hb, g/dL), hematocrit (Hct, %), and reticulocyte count (1e10/L) were estimated with a complete blood count. Fetal hemoglobin (HbF, %) and sickle hemoglobin (HbS, %) content were estimated from capillary electrophoresis.

3.2.3 DCS Instrumentation

DCS data were acquired with a custom, in-house-built system consisting of a 852 nm long-coherence length laser (iBeam Smart, TOPTICA Photonics, Farmington, New York), two four-channel single photon counting modules (SPCM AQ4C-IO, Perkin-Elmer, Quebec, Canada), and an 8 channel counter/timer data acquisition board (PCIe6612, National Instruments, Austin, TX) that allowed for fast (20 Hz) quantification of the intensity autocorrection function, $g_2(t,\tau)$, at time, t, and delay time, τ.[188] The patient interface consisted of a flexible optical sensor with two source-detector spacings at 1.0 and 2.5 cm, denoted ρ_{short} and ρ_{long}, respectively. Seven single mode fibers (780HP, Thorlabs) were

bundled at the ρ_{long} detector optode to enhance SNR, while one single mode fiber was used at ρ_{short}. Care was taken to ensure compliance with ANSI standards for skin exposure.

3.2.4 Data Processing

To estimate cerebral blood flow, $g_2(\rho_{long}, t, \tau)$ was first averaged across all seven detectors with photon count rates > 10 kHz. Next, to enhance signal-to-noise ratio, both $g_2(\rho_{short}, t, \tau)$ and the averaged $g_2(\rho_{long}, t, \tau)$ were down sampled from 20 Hz to 1 Hz by frame averaging. Then, data from each source-detector spacing were independently fit to the semi-infinite homogenous solution to the correlation diffusion equation [270] to extract an index of blood flow ($BFi(\rho, t)$, cm^2/s). Fits were restricted to $g_2 > 1.2$ at ρ_{long} to enhance sensitivity to cortical blood flow.[203] In 2 participants, this threshold resulted in < 5 data points. For these individuals, the g_2 threshold was loosened to 1.05. For all g_2 fits, we assumed a fixed index of refraction of 1.4, and absorption and reduced scattering coefficients at 852 nm of 0.19 and 8.4 cm^{-1}, respectively.[271]

For each experimental paradigm, relative change in blood flow index as a function of time ($rBFi(t)$) was calculated as $\left(BFi\left(\rho_{long}, t\right) - BFi_0\right)/BFi_0 \times 100\%$ where the subscript 0 denotes the mean flow index at ρ_{long} during the baseline of the given paradigm. For resting state, baseline was chosen as the 2 minutes at the start of the resting state period. For breath-hold, baseline was chosen as the 30 seconds prior to the first breath-hold epoch. Change in EtCO2 as a function of time was estimated as $\Delta EtCO2(t) = EtCO2(t) - EtCO2_0$ using the same baseline periods as rBFi. To account for the gas transit time from the mask to the capnogram and the physiological delay between alveolar diffusion of CO2 in the lungs and arterial CO2 reaching the cerebrovasculature to

elicit a cerebral blood flow response, we time-aligned $rBFi(t)$ and $\Delta EtCO2(t)$ via cross correlation. For this analysis, the EtCO2 time series was incrementally shifted between -5 to 20s in steps of 0.01 s. For each shift, $\Delta EtCO2(t)$ was interpolated to the $rBFi(t)$ time axis, and Pearson's correlation coefficient between $rBFi(t)$ and $\Delta EtCO2(t)$ was estimated. Finally, $\Delta EtCO2(t)$ was shifted by the time lag, t_{xcorr}, that yielded the highest correlation coefficient between $rBFi(t)$ and $\Delta EtCO2(t)$.

3.2.5 Estimation of CVR

To estimate CVR, we employed a standard linear regression which assumes a linear relationship between $rBFi(t)$ and $\Delta EtCO2(t)$:

$$rBFi(t) = \beta_0 + \beta_1 * \Delta EtCO2\ (t)\ +\ \text{Ɛ}. (Eq. 17)$$

Here β_1 reflects CVR (%/mmHg), β_0 is the intercept, and Ɛ is the fit residual. For each experimental paradigm (i.e., resting state and breath-hold), linear regression (*regress*, MATLAB) was applied between the cross-correlated, time-aligned $rBFi(t)$ and $\Delta EtCO2(t)$ signals to obtain an estimate of CVR. To ensure that the model explains a significant amount of variability in the data, we discarded CVR estimates for which the model p-value for β_1 was > 0.05. We further discarded CVR values < 0. For breath-hold CVR, we required a minimum of 3 consecutive compliant epochs as an additional data quality metric. A compliant epoch was defined as: 1) no evidence of breathing during the breath-hold period, as determined by ethnographic observation and monitoring of the CO2 waveform morphology, and 2) EtCO2 peak after breath-hold greater than 1 mmHg of the EtCO2 immediately before breath-hold. Three participants displayed a substantial (> 5 mmHg) decreasing trend in EtCO2 across the entire breath-hold paradigm duration. For

these individuals, only the final 3 epochs where EtCO2 had stabilized were included for analysis.

3.2.6 Statistical Analysis

Summary statistics are presented as median (interquartile range) or count (percentage). First, the non-parametric Wilcoxon rank sum test was used to test differences in all measured parameters (age, sex, weight, height, systolic/diastolic/mean blood pressure, transcutaneous oxygen saturation, CVR, t_{xcorr}) between SCD and control groups due to the small sample size. Next, to investigate agreement of CVR between breath-hold and resting state paradigms, data were visually assessed using Bland Altman analysis to quantify the mean bias between the two paradigms.[245] Agreement was quantified with Lin's Concordance Correlation Coefficient (CCC).[272] CCC > 0.7 is considered strong agreement. Third, to explore the association between CVR and demographic/hematologic biomarkers, we used univariable linear regression of CVR and age, sex (both SCD and control), as well as between CVR and Hb, Hct, reticulocyte count, HbF, and HbS (SCD only). These associations are presented in terms of the slope estimate for the best fit line between two variables with 95% confidence intervals, Pearson Correlation Coefficient (r) to assess the linear correlation along with its corresponding p-value. Finally, a subgroup analysis was conducted by repeating all previous analyses on a subset of participants with average resting-state $BFI(\rho_{short}) < BFI(\rho_{long})$, indicative of enhanced brain sensitivity.[273] All statistical analysis was performed in MATLAB. Statistical significance was assessed at the 0.05 confidence level.

3.3 Results

3.3.1 Enrollment, Data Quality, and Demographics

A flowchart of the data used for final analysis is shown in **Figure 12**. A total of 16 SCD and 18 control children were enrolled but only 13 SCD and 16 control children datasets satisfied our DCS signal quality control criteria. Of these, 10/13 (77%) SCD and 13/16 (81%) controls had breath-hold data that passed quality criteria; 9/10 (90%) SCD and 7/9 (78%) controls had resting state data that passed quality criteria (**Figure 12**). Notably, the resting state paradigm was implemented after the initial 12 subjects were recruited, thus fewer resting state datasets were available for analysis; 13 participants (7 SCD and 6 controls) had *both* resting state and breath-hold datasets that passed quality criteria. In total, 12/15 unique SCD/control participants had at least one dataset that was included in the final analysis (**Table 8**). Fourteen (52%) were female with a median (IQR) age of 11 (10, 13) years. No differences in age, sex, weight, height, blood pressure, or transcutaneous oxygen saturation were observed between groups. Within the SCD group, all patients were taking hydroxyurea per standard of care at a median (IQR) dose of 850 (750, 900) mg/day.

.

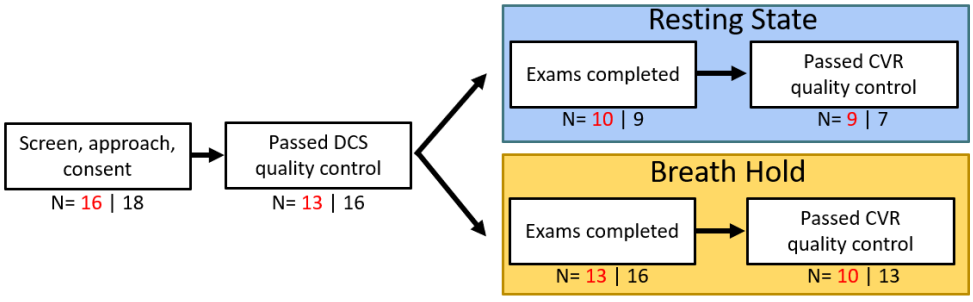

Figure 12. Flowchart of data included for analysis.
Red indicates n for the sickle cell disease group; black indicates n for the control group. Of the consented participants, the majority completed the full CVR exam that included both breath-hold and resting state assessments, while a subset just completed the breath-hold exam.

Table 8. Participant characteristics.
Data are reported as median (interquartile range) or count (percentage) for the SCD and control participants with data that was included in the final analysis for either breath-hold or resting state paradigms.

Parameter	SCD	Control	p-value
	General Characteristics		
N of participants	12	15	-
Age (years)	11.2 (10.6, 13.1)	11.5 (8.9, 12.2)	0.661
Sex (N; % Female)	6; 50%	8; 57.1%	-
Weight (kg)	40 (34, 47)	44 (30, 52)	0.931
Height (cm)	144 (142, 155)	153 (141, 160)	0.624
	Physiological Data		
Systolic blood pressure (mmHg)	111 (103, 117)	91 (65, 118)	0.290
Diastolic blood pressure (mmHg)	64 (60, 68)	58 (65, 66)	0.218
Mean blood pressure (mmHg)	80 (78, 83)	74 (73, 81)	0.217
Oxygen saturation (%)	99 (97, 100)	97 (96, 98)	0.220
	Genotype		
AA (N; %)	0; 0%	16; 100%	-
SS (N; %)	11; 100%	0; 0%	-
	Hematological Factors		
Hemoglobin (g/dL)	8.9 (7.9, 9.8)	-	-
Hematocrit (%)	25 (22, 28)	-	-
Reticulocytes (1E10/L)	18 (15, 27)	-	-
Fetal hemoglobin (%)	10 (7, 15)	-	-
Sickle hemoglobin (%)	86 (81, 90)	-	-
	Medications		
Hydroxyurea only (N; %)	8; 66.7%	-	-
Voxelotor only (N; %)	1; 8.3%	-	-
Hydroxyurea and Voxelotor (N; %)	2; 16.7%	-	-

p-values are from the Wilcoxon rank sum test.

3.3.2 CVR Comparison Among Groups

Median [IQR] CVR assessed during the breath-hold paradigm was significantly lower in SCD compared to controls (2.03 [1.31, 2.44] vs. 3.49 [3.00, 4.11] %/mmHg), p = 0.028, **Figure 13**). Moreover, median [IQR] t_{xcorr}, i.e., the time lag between rBFI and

EtCO2, was longer in the SCD group compared to controls (11.5 [6.5, 12.3] vs. 6.5 [1.5, 10.5] s), although this trend did not reach statistical significance (p = 0.23, **Figure 14**).

In the resting state paradigm, no CVR differences were observed between groups (median [IQR] of 1.88 [1.69, 3.26] in SCD vs. 1.81 [1.22, 2.82] %/mmHg in controls). Moreover, poor agreement was observed between CVR assessed in breath-hold vs. resting state paradigms in the subset of participants that completed both paradigms (N = 13, CCC = -0.40, **Figure 15**). Given the lack of group differentiation in resting state CVR and the poor agreement with breath-hold CVR, we focus the remainder of the analysis on CVR assessed during the breath-hold paradigm.

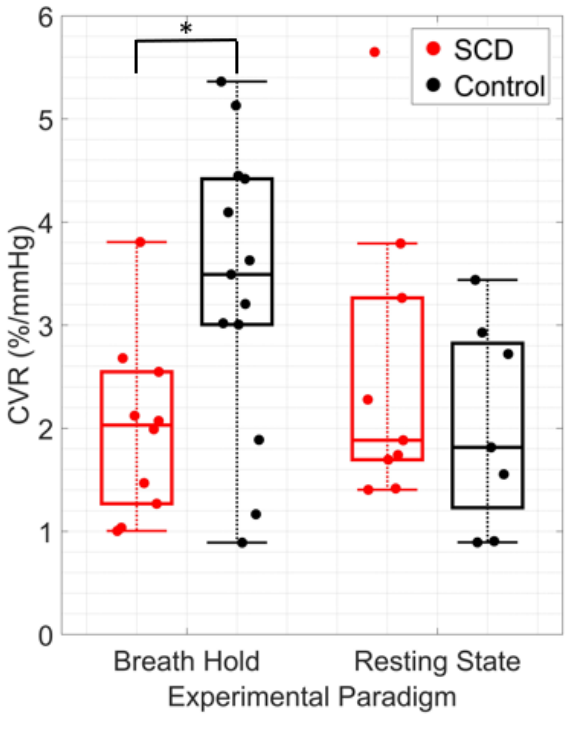

Figure 13. Cerebrovascular reactivity (CVR) by group and experimental paradigm. Boxplots of CVR (%/mmHg) in sickle cell disease (SCD, red) and control (black) groups during breath-hold (left) and resting state (right) experimental paradigms. For each boxplot, the central line denotes the median and the bottom and top edges of the box indicate the 25th and 75th percentiles, respectively. The whiskers extend to the most extreme data points not considered outliers. Individual dots represent each participant. *p < 0.05; significance between groups was assessed using a Wilcoxon rank-sum test.

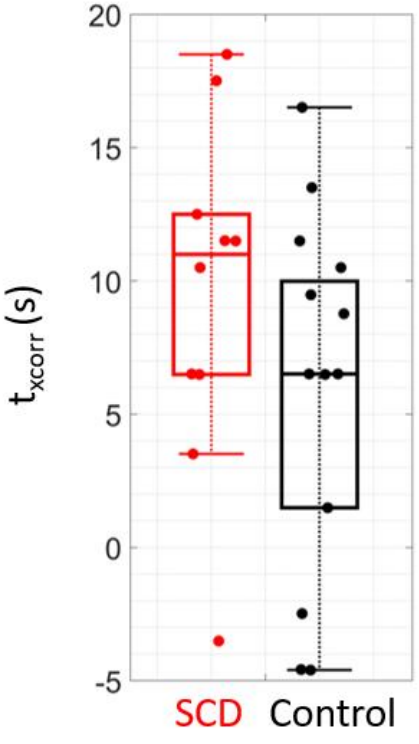

Figure 14. Cross correlation time lag by group.
Boxplots of t_{xcorr}, the time lag that yielded the highest correlation coefficient between blood flow and end tidal CO2 timeseries, for sickle cell (SCD, red, N = 10) and control (black, N = 13) groups in the breath-hold experimental paradigm.

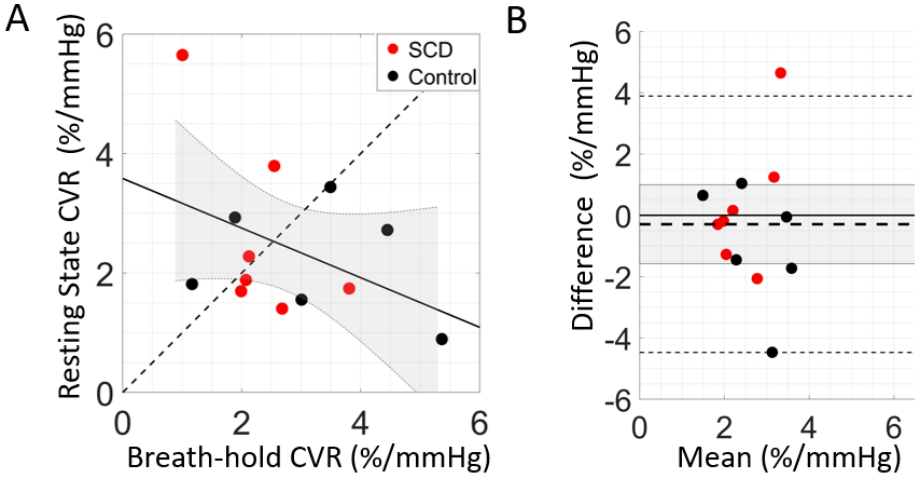

Figure 15. Agreement between cerebrovascular reactivity (CVR) paradigms.
(A) CVR assessed during breath-hold versus resting state paradigms (N = 13). The dotted line represents the line of unity, the solid line represents the best linear fit, and the shaded grey region denotes the 95% confidence interval. (B) Bland-Altman plot of the mean CVR between resting state and breath-hold versus the difference. Mean bias is denoted by the horizontal thick dotted black line along with its 95% confidence interval (shaded gray region), line of equality (solid thick black line), and limits of agreement (thin dotted black lines).

3.3.3 Association of CVR and demographic/hematologic factors

Grouping SCD and control data together, an inverse association between CVR and age was observed (r = -0.31), although this trend did not reach statistical significance (p = 0.14, **Figure 16A; Appendix 1, Table 9**). No sex differences in CVR were observed (p = 0.52, **Figure 16B; Appendix 1, Table 9**). Within the SCD group, no significant correlations between CVR and hematologic factors were found (**Appendix 1, Table 10**).

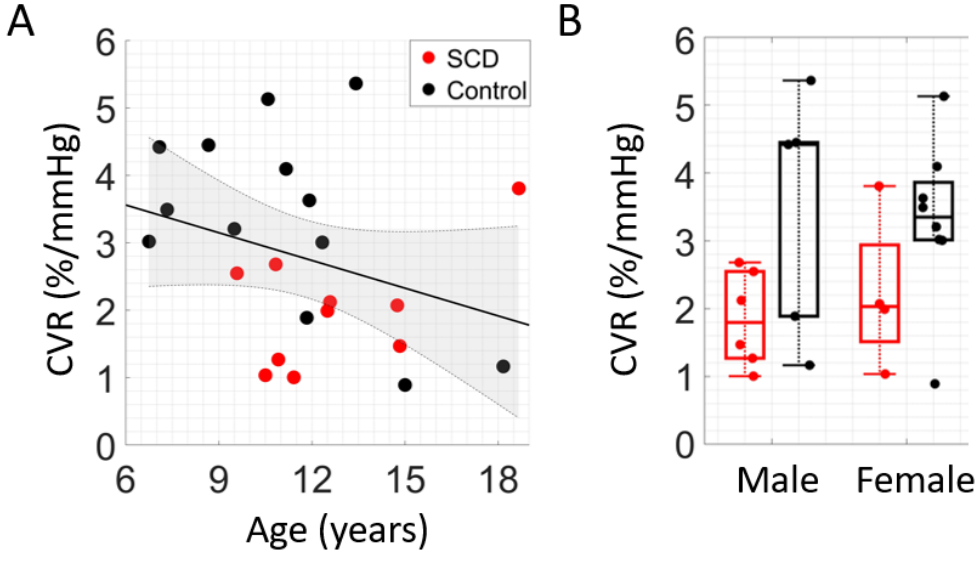

Figure 16. Association between breath-hold cerebrovascular reactivity (CVR) and demographic factors.
(A) Relationship between breath-hold CVR and age. Data points are color coded by group (red = SCD, black = control, N = 23). The solid line (black) represents the best linear fit and shaded region (gray) represents the 95% confidence interval. (B) Boxplot of CVR differences between sexes for SCD (red) and healthy controls (black).

3.3.4 Subgroup analysis of participants with enhanced brain sensitivity

The analysis presented in Sections 3.2-3.3 was repeated in a subgroup of participants with enhanced brain sensitivity, i.e., individuals for whom average resting-state $BFI(\rho_{short}) < BFI(\rho_{long})$ (7 SCD and 9 controls for breath-hold, **Figure 17**). Generally, similar trends were observed, although median [IQR] CVR differences between SCD and controls during the breath-hold paradigm became highly statistically significant (1.99 [1.15, 2.3] vs. 3.62 [3.2, 4.41] %/mmHg, p < 0.001, **Figure 17A**). The lag time between rBFI and EtCO2 was not statistically significant between groups (p = 0.98, **Figure 17B**). An inverse trend between CVR and age was still observed (p = 0.14, **Figure 17C**), and CVR was not different between sexes (**Figure 17D**). Finally, within the SCD group, a significant inverse correlation between CVR and reticulocyte count emerged (r = -0.90, p = 0.015; **Appendix 1,** Error! Reference source not found.); the remaining correlations with other hematological factors were not statistically significant.

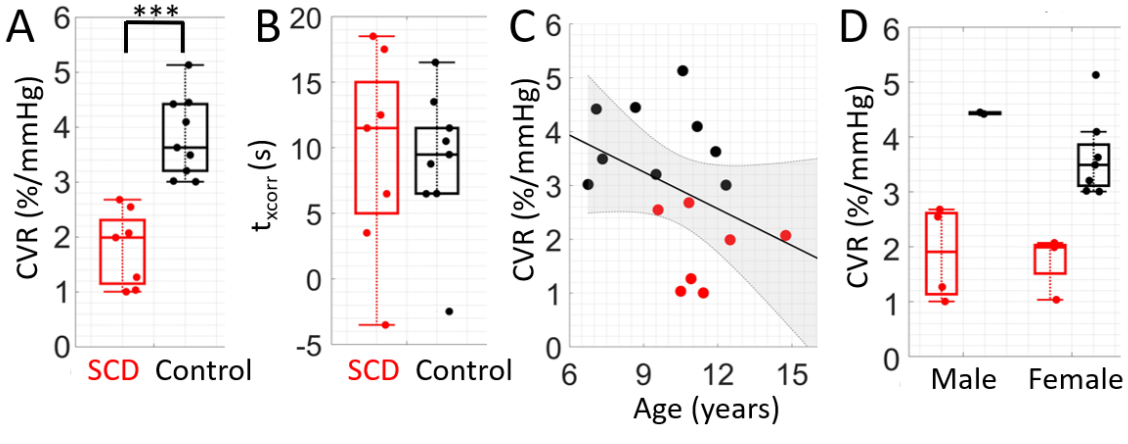

Figure 17. Subgroup analysis in participants with enhanced brain-sensitivity. Breath-hold paradigm results from individuals with average resting state $BFI(\rho_{short}) < BFI(\rho_{long})$. A) Boxplot of CVR (%/mmHg) in sickle cell (SCD, N=7) and control (N=9) groups. *** denotes p<0.001; significance was assessed with a Wilcoxon rank-sum test. B) Boxplots of t_{xcorr}, the time lag that yielded the highest correlation coefficient between blood flow and end tidal CO2 timeseries. (C) Relationship between CVR and age. The solid line (black) represents the best linear fit and shaded region (gray) represents the

95% confidence interval. (D) Boxplot of CVR in males vs. females. In all plots, red denotes SCD and black denotes controls.

3.4 Discussion

3.4.1 Breath-hold demonstrates CVR deficits in SCD children.

.

Here we use DCS for the first time to assess CVR in children with sickle cell disease compared to healthy controls. Using the breath-hold paradigm, we confirmed our primary hypothesis that CVR is significantly lower in SCD vs. controls (**Figure 13**). This trend agrees qualitatively with prior literature that observed CVR deficits with other modalities [210,261,262]. Quantitative comparison of our values to those previously published is challenging because of limitations in other datasets, including use of surrogate markers of CBF (e.g., BOLD signal change with MRI), or lack of EtCO2 monitoring to normalize the CBF response. Nevertheless, the ~40% decrease in CVR in SCD vs. controls is similar to the ~40-50% decrease previously reported with MRI using hypercapnia.[210,261,262] Thus, our results match expected trends, with the added advantage that they were obtained using a more tolerable and clinically-translatable breath-hold paradigm and lower cost optical neuromonitoring modality.

Breath-hold was well tolerated in this pediatric cohort. When asked to evaluate the difficulty of each experimental paradigm on a scale from 0-10, where 10 represents “easiest” and 0 indicates “hardest” difficulty, the median (IQR) breath-hold score was 8 (6.75,10) for SCD and 7 (8,5) for controls (

Figure 18). Comparatively, for the resting state paradigm, the qualitative median (IQR) score was 10 (10,8) for SCD and 8 (6,10) for controls. All participants completed the breath-hold exam, and compliance to the protocol was high (~80% of available epochs were included in the final analysis after applying our quality metrics). The main deviation we observed was the occasional need to adjust the breath-hold time per each participant’s

ability. To minimize the amount of equipment interfacing with the participant, we attempted to use a nasal cannula to monitor EtCO2. However, a subset of participants struggled to breathe exclusively through their nose and required frequent coaching during the exam. A properly-fitted mask that covers the nose and mouth is recommended for future studies to ensure high fidelity of the EtCO2 trace. Given the high compliance and ease of implementation, this work suggests that CVR assessment with breath-hold coupled with DCS may be feasible for routine screening of cerebrovascular dysfunction in children with SCD as young as 6y that may one day aid in assessing stroke[89] or guiding therapeutic management (e.g., blood transfusion) [274].

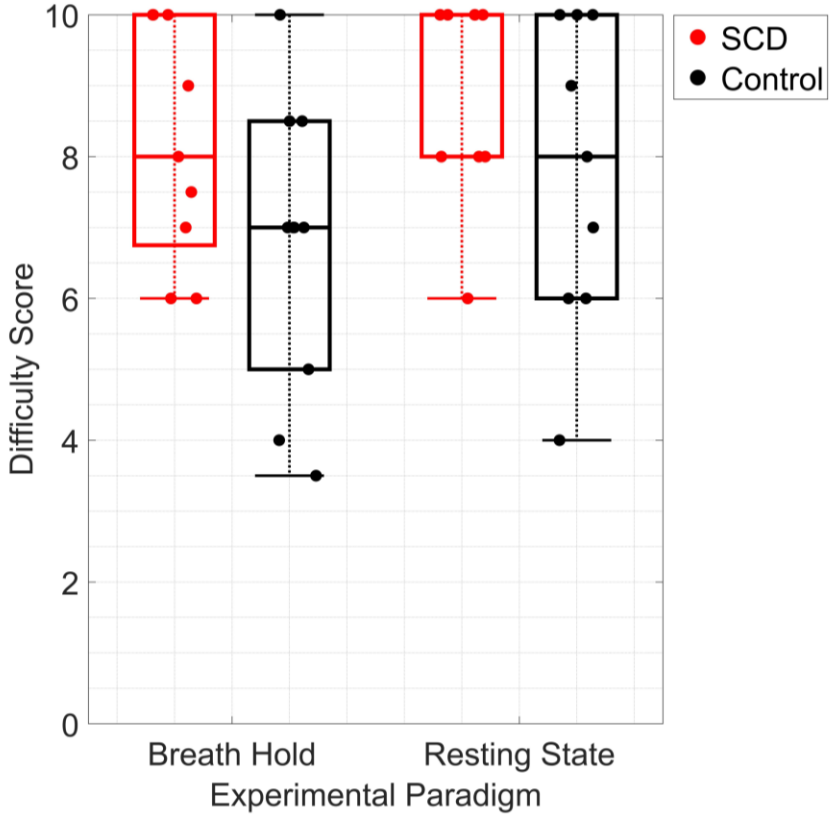

Figure 18. Qualitative evaluation of CVR paradigms.
Boxplot of difficulty score for each experimental paradigm for SCD (red, N=8) and healthy control (black, N=9) participants. Participants were asked "On a scale of 0 to 10, how difficult was the breath-hold/resting state exam?" where 10 represents "easiest" and 0 indicates "hardest" difficulty.

However, limitations in the breath-hold approach remain. First, a nontrivial fraction of data (N=6/29; ~21%) did not pass our quality control criteria (**Figure 12**). The reason for this poor pass rate is unclear. We noted a trend that resting $\mathrm{BFI}(\rho_{\mathrm{short}})$ was greater than $\mathrm{BFI}(\rho_{\mathrm{long}})$ in 30% of data that passed (N=7/23) versus 67% of data that failed (N=4/6), suggesting that brain sensitivity may be one factor that influences pass rate. Future work that enhances depth penetration using recent advances in DCS technology would be beneficial.[141] Second, repeatability along with the influence of the number of epochs, the length of each epoch, the differences between end-inspiration and end-expiration breath-holds[197], and time of day[275] were not quantified. Future work that explores variation in CVR across days/weeks would be valuable, particularly in children with SCD who often experience periods of relative hemodynamic instability, e.g., due to vaso-occlusive crisis. Third, while useful in an outpatient context given its ease of implementation, the breath-hold task requires active participation, which limits utility in younger children who may struggle to comply with long (20-30s) breath-holds, in patients with severe conditions, or in sedated individuals.[225,269] Fourth, inherent to the study protocol, EtCO2 data is lacking during the breath-hold, requiring interpolation during the period with null data. Finally, our estimation of CVR is predicated on the assumption of linearity between EtCO2 and CBF. Others have suggested more robust numerical approaches by convolving the EtCO2 signal with a hemodynamic response function that may help to account for any potential nonlinear behavior during the breath-hold.[224]

3.4.2 Resting state CVR

Contrary to breath-hold, differences in CVR between groups with the resting state paradigm were not observed. In the subset of participants who had both breath-hold and resting state exams available, we observed poor CVR agreement between the paradigms

(**Figure 15A**). This result, contrary to our hypothesis, suggests that the resting state and breath-hold exams do not yield equivalent CVR values among groups, perhaps indicating that an external stimulus is needed to invoke reliable changes in cerebral blood flow for CVR estimation when assessed by DCS. While assessment of CVR at rest would be ideal for integrating into a clinical workflow, more work is needed to elucidate the clinical value of this resting-state assessment with DCS.

3.4.3 Factors associated with CVR

In a secondary bivariable analysis, we explored the association of breath-hold CVR with age, sex, and hematologic factors (**Figure 16**; **Appendix 1,** Error! Reference source not found.**-10**). First, the weak, negative, trending but not significant association between CVR and age (**Figure 16A**) differed from the result observed by Leung and colleagues in which CVR assessed with BOLD-MRI changes in two phases; increasing until ~15 years of age then declining through 30 years of age.[120] Caution is warranted in interpreting this discrepancy. This difference may be due to the chosen modality, as the blood-oxygen-level-dependent MRI signal and the cerebral blood flow index DCS signal inherently measure different hemodynamic phenomena. Second, the lack of differences in CVR among sex we observed (**Figure 16B**, **Appendix 1,** Error! Reference source not found.) is consistent with other literature which demonstrated no sex differences.[276] Third, the lack of correlation between CVR and hematocrit concentration (**Appendix 1,** Error! Reference source not found.) differs from the positive association previously observed.[210] This difference may be attributable to the small SCD cohort size and the more limited range of hematocrit observed in our SCD population. Fourth, we observed an inverse correlation between CVR and reticulocyte count that became statistically significant in the sub-analysis of participants with enhanced brain-sensitivity (**Appendix 1,** Error! Reference

source not found.). This association, while preliminary, is a novel finding that may reflect a relationship between cerebrovascular health and disease severity. More work is needed to further explore and validate this finding.

3.4.4 Advantages of DCS as a CVR quantifying platform for children with SCD

The use of DCS as a CVR-quantifying device for routine assessments in clinical environments offers many strategic advantages over existing clinical neuromonitoring platforms. First, DCS is an economically viable alternative to existing neuromonitoring modalities. The capital investment required for a DCS system ($25-60K USD) is orders of magnitude less expensive than the capital investment required for an MRI ($500K-3M+ USD) and is comparable to TCD devices. Second, the small and portable form factor of DCS is comparable to existing TCD devices and far more advantageous than existing neuroimaging tools (e.g., MRI). Further, NIRS-based neuromonitoring devices have precedent as FDA-approved commercial medical devices (e.g., INVOS 7100 Regional Oximeter by Medtronic) further demonstrating the feasibility of diffuse optical tools into the clinical environment. Finally, the DCS-measured cerebral blood flow index is thought to be a more direct measure of microvascular CBF than existing bedside modalities like TCD or commercial NIRS. Taken together, DCS offers many unique advantages as a bedside portable CVR-quantifying platform in the clinical environment.

3.4.5 Study Limitations

This study is not without limitations. First, we did not randomize the order of the breath-hold and resting state paradigms among participants. While our experimental design was intended to provide a sufficient resting period prior to the breath-hold exam,

the best practice to avoid unintended systematic error would have been to randomize the order. Second, we did not acquire complete blood count panels in healthy children, limiting our ability to compare univariate associations with CVR between the SCD and control populations.

3.5 Conclusions

In this work, we demonstrate that diffuse correlation spectroscopy is sensitive to CVR impairments in children with sickle cell disease. This work suggests that bedside cerebrovascular function assessment using a breath-hold stimulus with DCS may be a feasible and potentially clinically useful technique to integrate into a routine outpatient clinical workflow for these patients.

3.6 Appendix 1: Summary of associations between CVR and demographic/hematologic factors

Table 9 provides a summary of the associations between CVR and demographic factors for the entire cohort (control and SCD children). **Table 10** provides a summary of the associations between CVR and hematologic factors for SCD participants.

Table 9 Bivariable analysis of breath-hold CVR and demographic factors.
Associations are presented in terms of the slope estimate for the line of best fit with 95% confidence intervals, along with Pearson's correlation coefficient (r) and p-values. Analysis was performed on the entire dataset (N = 23), and a sensitivity analysis on the subset with $BFI(\rho_{short}) < BFI(\rho_{long})$, indicative of enhanced brain sensitivity (N = 16).

	Full Dataset		**Subset Dataset BFI(ρ_{short}) < BFI(ρ_{long})**	
	Estimate (95% CI)	**r, p**	**Estimate (95% CI)**	**r, p**
Age (years)	-0.14 (-0.33, 0.05)	-0.31, 0.15	-0.28 (-0.53, 0.08)	-0.39, 0.13
Sex	0.37 (-0.83, 1.56)	0.14, 0.52	0.34 (-1.08, 1.76)	0.14, 0.61

Table 10 Bivariable analysis of breath-hold CVR and hematological factors within the sickle cell group
Associations are presented in terms of the slope estimate for the line of best fit with 95% confidence intervals, along with Pearson correlation coefficient (r) and p-values. Analysis was performed on the entire sickle group (N = 10), and a sensitivity analysis on the subset of individuals with $BFI(\rho_{short}) < BFI(\rho_{long})$, indicative of enhanced brain sensitivity (N= 7). Bolded text indicates statistical significance; p<0.05.

	Full Dataset		**Subset Dataset BFI(ρ_{short}) < BFI(ρ_{long})**	
	Estimate (95% CI)	**r, p**	**Estimate (95% CI)**	**r, p**
Hemoglobin	-0.06 (-0.51, 0.40)	-0.10, 0.78	-0.02 (-0.55, 0.51)	-0.04, 0.92
Hematocrit	-0.03 (-0.18, 0.12)	-0.14, 0.70	-0.02 (-0.18, 0.14)	-0.13, 0.78
Reticulocytes	-0.05 (-0.13 0.02)	-0.53, 0.15	**-0.06 (-0.10, -0.02)**	**-0.90, 0.01**
Fetal hemoglobin	-0.04 (-0.13, 0.04)	-0.38, 0.28	-0.01 (-0.10, 0.08)	-0.12, 0.80
Sickle hemoglobin	-0.01 (-0.11, 0.09)	-0.07, 0.86	0.01 (-0.14, 0.16)	0.12, 0.82

3.7 Appendix 2: Graphical User Interface to facilitate breath-holding

A graphical user interface (GUI) functioning as a rudimentary video game was developed in MATLAB to provide the participant end-user with a visual guide to facilitate the breath-hold examination. The GUI was designed to visually and functionally mimic a mechanical metronome to facilitate paced breathing prior to and after each breath-hold (**Figure 19**) in addition to help the participant prepare for and to time the duration of the end-expiration

breath-hold (**Figure 20**). The choice of a mechanical metronome as the visual display to the end-user was designed to provide a relatable experience for children who have exposure to practicing a musical instrument.

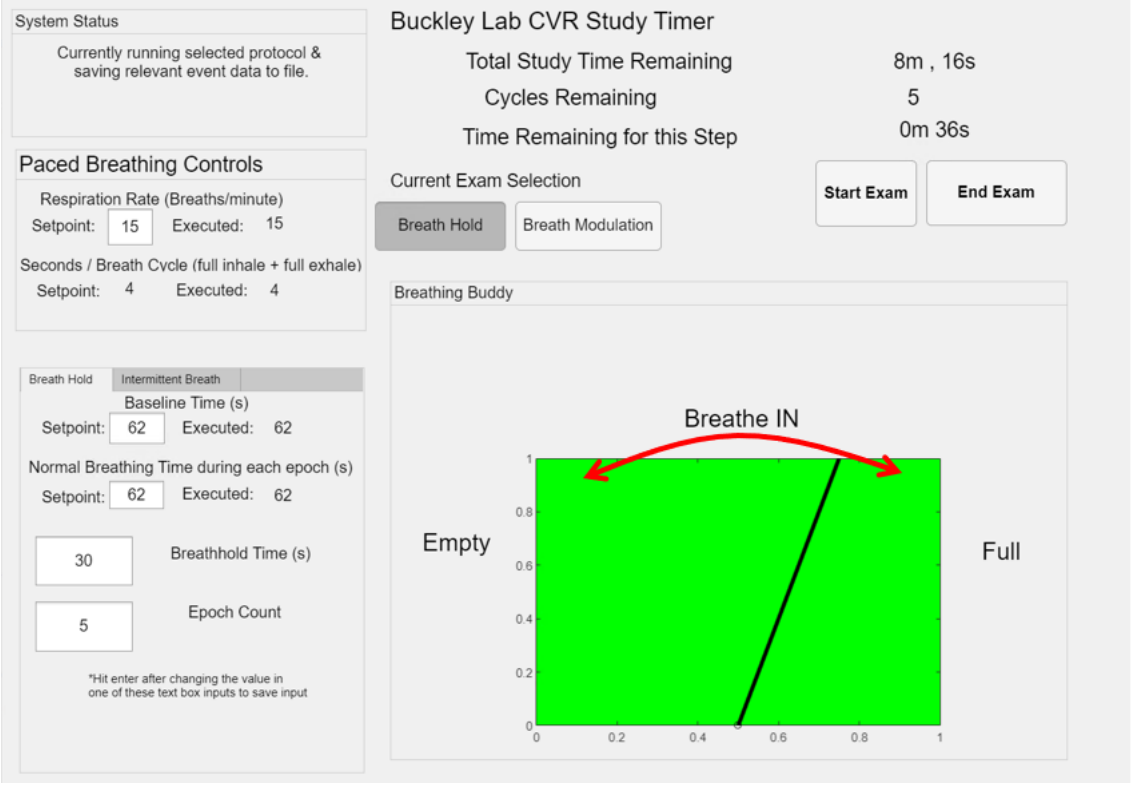

Figure 19 "Breathing Buddy" Graphical User Interface during paced breathing.
A visual depiction of the end-user interface used to guide participants in the breath-hold exam is provided for reference. User inputs are provided on the left-hand panel to control various exam parameters. Participants are instructed to watch the "Breathing Buddy" panel in the bottom right. The thick black line in this panel swings back and forth (red arrow, akin to a metronome) during the paced breathing portion of the breath-hold exam.

Figure 20 "Breathing Buddy" Graphical User Interface during breath-hold state.
A visual depiction of the end-user interface used to guide participants A) immediately before and B) during the breath-hold state.

Chapter 4 Conclusions

4.1 Original contributions

The following peer-reviewed journal articles derived from this work have been published:

1. **Kyle R. Cowdrick** et al. Agreement in cerebrovascular reactivity assessed with diffuse correlation spectroscopy across experimental paradigms improves with short separation regression. Neurophotonics 10 (2023). https://doi.org/10.1117/1.NPh.10.2.025002

The following publications derived from this work are in preparation:

1. **Kyle R. Cowdrick** et al. *Impaired cerebrovascular reactivity in pediatric sickle cell disease using diffuse correlation spectroscopy.* (Planned Q2 2023 submission to Biomedical Optics Express).
2. Tara Urner, **Kyle R. Cowdrick** et al. *Characterization of Pulsatile Microvascular Cerebral Blood Flow Waveforms Measured by Diffuse Correlation Spectroscopy* (In Review,Q2 2023 Biomedical Optics Express)

I have presented the various findings derived from this work at the following invited seminars:

1. May 2022: **Kyle R. Cowdrick, MSE**. *Comparison of Methods to Assess Cerebrovascular Reactivity in Healthy Adults Using Diffuse Correlation*

Spectroscopy. Invited in-person seminar for the Georgia Tech-Emory BME Department Departmental Seminar Series. Atlanta, GA. May 6, 2022.

2. February 2022: **Kyle R. Cowdrick, MSE**. E*nhancing the Scientific Value Proposition of Diffuse Optics in Pediatric Clinical Applications.* Invited in-person seminar for the VCU BME Department Graduate Seminar Series at Virginia Commonwealth University. Richmond, VA. February 22,2022.
3. September 2021: **Kyle R. Cowdrick, MSE**. D*iffuse Optics Seeking an Ideal Value-Added Clinical Application: Exploratory Research for Pediatric Settings.* Invited in-person seminar at The Institute of Photonic Sciences (ICFO). Barcelona, Spain. September 15, 2021. (Abstract)

I have presented the following peer-reviewed abstracts derived from this work in an oral presentation format at the following major conferences:

1. October 2022: **Kyle R Cowdrick** et al. *Agreement Among Experimental Cerebrovascular Reactivity Paradigms Assessed with Diffuse Correlation Spectroscopy Improves with Short Separation Regression.* Oral in-person presentation for the Society for fNIRS's 2022 conference. Boston, MA. October 10, 2022.
2. April 2022: **Kyle Cowdrick** et al. *Comparison of Methods to Assess Cerebrovascular Reactivity in Healthy Adults Using Diffuse Correlation Spectroscopy.* Oral in-person presentation for Optica's BioMed 2022 conference. Fort Lauderdale, Florida. April 25, 2022.
3. March 2021: **Kyle Cowdrick, MS**E, Erin Buckley PhD. *Comparison of Methods to Assess Cerebrovascular Reactivity Using Diffuse Correlation Spectroscopy.* SPIE BIOS 2021 Conference: Clinical and Translational Neurophotonics.

4.1.1 Aim 1

The results derived from Aim 1 resulted in a first validation that the more tolerable breath-hold experimental paradigm agrees strongly with the gold standard hypercapnia paradigm in healthy adult subjects measured by DCS when utilizing a specific numerical method, namely, a linear regression with a short separation regression. This finding lends more confidence that when comparing CVR results among these two experimental paradigms using this numerical approach, the CVR measured will yield a sufficiently accurate comparison with DCS. In this work, we were able to demonstrate that CVR assessments with DCS are feasible to perform in this study population regardless of experimental paradigm. Through our experimental design, we were able to provide a useful framework that can be leveraged for more systematic evaluations of CVR measured by DCS (discussed in **Chapter 4.2.1**). Further, with regards to the execution of the hypercapnia paradigm, we provide a very cost-effective method for performing these exams when compared to a computer-controlled approach[265], making the interventions more accessible to the broader research community.

4.1.2 Aim 2

The work presented in Aim 2 reflects the anticipated first published investigation in which DCS was used to assess CVR in a population of children with sickle cell disease. The primary contribution of this work is the demonstration that SCD children exhibit significant CVR deficits compared to healthy pediatric controls. In this aim, we demonstrate the feasibility of DCS to detect reductions in CVR in a SCD population, a result which is expected from existing literature using other modalities. Although more validation is required to confirm the findings of this pilot study in a larger cohort, this finding

lends support to the clinical value of DCS-measured CVR in a routine outpatient clinical workflow.

4.2 Recommendations for future study

Future directions are discussed in two broad categories, the first specific to the two aims presented in this dissertation and the second more broadly related to the overall theme of this dissertation, namely, further enhancing and discerning the clinical value of CVR assessments using DCS.

4.2.1 Recommended explorations concerning the robustness of CVR assessments by DCS.

The most natural progression of the work presented in this dissertation entails performing a systematic evaluation regarding the robustness of DCS-mediated CVR assessments as the repeatability of these measurements remains unexplored. Future work should assess CVR repeatability among hypercapnia, breath-hold, and resting state paradigms to determine the extent to which DCS-measured CVR is reliable. This recommendation would be a natural expansion of Aim 1 and would be most feasibly executed in clinically stable individuals such as healthy adults. To apply findings to children with SCD disease and expand upon Aim 2, this repeatability examination should also be performed in healthy children. An example experimental design would assess CVR among all 3 paradigms across multiple study days, e.g., using Day 1, 7, 30 days as a starting place for evaluation. The paradigms would be randomly ordered for a given study day. Given recent work[202] that has explored CVR assessments in healthy individuals using next generation NIRS platforms such as trNIRS and the known challenges in using NIRS-derived parameters as a proxy measurement of CBF, a repeatability assessment

that compares CVR derived from both DCS and a NIRS modality would add further value to the field by comparing the repeatability of CVR assessments between the two optical neuromonitoring modalities.

If the study framework above yields a conclusion that CVR assessments by optical neuromonitoring modalities are less repeatable than desired, future work can investigate whether alternative designs of the experimental paradigms or numerical methods used in Aim 1 can improve repeatability. When considering the former theme, for example, Aim 1 utilized a hypercapnia challenge that involved a "step design", or steady state inhalation of CO_2 for up to 6 minutes in duration. Other studies in fMRI have utilized hypercapnia "block " designs that involve shorter period (~1-2 minutes) of CO_2 inhalation but repeat the intervention 3-5 times after 1-3 minutes of rest.[6] The degree to which different designs within the experimental paradigms influence optically measured CVR repeatability is a topic ripe for exploration. Regarding the latter theme, two relatively simple numerical methods were utilized in Aim 1 to quantify CVR (linear regression, general linear model with short separation regression). Other numerical approaches have been extensively explored by the fMRI community[224,231] evaluating general linear models with additional regressors with the aim to assess the repeatability and reliability of the numerical techniques used to quantify CVR. It is recently suggested that the local CBF response to CO_2 can be characterized by non-linear behavior which may influence the calculation of CVR.[92] A thorough comparison of multiple numerical techniques would further aid our understanding concerning the robustness of optically derived measures of CVR.

4.2.2 Recommended explorations to discern the value of using optically derived CVR measures to address unmet clinical needs.

The work presented in this dissertation takes a first step in enhancing the clinical value proposition of CVR by exploring more accessible ways to assess this biomarker in outpatient clinical environments. However, more work is needed to discern the degree to which CVR assessment by DCS sufficiently addresses unmet clinical needs if such a platform is to be successfully translated from research concept to routine diagnostic reality. Three areas of further work are discussed briefly that if addressed, will further enhance the clinical value of DCS-mediated assessments of cerebrovascular function: voice of the customer research, outcomes-focused clinical research, and health economics research.

"Voice of the customer" research[43] refers to performing rigorous, systematic qualitative research with essential stakeholders in the healthcare value chain[277] and is used to identify promising targets for medtech innovation and de-risk the technology transfer of a potential medical device solution. VoC comprises performing clinical observations in healthcare environments and conducting informational interviews with key opinion leaders and diverse stakeholders to identify— or in the case of DCS as a cerebral neuromonitoring modality—validate perceived unmet clinical needs. The CVR field would greatly benefit from VoC research. It is imperative to validate whether a few essential hypotheses understood by the CVR and DCS research communities are shared among clinical providers and other essential healthcare stakeholders (e.g., including but not limited to nurses, advanced practice providers, payor stakeholders, healthcare finance stakeholders, investors):

1) "There is a strong clinical need for bedside CVR monitoring that if provided to physicians on-demand, CVR assessments can meaningfully reduce risk of adverse patient outcomes due to cerebrovascular dysfunction."

2) “Out of all possible biomarkers that assess cerebrovascular or neuronal health that are currently unavailable to clinicians, assessment of CVR is the most important clinical biomarker to quantify.”

3) “CVR measured by DCS optical neuromonitoring providers differentiated advantages compared to other neuromonitoring modalities such that it is the preferred approach for providing on-demand, bedside CVR assessments.”

Informational interview questions structured around these hypotheses can yield insights that when aggregated through appropriate qualitative research and design thinking techniques[43], can either validate these hypotheses or indicate that other targets for innovation would have a higher impact on healthcare delivery. To illustrate this point in reference to hypothesis #2, CVR is certainly not the only cerebral hemodynamic biomarker measurable by diffuse optical neuromonitoring tools that is of interest to clinicians. As discussed previously in **Chapter 1.5**, commercially available cwNIRS systems already provide a measure of regional oxygen saturation (rSO_2) to physicians in critical care and surgical settings while DCS can provide an assessment of CBF in addition to CVR.

A potentially exiting technical advancement which may serve as a more viable target for innovation, technology transfer, and clinical adoption when compared to CVR assessment by DCS is the use of diffuse optical spectroscopies to noninvasively quantify ICP. Recent proof of concept studies have demonstrated the ability of both DCS[278–281] and fdNIRS[278,282] systems to analyze the morphologic properties of CBF and hemoglobin-derived (e.g. HbO, HbT) pulsatile waveforms by using machine learning techniques and derive estimates of ICP. Initial validations of this approach has been demonstrated in non-human primate models[278,279,282] and in pediatric critical care populations[280,281] with heterogenous clinical indications. While exciting, there is much more work required to

demonstrate the clinical utility of this approach given the critical nature of ICP assessment requires a replacement noninvasive measure to have an extremely high degree of accuracy. Anecdotally, it is not difficult to recognize the value *prima facie* of a noninvasive ICP assessment with respect to the spiral innovation model. From a clinical perspective, any neurosurgery is associated with risk and surgical implantation of ICP monitors is no exception. The risk of intracranial hemorrhage can be as high as 10% in adults and higher in children while the risk of infection ranges from 5-20% when using ICP monitors with external ventricular drains.[283] Technical failures such as catheter displacement or blockage with biological debris may occur. While easily recognized, the ICP can be underestimated (e.g., in the case of blockage) and misrepresent a patient's brain status at a critical time where medical intervention could prevent neurologic injury.[283] It is a compelling prospect to provide accurate noninvasive assessments of ICP while completely eradicating these potential risks, especially when such risks are higher in pediatric populations. From an economic perspective, providing an accurate assessment of ICP without the use of a neurosurgical procedure may broadly enable cost savings to hospitals and insurance payors. From a technology perspective, while there are at least 12 competing technologies[284] under investigation to perform noninvasive ICP assessments, the many benefits of diffuse optical neuromonitoring techniques—DCS in particular— has been previously highlighted in **Chapter 1.5**. Conversely from a strategic perspective, there is a larger array of activity in CVR field (~4300 publications)*[4] compared to non-invasive measures of ICP (~1300 publications)*[5] suggesting CVR is a biomarker of greater interest in the cerebral neuromonitoring field. However, this may be due to the reality that interest in non-invasive ICP is a relatively newer concept, as it was ~2010 before a qualitatively exponential rise of publications in the available literature was

*[4] PubMed search terms; "cerebrovascular reactivity" OR "CVR"; 4/4/23
*[5] PubMed search terms: non-invasive ICP OR non-invasive intracranial pressure OR noninvasive ICP; 4/4/23

demonstrated compared to ~1990 for CVR. To expand upon and validate these anecdotal observations, systematic voice of the customer and ethnographic research (representative example provided[285]) is needed to determine the degree to which CVR monitoring is clinically useful compared to other available biomarkers of cerebral health such as noninvasive assessments of ICP.

Outcomes-focused clinical research is required to confirm that in a high-priority clinical indication (identified from both VoC research and a systematic review of the literature), impairments of CVR are associated with adverse clinical outcomes (e.g., neurologic morbidity, greater length of hospital stay, death). It is important to establish a clear link of CVR with outcome to demonstrate a strong value proposition which suggests that interventions aimed to treat and restore CVR impairments may reduce adverse outcomes. A focus on outcomes-based research would set the stage for interventional randomized clinical trials to investigate whether CVR assessment makes a strong impact in individualized disease management. Regardless if such trials would be required to secure FDA-approval of the technology, they would be necessary to support adoption of a CVR quantifying platform by physician end users and support the financial cost-benefit argument by hospital customers to purchase the platform. It is likely that outcomes-based research in CVR using DCS would be conducted in a multi-site manner leveraging the expertise of other global experts in DCS for cerebral neuromonitoring to reduce the time associated with conducting compelling outcomes-based research by expanding and diversifying the total available patient population.

Finally in tandem with outcomes-focused research, a foray into health economics research is required to support both the clinical and economic value proposition of CVR monitoring by DCS. As discussed in **Chapter 1.5.1.2**, existing cerebral optical neuromonitoring platforms based on the cwNIRS technique are currently not consistently

covered by insurance providers. Payment incentives are by no means a guarantee for NIRS-based neuromonitoring devices. Any financial argument to support the adoption of a CVR quantifying DCS platform would have to rely on demonstrating the ability of the platform to mitigate adverse patient outcomes and consequently, reduce the cost to the hospital/healthcare system. A health economics analysis would require examination of potential financial benefits to the system and the associated projected per-patient savings of decreased lengths of stay, decreased additional interventions required associated with adverse events (e.g., less need for rehabilitee therapy post-injury, decrease in pharmaceutical interventions, decrease in neurosurgical interventions). The implementation of this area of research is necessarily tied to conducting robust outcomes-focused studies through formal clinical trials. If observational studies of CVR assessment by DCS are unable to draw a link between CVR and adverse outcomes, interventional trials will not be able to process and consequently, there will be no viable economic argument to support successful transfer of a CVR quantifying DCS platform from research concept to routine clinical reality.

REFERENCES

1. Fisher, J. A. & Mikulis, D. J. Cerebrovascular Reactivity: Purpose, Optimizing Methods, and Limitations to Interpretation – A Personal 20-Year Odyssey of (Re)searching. *Front Physiol* **12**, 629651 (2021).

2. Clarke, D. D. & Sokoloff, L. Regulation of Cerebral Metabolic Rate. *Basic Neurochemistry: Molecular, Cellular and Medical Aspects. 6th edition* (1999).

3. Fantini, S., Sassaroli, A., Tgavalekos, K. T. & Kornbluth, J. Cerebral blood flow and autoregulation: current measurement techniques and prospects for noninvasive optical methods. *Neurophotonics* **3**, (2016).

4. Willie, C. K., Tzeng, Y.-C., Fisher, J. A. & Ainslie, P. N. Integrative regulation of human brain blood flow: Integrative regulation of human brain blood flow. *The Journal of Physiology* **592**, 841–859 (2014).

5. Markus, H. Cerebral perfusion and stroke. *J Neurol Neurosurg Psychiatry* **75**, 353–361 (2004).

6. Liu, P., De Vis, J. B. & Lu, H. Cerebrovascular reactivity (CVR) MRI with CO2 challenge: A technical review. *NeuroImage* (2018) doi:10.1016/j.neuroimage.2018.03.047.

7. De Vis, J. B. *et al.* Calibrated MRI to Evaluate Cerebral Hemodynamics in Patients with an Internal Carotid Artery Occlusion. *J Cereb Blood Flow Metab* **35**, 1015–1023 (2015).

8. Donahue, M. J. *et al.* Relationships between hypercarbic reactivity, cerebral blood flow, and arterial circulation times in patients with Moyamoya Disease. *J Magn Reson Imaging* **38**, (2013).

9. Gupta, A. *et al.* Cerebrovascular Reserve and Stroke Risk in Patients with Carotid Stenosis or Occlusion: A Systematic Review and Meta-Analysis. *Stroke* **43**, 2884–2891 (2012).

10. Mandell Daniel M. *et al.* Mapping Cerebrovascular Reactivity Using Blood Oxygen Level-Dependent MRI in Patients With Arterial Steno-occlusive Disease. *Stroke* **39**, 2021–2028 (2008).

11. Mikulis, D. J. *et al.* Preoperative and postoperative mapping of cerebrovascular reactivity in moyamoya disease by using blood oxygen level—dependent magnetic resonance imaging. *Journal of Neurosurgery* **103**, 347–355 (2005).

12. Marstrand J.R. *et al.* Cerebral Perfusion and Cerebrovascular Reactivity Are Reduced in White Matter Hyperintensities. *Stroke* **33**, 972–976 (2002).

13. Fujiwara, Y. *et al.* Simultaneous Impairment of Intracranial and Peripheral Artery Vasoreactivity in CADASIL Patients. *CED* **33**, 128–134 (2012).

14. Geranmayeh, F., Wise, R. J., Leech, R. & Murphy, K. Measuring Vascular Reactivity With Breath-Holds After Stroke: A Method to Aid Interpretation of Group-Level BOLD Signal Changes in Longitudinal fMRI Studies. *Hum Brain Mapp* **36**, 1755–1771 (2015).

15. Krainik Alexandre, Hund-Georgiadis Margret, Zysset Stefan, & von Cramon D. Yves. Regional Impairment of Cerebrovascular Reactivity and BOLD Signal in Adults After Stroke. *Stroke* **36**, 1146–1152 (2005).

16. Neu, P., Schlattmann, P., Schilling, A. & Hartmann, A. Cerebrovascular reactivity in major depression: a pilot study. *Psychosom Med* **66**, 6–8 (2004).

17. Markus, H. & Cullinane, M. Severely impaired cerebrovascular reactivity predicts stroke and TIA risk in patients with carotid artery stenosis and occlusion. *Brain* **124**, 457–467 (2001).

18. Silvestrini Mauro, Troisi Elio, Matteis Maria, Cupini Letizia M., & Caltagirone Carlo. Transcranial Doppler Assessment of Cerebrovascular Reactivity in Symptomatic and Asymptomatic Severe Carotid Stenosis. *Stroke* **27**, 1970–1973 (1996).

19. Webster, M. W. *et al.* Compromised cerebral blood flow reactivity is a predictor of stroke in patients with symptomatic carotid artery occlusive disease. *Journal of Vascular Surgery* **21**, 338–345 (1995).

20. Lee, J. K. *et al.* A pilot study of cerebrovascular reactivity autoregulation after pediatric cardiac arrest. *Resuscitation* **85**, 1387–1393 (2014).

21. Mathieu, F. *et al.* Continuous Near-Infrared Spectroscopy Monitoring in Adult Traumatic Brain Injury: A Systematic Review. *J Neurosurg Anesthesiol* (2019) doi:10.1097/ANA.0000000000000620.

22. Zeiler, F. A. *et al.* Intracranial and Extracranial Injury Burden as Drivers of Impaired Cerebrovascular Reactivity in Traumatic Brain Injury. *Journal of Neurotrauma* **35**, 1569–1577 (2018).

23. Zeiler, F. A. *et al.* Critical Thresholds of Intracranial Pressure-Derived Continuous Cerebrovascular Reactivity Indices for Outcome Prediction in Noncraniectomized Patients with Traumatic Brain Injury. *Journal of Neurotrauma* **35**, 1107–1115 (2017).

24. Zeiler, F. A. *et al.* Transcranial Doppler Systolic Flow Index and ICP-Derived Cerebrovascular Reactivity Indices in Traumatic Brain Injury. *J. Neurotrauma* **35**, 314–322 (2018).

25. Kenney, K. *et al.* Cerebral Vascular Injury in Traumatic Brain Injury. *Experimental Neurology* **275**, 353–366 (2016).

26. Diedler, J. *et al.* The limitations of near-infrared spectroscopy to assess cerebrovascular reactivity: the role of slow frequency oscillations. *Anesth. Analg.* **113**, 849–857 (2011).

27. Lavinio, A. *et al.* Cerebrovascular reactivity and autonomic drive following traumatic brain injury. *Acta Neurochir. Suppl.* **102**, 3–7 (2008).

28. Chan, S., Evans, K. C., Rosen, B. R., Song, T. & Kwong, K. K. A case study of magnetic resonance imaging of cerebrovascular reactivity: A powerful imaging marker for mild traumatic brain injury. *Brain Injury* **29**, 403–407 (2015).

29. Svaldi, D. O. *et al.* Cerebrovascular Reactivity Alterations in Asymptomatic High School Football Players. *Developmental Neuropsychology* **40**, 80–84 (2015).

30. Tsvetanov, K. A. *et al.* The effect of ageing on fMRI: Correction for the confounding effects of vascular reactivity evaluated by joint fMRI and MEG in 335 adults. *Human Brain Mapping* **36**, 2248–2269 (2015).

31. Song, Z., McDonough, I. M., Liu, P., Lu, H. & Park, D. C. Cortical amyloid burden and age moderate hippocampal activity in cognitively-normal adults. *NeuroImage: Clinical* **12**, 78–84 (2016).

32. Tchistiakova, E., Anderson, N. D., Greenwood, C. E. & MacIntosh, B. J. Combined effects of type 2 diabetes and hypertension associated with cortical thinning and impaired cerebrovascular reactivity relative to hypertension alone in older adults. *NeuroImage: Clinical* **5**, 36–41 (2014).

33. Liu, P. *et al.* Age-related differences in memory-encoding fMRI responses after accounting for decline in vascular reactivity. *NeuroImage* **78**, 415–425 (2013).

34. Liu, P. *et al.* A comparison of physiologic modulators of fMRI signals. *Human Brain Mapping* **34**, 2078–2088 (2013).

35. van Oers, C. A. M. M. *et al.* Contribution of the left and right inferior frontal gyrus in recovery from aphasia. A functional MRI study in stroke patients with preserved hemodynamic responsiveness. *NeuroImage* **49**, 885–893 (2010).

36. Kannurpatti, S. S. & Biswal, B. B. Detection and scaling of task-induced fMRI-BOLD response using resting state fluctuations. *NeuroImage* **40**, 1567–1574 (2008).

37. Biswal, B. B., Kannurpatti, S. S. & Rypma, B. Hemodynamic scaling of fMRI-BOLD signal: validation of low-frequency spectral amplitude as a scalability factor. *Magnetic Resonance Imaging* **25**, 1358–1369 (2007).

38. Thomason, M. E., Foland, L. C. & Glover, G. H. Calibration of BOLD fMRI using breath-holding reduces group variance during a cognitive task. *Human Brain Mapping* **28**, 59–68 (2007).

39. Li, T.-Q., Moseley, M. E. & Glover, G. A FAIR Study of Motor Cortex Activation under Normo- and Hypercapnia Induced by Breath Challenge. *NeuroImage* **10**, 562–569 (1999).

40. Hoge, R. D. *et al.* Investigation of BOLD signal dependence on cerebral blood flow and oxygen consumption: The deoxyhemoglobin dilution model. *Magnetic Resonance in Medicine* **42**, 849–863 (1999).

41. Davis, T. L., Kwong, K. K., Weisskoff, R. M. & Rosen, B. R. Calibrated functional MRI: Mapping the dynamics of oxidative metabolism. *Proc Natl Acad Sci U S A* **95**, 1834–1839 (1998).

42. Bright, M. G. & Murphy, K. Reliable quantification of BOLD fMRI cerebrovascular reactivity despite poor breath-hold performance. *Neuroimage* **83**, 559–568 (2013).

43. *Biodesign: the process of innovating medical technologies*. (Cambridge University Press, 2015).

44. Yazdi, Y. & Acharya, S. A New Model for Graduate Education and Innovation in Medical Technology. *Annals of Biomedical Engineering* **41**, 1822–1833 (2013).

45. Kinsel, D. Design Control Requirements for Medical Device Development. *World J Pediatr Congenit Heart Surg* **3**, 77–81 (2012).

46. Ornim Medical lays off most employees. *Globes* (2018).

47. Tress, E. E., Kochanek, P. M., Saladino, R. A. & Manole, M. D. Cardiac arrest in children. *J Emerg Trauma Shock* **3**, 267–272 (2010).

48. Kleinman, M. E. *et al.* Part 14: Pediatric Advanced Life Support: 2010 American Heart Association Guidelines for Cardiopulmonary Resuscitation and Emergency Cardiovascular Care. *Circulation* **122**, S876–S908 (2010).

49. Kattwinkel, J. *et al.* Part 15: Neonatal Resuscitation: 2010 American Heart Association Guidelines for Cardiopulmonary Resuscitation and Emergency Cardiovascular Care. *Circulation* **122**, S909–S919 (2010).

50. Kurz, J. E., Smith, C. M. & Wainwright, M. S. Thermoregulate, autoregulate and ventilate: brain-directed critical care for pediatric cardiac arrest. *Curr. Opin. Pediatr.* **29**, 259–265 (2017).

51. Nolan, J. P. *et al.* Post-cardiac arrest syndrome: Epidemiology, pathophysiology, treatment, and prognostication. *Resuscitation* **79**, 350–379 (2008).

52. White, B. C. *et al.* Global brain ischemia and reperfusion. *Ann Emerg Med* **27**, 588–594 (1996).

53. van den Brule, J. M. D., van der Hoeven, J. G. & Hoedemaekers, C. W. E. Cerebral Perfusion and Cerebral Autoregulation after Cardiac Arrest. *Biomed Res Int* **2018**, (2018).

54. Lee, J. K. *et al.* A pilot study of cerebrovascular reactivity autoregulation after pediatric cardiac arrest. *Resuscitation* **85**, 1387–1393 (2014).

55. Lovett, M. E., Maa, T., Chung, M. G. & O'Brien, N. F. Cerebral blood flow velocity and autoregulation in paediatric patients following a global hypoxic-ischaemic insult. *Resuscitation* **126**, 191–196 (2018).

56. Ameloot, K. *et al.* An observational near-infrared spectroscopy study on cerebral autoregulation in post-cardiac arrest patients: Time to drop 'one-size-fits-all' hemodynamic targets? *Resuscitation* **90**, 121–126 (2015).

57. Sundgreen, C. *et al.* Autoregulation of cerebral blood flow in patients resuscitated from cardiac arrest. *Stroke* **32**, 128–132 (2001).

58. Pham, P., Bindra, J., Chuan, A., Jaeger, M. & Aneman, A. Are changes in cerebrovascular autoregulation following cardiac arrest associated with neurological outcome? Results of a pilot study. *Resuscitation* **96**, 192–198 (2015).

59. Beckstead, J. E., Tweed, W. A., Lee, J. & MacKeen, W. L. Cerebral blood flow and metabolism in man following cardiac arrest. *Stroke* **9**, 569–573 (1978).

60. Aaslid, R., Lindegaard, K. F., Sorteberg, W. & Nornes, H. Cerebral autoregulation dynamics in humans. *Stroke* **20**, 45–52 (1989).

61. Mangus, D. B. *et al.* A systematic review of neuroprotective strategies after cardiac arrest: from bench to bedside (Part I – Protection via specific pathways). *Med Gas Res* **4**, 9 (2014).

62. Laurikkala, J. *et al.* Association of deranged cerebrovascular reactivity with brain injury following cardiac arrest: a post-hoc analysis of the COMACARE trial. *Crit Care* **25**, 350 (2021).

63. Balouris, S. A. *et al.* Development and validation of the Cerebral Performance Categories-Extended (CPC-E). *Resuscitation* **94**, 98–105 (2015).

64. Rittenberger, J. C., Raina, K., Holm, M. B., Kim, Y. J. & Callaway, C. W. Association between Cerebral Performance Category, Modified Rankin Scale, and Discharge Disposition after Cardiac Arrest. *Resuscitation* **82**, 1036–1040 (2011).

65. Elmer, J. & Callaway, C. W. The Brain after Cardiac Arrest. *Semin Neurol* **37**, 19–24 (2017).

66. Kavanagh, P. L., Fasipe, T. A. & Wun, T. Sickle Cell Disease: A Review. *JAMA* **328**, 57–68 (2022).

67. Juttukonda, M. R., Vaclavu, L., Kirkham, F. J., Fields, M. E. & Bush, A. M. Editorial: Cerebral oxygen supply and demand in sickle cell disease: Evidence of local ischemia despite global hyperemia. *Frontiers in Physiology* **13**, (2022).

68. Juttukonda, M. R. *et al.* Differential cerebral hemometabolic responses to blood transfusions in adults and children with sickle cell anemia. *Journal of Magnetic Resonance Imaging* **49**, 466–477 (2019).

69. Ford, A. L. *et al.* Silent infarcts in sickle cell disease occur in the border zone region and are associated with low cerebral blood flow. *Blood* **132**, 1714–1723 (2018).

70. DeBaun, M. R. *et al.* Silent cerebral infarcts: a review on a prevalent and progressive cause of neurologic injury in sickle cell anemia. *Blood* **119**, 4587–96 (2012).

71. Wang, W. *et al.* Neuropsychologic performance in school-aged children with sickle cell disease: a report from the Cooperative Study of Sickle Cell Disease. *The Journal of pediatrics* **139**, 391–7 (2001).

72. Schatz, J., Brown, R. T., Pascual, J. M., Hsu, L. & DeBaun, M. R. Poor school and cognitive functioning with silent cerebral infarcts and sickle cell disease. *Neurology* **56**, 1109–11 (2001).

73. Kim, Y. S. *et al.* Dynamic cerebral autoregulation in homozygous Sickle cell disease. *Stroke; a journal of cerebral circulation* **40**, 808–14 (2009).

74. Macedo-Campos, R. de S., Adegoke, S. A., Figueiredo, M. S., Braga, J. A. P. & Silva, G. S. Cerebral Vasoreactivity in Children with Sickle Cell Disease: A Transcranial Doppler Study. *Journal of Stroke and Cerebrovascular Diseases* **27**, 2703–2706 (2018).

75. Kosinski, P. D. *et al.* The severity of anaemia depletes cerebrovascular dilatory reserve in children with sickle cell disease: a quantitative magnetic resonance imaging study. *British Journal of Haematology* **176**, 280–287 (2017).

76. Kim, J. A., Leung, J., Lerch, J. P. & Kassner, A. Reduced cerebrovascular reserve is regionally associated with cortical thickness reductions in children with sickle cell disease. *Brain Research* **1642**, 263–269 (2016).

77. Kedar, A., Drane, W. E., Shaeffer, D., Nicole, M. & Adams, C. Measurement of cerebrovascular flow reserve in pediatric patients with sickle cell disease. *Pediatric Blood & Cancer* **46**, 234–238 (2006).

78. Prohovnik, I., Hurlet-Jensen, A., Adams, R., De Vivo, D. & Pavlakis, S. G. Hemodynamic Etiology of Elevated Flow Velocity and Stroke in Sickle-Cell Disease. *J Cereb Blood Flow Metab* **29**, 803–810 (2009).

79. Václavů, L. *et al.* Hemodynamic provocation with acetazolamide shows impaired cerebrovascular reserve in adults with sickle cell disease. *Haematologica* **104**, 690–699 (2018).

80. Nur, E. *et al.* Cerebrovascular reserve capacity is impaired in patients with sickle cell disease. *Blood* **114**, 3473–3478 (2009).

81. Fields, M. E. *et al.* Regional oxygen extraction predicts border zone vulnerability to stroke in sickle cell disease. *Neurology* **90**, e1134–e1142 (2018).

82. Juttukonda, M. R. *et al.* Differential cerebral hemometabolic responses to blood transfusions in adults and children with sickle cell anemia. *Journal of Magnetic Resonance Imaging* **49**, 466–477 (2019).

83. Jordan, L. C. *et al.* Non-invasive imaging of oxygen extraction fraction in adults with sickle cell anaemia. *Brain* **139**, 738–750 (2016).

84. Quinn, C. T. & Dowling, M. M. Cerebral Tissue Hemoglobin Saturation in Children with Sickle Cell Disease. *Pediatr Blood Cancer* **59**, 881–887 (2012).

85. Raj, A., Bertolone, S. J., Mangold, S. & Edmonds, H. L. Assessment of cerebral tissue oxygenation in patients with sickle cell disease: effect of transfusion therapy. *J. Pediatr. Hematol. Oncol.* **26**, 279–283 (2004).

86. Ford, A. L. *et al.* Silent infarcts in sickle cell anemia occur in the borderzone region and are associated with low cerebral blood flow. *Blood* blood-2018-04-841247 (2018) doi:10.1182/blood-2018-04-841247.

87. Jordan, L. C. & DeBaun, M. R. Cerebral hemodynamic assessment and neuroimaging across the lifespan in sickle cell disease. *J Cereb Blood Flow Metab* **38**, 1438–1448 (2018).

88. Stotesbury, H. *et al.* Vascular Instability and Neurological Morbidity in Sickle Cell Disease: An Integrative Framework. *Front Neurol* **10**, (2019).

89. DeBaun, M. R. *et al.* American Society of Hematology 2020 guidelines for sickle cell disease: prevention, diagnosis, and treatment of cerebrovascular disease in children and adults. *Blood Adv* **4**, 1554–1588 (2020).

90. Munn, Z. & Jordan, Z. The patient experience of high technology medical imaging: a systematic review of the qualitative evidence. *JBI Evidence Synthesis* **9**, 631 (2011).

91. Dewey, M., Schink, T. & Dewey, C. F. Claustrophobia during magnetic resonance imaging: Cohort study in over 55,000 patients. *Journal of Magnetic Resonance Imaging* **26**, 1322–1327 (2007).

92. Duffin, J. *et al.* Cerebrovascular Resistance: The Basis of Cerebrovascular Reactivity. *Front. Neurosci.* **12**, (2018).

93. Sørensen, H. Is cerebral monitoring useful? Focus must shift from mere observation to testing interventions. *Acta Anaesthesiol Scand* (2020) doi:10.1111/aas.13562.

94. Brassard, P. *et al.* Losing the dogmatic view of cerebral autoregulation. *Physiological Reports* **9**, e14982 (2021).

95. Petersen, N. H. Bedside Assessment of Cerebral Autoregulation: Working Toward a Common Monitoring Standard. *Neurocrit Care* (2021) doi:10.1007/s12028-021-01304-2.

96. Brady, K. M. *et al.* Personalizing the Definition of Hypotension to Protect the Brain: *Anesthesiology* 1 (2019) doi:10.1097/ALN.0000000000003005.

97. Kooi, E. M. W. & Richter, A. E. Cerebral Autoregulation in Sick Infants: Current Insights. *Clin Perinatol* **47**, 449–467 (2020).

98. Duffin, J., Mikulis, D. J. & Fisher, J. A. Control of Cerebral Blood Flow by Blood Gases. *Front. Physiol.* **12**, (2021).

99. Das, A., Murphy, K. & Drew, P. J. Rude mechanicals in brain haemodynamics: non-neural actors that influence blood flow. *Philosophical Transactions of the Royal Society B: Biological Sciences* **376**, 20190635 (2021).

100. Ainslie, P. N. & Duffin, J. Integration of cerebrovascular CO2 reactivity and chemoreflex control of breathing: mechanisms of regulation, measurement, and interpretation. *Am. J. Physiol. Regul. Integr. Comp. Physiol.* **296**, R1473-1495 (2009).

101. Iadecola, C. The Neurovascular Unit Coming of Age: A Journey through Neurovascular Coupling in Health and Disease. *Neuron* **96**, 17–42 (2017).

102. Grubb, S. *et al.* Precapillary sphincters maintain perfusion in the cerebral cortex. *Nature Communications* **11**, 1–12 (2020).

103. Atkinson, J. L. D., Anderson, R. E. & Sundt, T. M. The effect of carbon dioxide on the diameter of brain capillaries. *Brain Research* **517**, 333–340 (1990).

104. *Cerebral blood flow and metabolism*. (Lippincott Williams & Wilkins, 2002).

105. Busija, D. W. & Heistad, D. D. Factors involved in the physiological regulation of the cerebral circulation. *Rev Physiol Biochem Pharmacol* **101**, 161–211 (1984).

106. Wei, E. P., Kontos, H. A. & Patterson, J. L. Dependence of pial arteriolar response to hypercapnia on vessel size. *Am J Physiol* **238**, 697–703 (1980).

107. Attwell, D. *et al.* Glial and neuronal control of brain blood flow. *Nature* **468**, 232–243 (2010).

108. Lindauer, U., Megow, D., Matsuda, H. & Dirnagl, U. Nitric oxide: a modulator, but not a mediator, of neurovascular coupling in rat somatosensory cortex. *Am J Physiol* **277**, H799-811 (1999).

109. Purves, D. *et al.* Neuroglial Cells. *Neuroscience. 2nd edition* (2001).

110. Attwell, D., Mishra, A., Hall, C. N., O'Farrell, F. M. & Dalkara, T. What is a pericyte? *J Cereb Blood Flow Metab* **36**, 451–455 (2016).

111. Itoh, Y. & Suzuki, N. Control of brain capillary blood flow. *J. Cereb. Blood Flow Metab.* **32**, 1167–1176 (2012).

112. Hall, C. N. *et al.* Capillary pericytes regulate cerebral blood flow in health and disease. *Nature* **508**, 55–60 (2014).

113. Puro, D. G. Physiology and pathobiology of the pericyte-containing retinal microvasculature: new developments. *Microcirculation* **14**, 1–10 (2007).

114. Peppiatt, C. M., Howarth, C., Mobbs, P. & Attwell, D. Bidirectional control of CNS capillary diameter by pericytes. *Nature* **443**, 700–704 (2006).

115. Jill Hunter, Douglas Nordli, & John Dashe. Approach to neuroimaging in children - UpToDate. *UptoDate* Topic 6156 Version 20.0 (2019).

116. Giovannella, M. *et al.* Validation of diffuse correlation spectroscopy against 15O-water PET for regional cerebral blood flow measurement in neonatal piglets: *Journal of Cerebral Blood Flow & Metabolism* (2019) doi:10.1177/0271678X19883751.

117. Smeeing, D. P. J., Hendrikse, J., Petersen, E. T., Donahue, M. J. & de Vis, J. B. Arterial Spin Labeling and Blood Oxygen Level-Dependent MRI Cerebrovascular Reactivity in Cerebrovascular Disease: A Systematic Review and Meta-Analysis. *Cerebrovasc. Dis.* **42**, 288–307 (2016).

118. Watchmaker, J. M. *et al.* Hemodynamic mechanisms underlying elevated oxygen extraction fraction (OEF) in moyamoya and sickle cell anemia patients. *J Cereb Blood Flow Metab* **38**, 1618–1630 (2018).

119. De Vis, J. b. *et al.* Age-related changes in brain hemodynamics; A calibrated MRI study. *Human Brain Mapping* **36**, 3973–3987 (2015).

120. Leung, J., Kosinski, P. D., Croal, P. L. & Kassner, A. Developmental trajectories of cerebrovascular reactivity in healthy children and young adults assessed with magnetic resonance imaging. *The Journal of Physiology* **594**, 2681–2689 (2016).

121. D'Andrea, A. *et al.* Transcranial Doppler Ultrasound: Physical Principles and Principal Applications in Neurocritical Care Unit. *J Cardiovasc Echogr* **26**, 28–41 (2016).

122. Purkayastha, S. & Sorond, F. Transcranial Doppler Ultrasound: Technique and Application. *Semin Neurol* **32**, 411–420 (2012).

123. Lagopoulos, J. Cerebral autoregulation. *Acta Neuropsychiatrica* **20**, 271–272 (2008).

124. Meel-van den Abeelen, A. S. S., van Beek, A. H. E. A., Slump, C. H., Panerai, R. B. & Claassen, J. A. H. R. Transfer function analysis for the assessment of cerebral autoregulation using spontaneous oscillations in blood pressure and cerebral blood flow. *Medical Engineering & Physics* **36**, 563–575 (2014).

125. Royl, G. *et al.* Hypothermia effects on neurovascular coupling and cerebral metabolic rate of oxygen. *NeuroImage* **40**, 1523–1532 (2008).

126. Naqvi, J., Yap, K. H., Ahmad, G. & Ghosh, J. Transcranial Doppler Ultrasound: A Review of the Physical Principles and Major Applications in Critical Care. *International Journal of Vascular Medicine* **2013**, e629378 (2013).

127. Han, S. J. *et al.* The Presto 1000: A novel automated transcranial Doppler ultrasound system. *J Clin Neurosci* **22**, 1771–1775 (2015).

128. Lucid™ TCD 2.0. *NovaSignal* https://novasignal.com/solutions/lucid-tcd/.

129. PhysioSonics Announces FDA Clearance for Presto 1000 Flow Monitor for Ultrasound Cranial Monitoring. *Imaging Technology News* https://www.itnonline.com/content/physiosonics-announces-fda-clearance-presto-1000-flow-monitor-ultrasound-cranial-monitoring (2013).

130. NovaSignal- About. *NovaSignal* https://novasignal.com/company/about/.

131. Liebeskind, D. *SONAS Ultrasound Device for the Detection of Ischemic and Hemorrhagic Stroke*. https://clinicaltrials.gov/ct2/show/NCT03296852 (2019).

132. NovaSignal Corp. *RoBotic TCD Ultrasound BubbLe Study Compared to Transthoracic Echocardiography for Detection of Right to Left Shunt*. https://clinicaltrials.gov/ct2/show/NCT04604015 (2020).

133. Gore, J. C. Principles and practice of functional MRI of the human brain. *J Clin Invest* **112**, 4–9 (2003).

134. Li, Z., Zhu, Y., Childress, A. R., Detre, J. A. & Wang, Z. Relations between BOLD fMRI-Derived Resting Brain Activity and Cerebral Blood Flow. *PLOS ONE* **7**, e44556 (2012).

135. Simon, A. B. & Buxton, R. B. Understanding the dynamic relationship between cerebral blood flow and the BOLD signal: Implications for quantitative functional MRI. *Neuroimage* **116**, 158–167 (2015).

136. Pernet, C. R. Misconceptions in the use of the General Linear Model applied to functional MRI: a tutorial for junior neuro-imagers. *Front. Neurosci.* **8**, (2014).

137. Monti, M. M. Statistical Analysis of fMRI Time-Series: A Critical Review of the GLM Approach. *Front. Hum. Neurosci.* **5**, (2011).

138. Lindquist, M. A., Loh, J. M., Atlas, L. Y. & Wager, T. D. Modeling the Hemodynamic Response Function in fMRI: Efficiency, Bias and Mis-modeling. *Neuroimage* **45**, S187–S198 (2009).

139. Liu, P. *et al.* Multi-vendor and multisite evaluation of cerebrovascular reactivity mapping using hypercapnia challenge. *NeuroImage* **245**, 118754 (2021).

140. Sobczyk, O. *et al.* The Reproducibility of Cerebrovascular Reactivity Across MRI Scanners. *Front. Physiol.* **12**, (2021).

141. Ayaz, H. *et al.* Optical imaging and spectroscopy for the study of the human brain: status report. *NPh* **9**, S24001 (2022).

142. Cournoyer, A. *et al.* Near-infrared Spectroscopy Monitoring During Cardiac Arrest: A Systematic Review and Meta-analysis. *Acad Emerg Med* **23**, 851–862 (2016).

143. Kocsis, L., Herman, P. & Eke, A. The modified Beer–Lambert law revisited. *Phys. Med. Biol.* **51**, N91–N98 (2006).

144. Durduran, T., Choe, R., Baker, W. B. & Yodh, A. G. Diffuse optics for tissue monitoring and tomography. *Rep. Prog. Phys.* **73**, 43 (2010).

145. Mccormick, P. W. *et al.* Noninvasive cerebral optical spectroscopy for monitoring cerebral oxygen delivery and hemodynamics. *Critical Care Medicine* **19**, 89–97 (1991).

146. Khozhenko, A., Lamperti, M., Terracina, S. & Bilotta, F. Can Cerebral Near-infrared Spectroscopy Predict Cerebral Ischemic Events in Neurosurgical Patients? A Narrative Review of the Literature. *Journal of Neurosurgical Anesthesiology* **31**, 378–384 (2019).

147. Finucane, E., Jooste, E. & Machovec, K. A. Neuromonitoring Modalities in Pediatric Cardiac Anesthesia: A Review of the Literature. *Journal of Cardiothoracic and Vascular Anesthesia* **34**, 3420–3428 (2020).

148. Maas, A. I. R. & Citerio, G. Noninvasive monitoring of cerebral oxygenation in traumatic brain injury: a mix of doubts and hope. *Intensive Care Med* **36**, 1283–1285 (2010).

149. Kahn, R. A. & Anyanwu, A. Near-infrared spectroscopy in vegetables and humans: An observational study. *Eur J Anaesthesiol* **35**, 907–910 (2018).

150. Genbrugge, C. *et al.* Regional Cerebral Oximetry During Cardiopulmonary Resuscitation: Useful or Useless? *J Emerg Med* **50**, 198–207 (2016).

151. Fantini, S. & Sassaroli, A. Frequency-Domain Techniques for Cerebral and Functional Near-Infrared Spectroscopy. *Frontiers in Neuroscience* **14**, (2020).

152. Ferrari, M. & Quaresima, V. A brief review on the history of human functional near-infrared spectroscopy (fNIRS) development and fields of application. *NeuroImage* **63**, 921–935 (2012).

153. Scholkmann, F. *et al.* A review on continuous wave functional near-infrared spectroscopy and imaging instrumentation and methodology. *NeuroImage* **85**, 6–27 (2014).

154. Quaresima, V. & Ferrari, M. Functional Near-Infrared Spectroscopy (fNIRS) for Assessing Cerebral Cortex Function During Human Behavior in Natural/Social Situations: A Concise Review. *Organizational Research Methods* **22**, 46–68 (2019).

155. Westgarth, M. M. P., Hogan, C. A., Neumann, D. L. & Shum, D. H. K. A systematic review of studies that used NIRS to measure neural activation during emotion processing in healthy individuals. *Social Cognitive and Affective Neuroscience* **16**, 345–369 (2021).

156. Medtronic Patient Monitoring Division. INVOS™ 7100 Cerebral Oximetry System | Medtronic. *Medtronic* https://www.medtronic.com/covidien/en-us/products/cerebral-somatic-oximetry/invos-7100-system.html (2023).

157. Masimo Corporation. Root with O3 Regional Oximetry. *Masimo* https://www.masimo.com/technology/brain-monitoring/cerebral-oximetry/ (2023).

158. Edwards Life Sciences. ForeSight tissue oximetry sensor. *www.edwards.com* https://www.edwards.com/healthcare-professionals/products-services/tissue-oximetry/foresight (2023).

159. Nonin Medical Corporation. Cerebral and Tissue Oximetry (Nonin SenSmart X-100 Specifications). *Nonin Medical Corporation* https://www.nonin.com/technologies/cerebral-tissue-oximetry/ (2023).

160. Medtronic. 2022 Billing and Coding Guidelines: Invos cerebral/somatic oximetry. (2022).

161. Schwarz, G., Litscher, G., Kleinert, R. & Jobstmann, R. Cerebral Oximetry in Dead Subjects. *Journal of Neurosurgical Anesthesiology* **8**, 189–193 (1996).

162. Cardim, D. & Griesdale, D. E. Near-infrared spectroscopy: unfulfilled promises. *British Journal of Anaesthesia* **121**, 523–526 (2018).

163. Lewis, C., Parulkar, S. D., Bebawy, J., Sherwani, S. & Hogue, C. W. Cerebral Neuromonitoring During Cardiac Surgery: A Critical Appraisal With an Emphasis on Near-Infrared Spectroscopy. *Journal of Cardiothoracic and Vascular Anesthesia* **32**, 2313–2322 (2018).

164. Maillard, J., Sologashvili, T., Diaper, J., Licker, M.-J. & Keli Barcelos, G. A Case of Persistence of Normal Tissue Oxygenation Monitored by Near-Infrared Spectroscopy (NIRS) Values Despite Prolonged Perioperative Cardiac Arrest. *Am J Case Rep* **20**, 21–25 (2019).

165. Schneider, A. *et al.* Comparison of four near-infrared spectroscopy devices shows that they are only suitable for monitoring cerebral oxygenation trends in preterm infants. *Acta Paediatr.* **103**, 934–938 (2014).

166. Boas, D. A. & Franceschini, M. A. Haemoglobin oxygen saturation as a biomarker: the problem and a solution. *Philos Trans A Math Phys Eng Sci* **369**, 4407–4424 (2011).

167. Grant, P. E. *et al.* Increased cerebral blood volume and oxygen consumption in neonatal brain injury. *J Cereb Blood Flow Metab* **29**, 1704–1713 (2009).

168. Roche-Labarbe, N. *et al.* Noninvasive optical measures of CBV, StO2, CBF index, and rCMRO2 in human premature neonates' brains in the first six weeks of life. *Human Brain Mapping* **31**, 341–352 (2010).

169. Davidson, A. & Skowno, J. Neuromonitoring in paediatric anaesthesia. *Current Opinion in Anesthesiology* **32**, 370–376 (2019).

170. Clark, J. B., Barnes, M. L., Undar, A. & Myers, J. L. Multimodality neuromonitoring for pediatric cardiac surgery: our approach and a critical appraisal of the available evidence. *World J Pediatr Congenit Heart Surg* **3**, 87–95 (2012).

171. Young, A. M. H. *et al.* Multimodality neuromonitoring in severe pediatric traumatic brain injury. *Pediatr Res* **83**, 41–49 (2018).

172. Strike, S. A. *et al.* Intraoperative Neuromonitoring in Pediatric and Adult Spine Deformity Surgery: *Clinical Spine Surgery* **30**, E1174–E1181 (2017).

173. Bembea, M. M., Felling, R., Anton, B., Salorio, C. F. & Johnston, M. V. Neuromonitoring During Extracorporeal Membrane Oxygenation: A Systematic Review of the Literature. *Pediatric Critical Care Medicine* **16**, 558–564 (2015).

174. Galgano, M. A. & Tovar-Spinoza, Z. Multimodality Neuromonitoring in Pediatric Neurocritical Care: Review of the Current Resources. *Cureus* **7**, (2015).

175. Smith, M. Multimodality Neuromonitoring in Adult Traumatic Brain Injury: A Narrative Review. *Anesthesiology* **128**, 401–415 (2018).

176. Davies, D. J. *et al.* Frequency-domain vs continuous-wave near-infrared spectroscopy devices: a comparison of clinically viable monitors in controlled hypoxia. *J Clin Monit Comput* **31**, 967–974 (2017).

177. Boas, D. A., Campbell, L. E. & Yodh, A. G. Scattering and Imaging with Diffusing Temporal Field Correlations. *Physical Review Letters* **75**, 1855–1858 (1995).

178. Boas, D. A. & Yodh, A. G. Spatially varying dynamical properties of turbid media probed with diffusing temporal light correlation. *Journal of the Optical Society America A* **14**, 192–215 (1997).

179. Boas, D. A. *et al.* Establishing the diffuse correlation spectroscopy signal relationship with blood flow. *Neurophotonics* **3**, 031412–031412 (2016).

180. Durduran, T. & Yodh, A. G. Diffuse correlation spectroscopy for non-invasive, micro-vascular cerebral blood flow measurement. *NeuroImage* **85, Part 1**, 51–63 (1).

181. Mesquita, R. C. *et al.* Direct measurement of tissue blood flow and metabolism with diffuse optics. *Philosophical transactions. Series A, Mathematical, physical, and engineering sciences* **369**, 4390–406 (2011).

182. Erin M Buckley. CEREBRAL HEMODYNAMICS IN HIGH-RISK NEONATES PROBED BY DIFFUSE OPTICAL SPECTROSCOPIES. *University of Pennsylvania* 221 (2011).

183. Chao Zhou. In-vivo optical imaging and spectroscopy of cerebral hemodynamics. *Dissertations available from ProQuest* 1–325 (2007).

184. Sathialingam, E. *et al.* Hematocrit significantly confounds diffuse correlation spectroscopy measurements of blood flow. *Biomed Opt Express* **11**, 4786–4799 (2020).

185. Haskell, R. C. *et al.* Boundary conditions for the diffusion equation in radiative transfer. *J. Opt. Soc. Am. A, JOSAA* **11**, 2727–2741 (1994).

186. Scholkmann, F. & Wolf, M. General equation for the differential pathlength factor of the frontal human head depending on wavelength and age. *JBO* **18**, 105004 (2013).

187. Lee, S. Y. *et al.* Noninvasive optical assessment of resting-state cerebral blood flow in children with sickle cell disease. *Neurophotonics* **6**, 1 (2019).

188. Wang, D. *et al.* Fast blood flow monitoring in deep tissues with real-time software correlators. *Biomed Opt Express* **7**, 776–797 (2016).

189. International Electrotechnical Commission. IEC 60825-14: 2004 Safety of laser products, Part 14: A user's guide. *International Standard* (2004).

190. Center for Devices and Radiological Health. Laser Products - Conformance with IEC 60825-1 Ed. 3 and IEC 60601-2-22 Ed. 3.1 (Laser Notice No. 56). *U.S. Food and Drug Administration* https://www.fda.gov/regulatory-information/search-fda-guidance-documents/laser-products-conformance-iec-60825-1-ed-3-and-iec-60601-2-22-ed-31-laser-notice-no-56 (2019).

191. Kiguchi, M. *et al.* Comparison of light intensity on the brain surface due to laser exposure during optical topography and solar irradiation. *JBO* **12**, 062108 (2007).

192. Zhang, G. *et al.* Brain perfusion monitoring with frequency-domain and continuous-wave near-infrared spectroscopy: a cross-correlation study in newborn piglets. *Phys. Med. Biol.* **45**, 3143–3158 (2000).

193. Buckley, E. M. *et al.* Validation of diffuse correlation spectroscopic measurement of cerebral blood flow using phase-encoded velocity mapping magnetic resonance imaging. *Journal of biomedical optics* **17**, 037007 (2012).

194. Yu, G. *et al.* Validation of diffuse correlation spectroscopy for muscle blood flow with concurrent arterial spin labeled perfusion MRI. *Opt. Express, OE* **15**, 1064–1075 (2007).

195. Kassner, A. & Roberts, T. P. L. Beyond Perfusion: Cerebral Vascular Reactivity and Assessment of Microvascular Permeability. *Topics in Magnetic Resonance Imaging* **15**, 58 (2004).

196. Liu, P. *et al.* Cerebrovascular reactivity mapping without gas challenges. *NeuroImage* **146**, 320–326 (2017).

197. Urback, A. L., MacIntosh, B. J. & Goldstein, B. I. Cerebrovascular reactivity measured by functional magnetic resonance imaging during breath-hold challenge: A systematic review. *Neuroscience & Biobehavioral Reviews* **79**, 27–47 (2017).

198. Croal, P. L. *et al.* Assessment of cerebral blood flow with magnetic resonance imaging in children with sickle cell disease: A quantitative comparison with transcranial Doppler ultrasonography. *Brain Behav* **7**, e00811 (2017).

199. Jain, V. *et al.* Cerebral oxygen metabolism in neonates with congenital heart disease quantified by MRI and optics. *Journal of Cerebral Blood Flow and Metabolism* **34**, 380–388 (2014).

200. Busch, D. R. *et al.* Cerebral Blood Flow Response to Hypercapnia in Children with Obstructive Sleep Apnea Syndrome. *Sleep* **39**, 209–16 (2016).

201. Durduran, T. *et al.* Optical measurement of cerebral hemodynamics and oxygen metabolism in neonates with congenital heart defects. *J Biomed Opt* **15**, 037004 (2010).

202. Milej, D. *et al.* Characterizing dynamic cerebral vascular reactivity using a hybrid system combining time-resolved near-infrared and diffuse correlation spectroscopy. *Biomedical Optics Express* **11**, 4571 (2020).

203. Selb, J. *et al.* Sensitivity of near-infrared spectroscopy and diffuse correlation spectroscopy to brain hemodynamics: simulations and experimental findings during hypercapnia. *Neurophotonics* **1**, (2014).

204. Zirak, P., Delgado-Mederos, R., Dinia, L., Martí-Fàbregas, J. & Durduran, T. Microvascular versus Macrovascular Cerebral Vasomotor Reactivity in Patients with Severe Internal Carotid Artery Stenosis or Occlusion. *Academic Radiology* **21**, 168–174 (2014).

205. Zirak, P., Delgado-Mederos, R., Martí-Fàbregas, J. & Durduran, T. Effects of acetazolamide on the micro- and macro-vascular cerebral hemodynamics: a diffuse optical and transcranial doppler ultrasound study. *Biomedical Optics Express* **1**, 1443 (2010).

206. Goff, D. A., Buckley, E. M., Durduran, T., Wang, J. & Licht, D. J. Noninvasive Cerebral Perfusion Imaging in High-Risk Neonates. *Seminars in Perinatology* **34**, 46–56 (2010).

207. Mesquita, R. C. *et al.* Influence of probe pressure on the diffuse correlation spectroscopy blood flow signal: extra-cerebral contributions. *Biomed Opt Express* **4**, 978–994 (2013).

208. Baker, W. B. *et al.* Pressure modulation algorithm to separate cerebral hemodynamic signals from extracerebral artifacts. *Neurophotonics* **2**, 035004 (2015).

209. Milej, D., Abdalmalak, A., Rajaram, A. & St. Lawrence, K. Direct assessment of extracerebral signal contamination on optical measurements of cerebral blood flow, oxygenation, and metabolism. *Neurophotonics* **7**, (2020).

210. Kosinski, P. D. *et al.* The severity of anaemia depletes cerebrovascular dilatory reserve in children with sickle cell disease: a quantitative magnetic resonance imaging study. *Br J Haematol* **176**, 280–287 (2017).

211. Cowdrick, K. R. *et al.* Agreement in cerebrovascular reactivity assessed with diffuse correlation spectroscopy across experimental paradigms improves with short separation regression. *Neurophotonics* **10**, (2023).

212. Fierstra, J. *et al.* Measuring cerebrovascular reactivity: what stimulus to use? *J Physiol* **591**, 5809–5821 (2013).

213. Settakis, G. *et al.* Acetazolamide as a vasodilatory stimulus in cerebrovascular diseases and in conditions affecting the cerebral vasculature. *Eur. J. Neurol.* **10**, 609–620 (2003).

214. Ziyeh, S. *et al.* Blood Oxygen Level–Dependent MRI of Cerebral CO_2 Reactivity in Severe Carotid Stenosis and Occlusion. *Stroke* **36**, 751–756 (2005).

215. Lu, H. *et al.* Alterations in Cerebral Metabolic Rate and Blood Supply across the Adult Lifespan. *Cereb Cortex* **21**, 1426–1434 (2011).

216. Prokopiou, P. C., Pattinson, K. T. S., Wise, R. G. & Mitsis, G. D. Modeling of dynamic cerebrovascular reactivity to spontaneous and externally induced CO2 fluctuations in the human brain using BOLD-fMRI. *NeuroImage* **186**, 533–548 (2019).

217. Lu, H. *et al.* MRI Mapping of Cerebrovascular Reactivity via Gas Inhalation Challenges. *J Vis Exp* (2014) doi:10.3791/52306.

218. Tancredi, F. B. & Hoge, R. D. Comparison of Cerebral Vascular Reactivity Measures Obtained Using Breath-Holding and CO_2 Inhalation. *Journal of Cerebral Blood Flow & Metabolism* **33**, 1066–1074 (2013).

219. Spano, V. R. *et al.* CO2 Blood Oxygen Level–dependent MR Mapping of Cerebrovascular Reserve in a Clinical Population: Safety, Tolerability, and Technical Feasibility. *Radiology* **266**, 592–598 (2013).

220. Wise, R. G. *et al.* Dynamic Forcing of End-Tidal Carbon Dioxide and Oxygen Applied to Functional Magnetic Resonance Imaging. *J Cereb Blood Flow Metab* **27**, 1521–1532 (2007).

221. Yezhuvath, U. S., Lewis-Amezcua, K., Varghese, R., Xiao, G. & Lu, H. On the assessment of cerebrovascular reactivity using hypercapnia BOLD MRI. *NMR in Biomedicine* **22**, 779–786 (2009).

222. Kastrup, A., Krüger, G., Neumann-Haefelin, T. & Moseley, M. E. Assessment of cerebrovascular reactivity with functional magnetic resonance imaging: comparison of CO2 and breath-holding. *Magnetic Resonance Imaging* **19**, 13–20 (2001).

223. Moreton, F. C., Dani, K. A., Goutcher, C., O'Hare, K. & Muir, K. W. Respiratory challenge MRI: Practical aspects. *NeuroImage: Clinical* **11**, 667–677 (2016).

224. Murphy, K., Harris, A. D. & Wise, R. G. Robustly measuring vascular reactivity differences with breath-hold: normalising stimulus-evoked and resting state BOLD fMRI data. *Neuroimage* **54**, 369–379 (2011).

225. Liu, P. *et al.* Cerebrovascular reactivity mapping without gas challenges. *NeuroImage* **146**, 320–326 (2017).

226. Busch, D. R. *et al.* Cerebral Blood Flow Response to Hypercapnia in Children with Obstructive Sleep Apnea Syndrome. *Sleep* **39**, 209–216 (2016).

227. Tung, K.-C. *et al.* Alterations in resting functional connectivity due to recent motor task. *Neuroimage* **78**, 316–324 (2013).

228. Wise, R. G., Ide, K., Poulin, M. J. & Tracey, I. Resting fluctuations in arterial carbon dioxide induce significant low frequency variations in BOLD signal. *NeuroImage* **21**, 1652–1664 (2004).

229. Liu, P. *et al.* Cerebrovascular reactivity mapping using intermittent breath modulation. *NeuroImage* 116787 (2020) doi:10.1016/j.neuroimage.2020.116787.

230. Palazzo, P. *et al.* Lack of correlation between cerebral vasomotor reactivity and flow-mediated dilation in subjects without vascular disease. *Ultrasound Med Biol* **39**, 10–15 (2013).

231. Lipp, I., Murphy, K., Caseras, X. & Wise, R. G. Agreement and repeatability of vascular reactivity estimates based on a breath-hold task and a resting state scan. *Neuroimage* **113**, 387–396 (2015).

232. Wu, M. M. *et al.* Improved accuracy of cerebral blood flow quantification in the presence of systemic physiology cross-talk using multi-layer Monte Carlo modeling. *NPh* **8**, 015001 (2021).

233. Zhou, Y., Rodgers, Z. B. & Kuo, A. H. Cerebrovascular reactivity measured with arterial spin labeling and blood oxygen level dependent techniques. *Magnetic Resonance Imaging* **33**, 566–576 (2015).

234. Laurin, A. BP_annotate (MATLAB Central File Exchange). (2021).

235. Jain, V. *et al.* Cerebral oxygen metabolism in neonates with congenital heart disease quantified by MRI and optics. *Journal of Cerebral Blood Flow and Metabolism* **34**, 380–388 (2014).

236. Irwin, D. *et al.* Influences of tissue absorption and scattering on diffuse correlation spectroscopy blood flow measurements. *Biomedical Optics Express* **2**, 1969 (2011).

237. Li, J. *et al.* Noninvasive detection of functional brain activity with near-infrared diffusing-wave spectroscopy. *JBO* **10**, 044002 (2005).

238. Zhao, H., Sathialingam, E. & Buckley, E. M. Accuracy of diffuse correlation spectroscopy measurements of cerebral blood flow when using a three-layer analytical model. *Biomed Opt Express* **12**, 7149–7161 (2021).

239. Farina, A. *et al.* In-vivo multilaboratory investigation of the optical properties of the human head. *Biomed Opt Express* **6**, 2609–2623 (2015).

240. Verdecchia, K. *et al.* Assessment of a multi-layered diffuse correlation spectroscopy method for monitoring cerebral blood flow in adults. *Biomedical Optics Express* **7**, 3659 (2016).

241. Gagnon, L. *et al.* Short separation channel location impacts the performance of short channel regression in NIRS. *NeuroImage* **59**, 2518–2528 (2012).

242. Saager, R. B., Telleri, N. L. & Berger, A. J. Two-detector Corrected Near Infrared Spectroscopy (C-NIRS) detects hemodynamic activation responses more robustly than single-detector NIRS. *NeuroImage* **55**, 1679–1685 (2011).

243. Yücel, M. A. *et al.* Short separation regression improves statistical significance and better localizes the hemodynamic response obtained by near-infrared spectroscopy for tasks with differing autonomic responses. *NPh* **2**, 035005 (2015).

244. Lin, L. I. A concordance correlation coefficient to evaluate reproducibility. *Biometrics* **45**, 255–268 (1989).

245. Giavarina, D. Understanding Bland Altman analysis. *Biochem Med (Zagreb)* **25**, 141–151 (2015).

246. von Lühmann, A., Ortega-Martinez, A., Boas, D. A. & Yücel, M. A. Using the General Linear Model to Improve Performance in fNIRS Single Trial Analysis and Classification: A Perspective. *Frontiers in Human Neuroscience* **14**, 30 (2020).

247. Liu, T. T., Nalci, A. & Falahpour, M. The Global Signal in fMRI: Nuisance or Information? *Neuroimage* **150**, 213–229 (2017).

248. Chen, J. J. & Gauthier, C. J. The Role of Cerebrovascular-Reactivity Mapping in Functional MRI: Calibrated fMRI and Resting-State fMRI. *Front Physiol* **12**, 657362 (2021).

249. Favre, M. E., Lim, V., Falvo, M. J. & Serrador, J. M. Cerebrovascular reactivity and cerebral autoregulation are improved in the supine posture compared to upright in healthy men and women. *PLOS ONE* **15**, e0229049 (2020).

250. Sutin, J. *et al.* Time-domain diffuse correlation spectroscopy. *Optica* **3**, 1006 (2016).

251. Samaei, S. *et al.* Time-domain diffuse correlation spectroscopy (TD-DCS) for noninvasive, depth-dependent blood flow quantification in human tissue in vivo. *Sci Rep* **11**, 1817 (2021).

252. Kholiqov, O., Zhou, W., Zhang, T., Du Le, V. N. & Srinivasan, V. J. Time-of-flight resolved light field fluctuations reveal deep human tissue physiology. *Nature Communications* **11**, 1–15 (2020).

253. Zhou, W. *et al.* Functional interferometric diffusing wave spectroscopy of the human brain. *Science Advances* **7**, eabe0150 (2021).

254. Carp, S. A. *et al.* Diffuse correlation spectroscopy measurements of blood flow using 1064 nm light. *JBO* **25**, 097003 (2020).

255. Baker, W. B. *et al.* Modified Beer-Lambert law for blood flow. *Biomed. Opt. Express, BOE* **5**, 4053–4075 (2014).

256. Gagnon, L., Yücel, M. A., Boas, D. A. & Cooper, R. J. Further improvement in reducing superficial contamination in NIRS using double short separation measurements. *Neuroimage* **85**, (2014).

257. Battisti-Charbonney, A., Fisher, J. & Duffin, J. The cerebrovascular response to carbon dioxide in humans. *The Journal of Physiology* **589**, 3039–3048 (2011).

258. Claassen, J. A. H. R., Zhang, R., Fu, Q., Witkowski, S. & Levine, B. D. Transcranial Doppler estimation of cerebral blood flow and cerebrovascular conductance during modified rebreathing. *Journal of Applied Physiology* **102**, 870–877 (2007).

259. Taylor, A. J., Kim, J. H. & Ress, D. Characterization of the hemodynamic response function across the majority of human cerebral cortex. *Neuroimage* **173**, 322–331 (2018).

260. Peng, T., Niazy, R., Payne, S. J. & Wise, R. G. The effects of respiratory CO2 fluctuations in the resting-state BOLD signal differ between eyes open and eyes closed. *Magnetic Resonance Imaging* **31**, 336–345 (2013).

261. Leung, J., Duffin, J., Fisher, J. A. & Kassner, A. MRI-based cerebrovascular reactivity using transfer function analysis reveals temporal group differences between patients with sickle cell disease and healthy controls. *NeuroImage: Clinical* **12**, 624–630 (2016).

262. Kim, J. A., Leung, J., Lerch, J. P. & Kassner, A. Reduced cerebrovascular reserve is regionally associated with cortical thickness reductions in children with sickle cell disease. *Brain Research* **1642**, 263–269 (2016).

263. Macedo-Campos, R. de S., Adegoke, S. A., Figueiredo, M. S., Braga, J. A. P. & Silva, G. S. Cerebral Vasoreactivity in Children with Sickle Cell Disease: A Transcranial Doppler Study. *Journal of Stroke and Cerebrovascular Diseases* **27**, 2703–2706 (2018).

264. Forté, S. *et al.* Sickle cell cerebrovascular reactivity to a CO2 stimulus: Too little, too slow. *Frontiers in Physiology* **13**, (2022).

265. Sayin, E. S. *et al.* Assessment of cerebrovascular function in patients with sickle cell disease using transfer function analysis. *Physiological Reports* **10**, e15472 (2022).

266. Afzali-Hashemi, L. *et al.* Impairment of Cerebrovascular Hemodynamics in Patients With Severe and Milder Forms of Sickle Cell Disease. *Front Physiol* **12**, 645205 (2021).

267. Poublanc, J. *et al.* Measuring Cerebrovascular Reactivity: The Dynamic Response to a Step Hypercapnic Stimulus. *Journal of Cerebral Blood Flow & Metabolism* **35**, 1746–1756 (2015).

268. Sayin, E. S. *et al.* Assessing Cerebrovascular Resistance in Patients With Sickle Cell Disease. *Frontiers in Physiology* **13**, (2022).

269. Pinto, J., Bright, M. G., Bulte, D. P. & Figueiredo, P. Cerebrovascular Reactivity Mapping Without Gas Challenges: A Methodological Guide. *Front. Physiol.* **11**, (2021).

270. Durduran, T., Choe, R., Baker, W. B. & Yodh, A. G. Diffuse Optics for Tissue Monitoring and Tomography. *Rep Prog Phys* **73**, (2010).

271. Lee, S. Y. *et al.* Noninvasive optical assessment of resting-state cerebral blood flow in children with sickle cell disease. *NPh* **6**, 035006 (2019).

272. Lin, L. I.-K. A Concordance Correlation Coefficient to Evaluate Reproducibility. *Biometrics* **45**, 255–268 (1989).

273. Wu, M. M. *et al.* Complete head cerebral sensitivity mapping for diffuse correlation spectroscopy using subject-specific magnetic resonance imaging models. *Biomed. Opt. Express* **13**, 1131 (2022).

274. Lee, S. Y. *et al.* Quantifying the Cerebral Hemometabolic Response to Blood Transfusion in Pediatric Sickle Cell Disease With Diffuse Optical Spectroscopies. *Frontiers in Neurology* **13**, (2022).

275. Ainslie, P. N. *et al.* Early morning impairment in cerebral autoregulation and cerebrovascular CO2 reactivity in healthy humans: relation to endothelial function. *Experimental Physiology* **92**, 769–777 (2007).

276. Tallon, C. M., Barker, A. R., Nowak-Flück, D., Ainslie, P. N. & McManus, A. M. The influence of age and sex on cerebrovascular reactivity and ventilatory response to hypercapnia in children and adults. *Experimental Physiology* **105**, 1090–1101 (2020).

277. Henrique, D. B., Rentes, A. F., Filho, M. G. & Esposto, K. F. A new value stream mapping approach for healthcare environments. *Production Planning & Control* **27**, 24–48 (2016).

278. Relander, F. A. J. *et al.* Using near-infrared spectroscopy and a random forest regressor to estimate intracranial pressure. *NPh* **9**, 045001 (2022).

279. Ruesch, A. *et al.* Estimating intracranial pressure using pulsatile cerebral blood flow measured with diffuse correlation spectroscopy. *Biomed. Opt. Express, BOE* **11**, 1462–1476 (2020).

280. Fischer, J. B. *et al.* Non-invasive estimation of intracranial pressure by diffuse optics − a proof-of-concept study. *medRxiv* 2020.05.21.20109256 (2020) doi:10.1101/2020.05.21.20109256.

281. Tabassum, S. *et al.* Clinical translation of noninvasive intracranial pressure sensing with diffuse correlation spectroscopy. *Journal of Neurosurgery* **1**, 1–10 (2022).

282. Ruesch, A., Schmitt, S., Yang, J., Smith, M. A. & Kainerstorfer, J. M. Fluctuations in intracranial pressure can be estimated non-invasively using near-infrared spectroscopy in

non-human primates. *J Cereb Blood Flow Metab* 0271678X19891359 (2019) doi:10.1177/0271678X19891359.

283. Le Roux, P. Intracranial Pressure Monitoring and Management. in *Translational Research in Traumatic Brain Injury* (eds. Laskowitz, D. & Grant, G.) (CRC Press/Taylor and Francis Group, 2016).

284. Canac, N., Jalaleddini, K., Thorpe, S. G., Thibeault, C. M. & Hamilton, R. B. Review: pathophysiology of intracranial hypertension and noninvasive intracranial pressure monitoring. *Fluids and Barriers of the CNS* **17**, 40 (2020).

285. Gullotti, D. M. *et al.* Trends in Intraoperative Assessment of Spinal Alignment: A Survey of Spine Surgeons in the United States. *Global Spine Journal* **12**, 82S-86S (2022).